

"This is the peer reviewed version of the following article: [Advanced Materials Technologies, 2018], which has been published in final form at  
[<https://onlinelibrary.wiley.com/doi/full/10.1002/admt.201800200>] This article may be used for non-commercial purposes in accordance with Wiley Terms and Conditions for Self-Archiving

# Advanced Materials Technologies

## Graphene-based planar micro-supercapacitors: Recent advances and future challenges

--Manuscript Draft--

<b>Manuscript Number:</b>	admt.201800200R3
<b>Full Title:</b>	Graphene-based planar micro-supercapacitors: Recent advances and future challenges
<b>Article Type:</b>	Review
<b>Section/Category:</b>	
<b>Keywords:</b>	micro -supercapacitors; Graphene; thin -films; electrochemical performance; fabrication
<b>Corresponding Author:</b>	Francesca Iacopi, PhD University of Technology Sydney Broadway, New South Wales AUSTRALIA
<b>Additional Information:</b>	
<b>Question</b>	<b>Response</b>
Please submit a plain text version of your cover letter here.	<p>Dear Dr.Levy,</p> <p>On behalf of my co-authors, I would like to submit our review manuscript "Graphene-based planar micro-supercapacitors: Recent advances and future challenges" for potential publication in Advanced Materials Technologies.</p> <p>We believe this review will be a helpful resource for the energy storage community. As the need for adequate and reliable integrated power sources for the sensors and hardware systems for the Internet of Everything is set towards a massive expansion in the coming years, we explain in this manuscript how graphene -based planar supercapacitors have the potential to fill in at least a part of this vast gap.</p> <p>We have particularly focused on most recent advances and novel challenges for thin - film characterisation. We also point out that research and development of graphene-based micro-supercapacitors is still at an immature stage and has a vast scope for further advances, spanning from the understanding of fundamental electrochemistry and transport mechanisms to the more technological fabrication and integration aspects.</p> <p>.</p> <p>Thanks in advance for your consideration of our work, Sincerely,</p> <p>Francesca Iacopi</p>
Do you or any of your co-authors have a conflict of interest to declare?	No. The authors declare no conflict of interest.
<b>Corresponding Author Secondary Information:</b>	
<b>Corresponding Author's Institution:</b>	University of Technology Sydney
<b>Corresponding Author's Secondary Institution:</b>	
<b>First Author:</b>	Liang Jiaying

<b>First Author Secondary Information:</b>	
<b>Order of Authors:</b>	Liang Jiaying
	Anjon Mondal
	Da-Wei Wang
	Francesca Iacopi, PhD
<b>Order of Authors Secondary Information:</b>	
<b>Abstract:</b>	<p>The continuous development of integrated electronics, such as maintenance-free biosensors, remote and mobile environmental sensors, wearable personal electronics, nanorobotics etc. and their continued miniaturization has led to an increasing demand for miniaturized energy storage units. Micro-supercapacitors with graphene electrodes hold great promise as miniaturized, integrated power sources thanks to their fast charge/discharge rates, high power density and long cycling stability. In addition, planar interdigitated electrodes also have the capability to reduce ion diffusion distances leading to a greatly improved electrochemical performance. Either as standalone power sources or complementing energy harvesting units, it is expected that graphene-based micro-supercapacitors will play a key role as miniaturized power sources in electronic microsystems. This review highlights the recent development, challenges and prospects in this area, with an emphasis on the link between material and geometry design of planar graphene-based electrodes and their electrochemical performance and integrability.</p>

DOI: 10.1002/ admt.201800200

**Article type:** Review

Graphene-based planar micro-supercapacitors: Recent advances and future challenges

*Liang Jiaxing, Anjon Kumar Mondal, Da-Wei Wang\*, Francesca Iacopi\**

Liang Jiaxing

School of Chemical Engineering, The University of New South Wales, Sydney, NSW 2052, Australia

Dr. Anjon Kumar Mondal

School of Electrical and Data Engineering, Faculty of Engineering and Information Technology, University of Technology Sydney, Broadway, Sydney, NSW 2007, Australia

Centre for Clean Energy Technology, Faculty of Science, University of Technology Sydney, Broadway, Sydney, NSW 2007,

Dr. Da-Wei Wang

School of Chemical Engineering, The University of New South Wales, Sydney, NSW 2052, Australia

E-mail: da-wei.wang@unsw.edu.au

Prof. Francesca Iacopi

School of Electrical and Data Engineering, Faculty of Engineering and Information Technology, University of Technology Sydney, Broadway, Sydney, NSW 2007, Australia

Centre for Clean Energy Technology, Faculty of Science, University of Technology Sydney, Broadway, Sydney, NSW 2007, Australia

E-mail: francesca.iacopi@uts.edu.au

**Keywords:** micro-supercapacitors, graphene, thin-films, electrochemical performance, fabrication

The continuous development of integrated electronics, such as maintenance-free biosensors, remote and mobile environmental sensors, wearable personal electronics, nanorobotics etc. and their continued miniaturization has led to an increasing demand for miniaturized energy storage units. Micro-supercapacitors with graphene electrodes hold great promise as miniaturized, integrated power sources thanks to their fast charge/discharge rates, superior power performance and long cycling stability. In addition, planar interdigitated electrodes also have the capability to reduce ion diffusion distances leading to a greatly improved electrochemical performance. Either as standalone power sources or complementing energy harvesting units, it is expected that graphene-based micro-supercapacitors will play a key role as miniaturized power sources in electronic microsystems. This review highlights the recent

development, challenges and perspectives in this area, with an emphasis on the link between material and geometry design of planar graphene-based electrodes and their electrochemical performance and integrability.

## 1. Introduction

Supercapacitors (SCs) are of particular interest for their high power densities as shown in **Figure 1**,<sup>[1]</sup> and ultra-long cycle life with little capacity loss.<sup>[2-5]</sup> They also have wide operational temperature range and can be operated environmental friendly as well as maintenance free.<sup>[6, 7]</sup> A supercapacitor is generally composed by one (or more) pair of electrodes similarly to an electrostatic capacitor, where the typical dielectric material is replaced by a liquid or solid-state electrolyte. The energy in a supercapacitor is typically stored following two distinct mechanisms, and the corresponding SCs categories are referred to either as electrochemical double layer capacitors (EDLCs) or as pseudo-capacitors. In EDLCs, energy is stored/ released via surface ions absorption/desorption in the effect of electric field. Hence, the EDLCs type active materials usually have high specific surface area, e.g. activated carbon and graphene.<sup>[8-10]</sup> On the other hand, for those pseudocapacitive materials, for instance MoS<sub>2</sub>, Nb<sub>2</sub>O<sub>5</sub> and etc., redox reactions play a predominant role in energy storage.<sup>[11, 12]</sup> Obviously, energy storage through a combination of the two mechanisms above in the same supercapacitor cell is also possible, depending on the chosen electrode and electrolyte materials.

However, large volume supercapacitors cannot be integrated in a miniaturized system with other electronic devices, and a planar alternative must be pursued. The rapidly increasing demand for wireless, self-powered, maintenance-free sensors and portable electronics have translated into an increasing need for miniaturized energy storage devices.<sup>[13-15]</sup> These small-scale power sources have become indispensable, where the external power source is not at hand.<sup>[16]</sup> In fact, also autonomous electronic systems powered via integrated energy harvesters

would still need to ensure a sufficient and uninterrupted energy provision by storing the excess energy locally to cover temporary dips in supply.<sup>[17]</sup> Currently, micro-batteries are the most common miniaturized sources in self-powered micro-devices.<sup>[18]</sup>

Although micro-batteries are commercially available and their market demand is expanding, their application is limited by their low power density and short cycle life. Alternative to micro-batteries, micro-supercapacitors (MSCs) are fairly new miniaturized power sources in microelectronic systems. In recent years, thanks to the advantages offered by SCs, they have attracted tremendous attention for replacing micro-batteries.<sup>[19, 20]</sup> Recently, MSCs have been considered not only to complement sensing systems (humidity, temperature, etc.), which are normally low power consumption devices, but also for communication units, e.g. Wi-Fi, Bluetooth, 4G-network, with substantially more demanding power performance requirements.<sup>[21]</sup>

Different approaches to MSCs fabrication include sandwich structures based on thin-film electrodes,<sup>[22]</sup> core-shell structures with fibre shape electrodes,<sup>[23, 24]</sup> and planar interdigital microelectrode finger arrays with micro-scale sizes in at least two dimensions.<sup>[25, 26]</sup> In particular, the planar interdigitated electrode configuration offers technical advantages over the sandwich structure, including a separator-free structure, shorter ionic diffusion distances and a larger electrolyte-electrode contact surface, resulting in superior capability, which is vital when the 2D layered materials are used as electrodes.<sup>[27]</sup> The diffusion distance of the electrolyte ions can be further reduced by reducing the gap between the electrodes, resulting in faster frequency response, smaller ion transport resistance and higher power densities, which is essential for future miniaturized mobile electronics.<sup>[25]</sup> In addition, the planar design permits the active electrode materials to be easily extendable to a 3D configuration, enhancing the areal energy and power density.<sup>[28]</sup> Finally, the planar architecture of MSCs can be made highly flexible and easy to integrate into wearable electronics for practical application.<sup>[29, 30]</sup>

As a one-atom thick 2D carbon sheet, graphene enjoys a high surface area of around 2630 m<sup>2</sup> g<sup>-1</sup> and outstanding electrical conductivity, making it a very promising active material for supercapacitors.<sup>[31]</sup> Generally, under a high temperature and with a metal substrate, by applying a chemical vapour deposition method (CVD), graphene is synthesized and subsequently transferred to its final substrate. However, the widespread application of this graphene is limited by the such processing conditions and low throughput.<sup>[32]</sup> The presence of abundant hydrophilic groups on the surface of graphene oxide (GO), the oxidized form of graphene, enables efficient dispersion in aqueous and some of the organic solvents for thin-film synthesis via different techniques.<sup>(33)</sup> Although the electrical resistance of GO is higher, reduced GO (RGO) can be converted via various techniques, e.g. thermal, optical, chemical, or electrochemical process, etc., to reinstate the high electrical conductivity.<sup>[34, 35]</sup> By introducing various electroactive materials including carbon nanotubes (CNTs), metal oxides/hydroxides and conductive polymers, the electrochemical performance of graphene can be further improved.<sup>[36, 37]</sup>

In fact, the chosen fabrication approaches are likely to influence the overall performances of MSCs and therefore determine whether the device will be successfully integrated in flexible or rigid electronics. The preparation of thin-film microelectrodes is facilitated by the advancement of processing techniques, e.g. chlorination, masking, gold sputtering, and selective etching methods of carbide derived carbon<sup>[20]</sup> and electrophoretic deposition of onion-like carbon.<sup>[38]</sup>

Owing to the 2D flat morphology and atomic layer thickness of graphene, it is possible to design thin film planar interdigitated MSCs. In order to develop planar MSCs, graphene-based films can be formed and patterned by using thin film based techniques.<sup>[39]</sup> An additional benefit of the thin-film based approach is that the graphene may be grown directly on the substrates of choice, for example, Si<sup>[40]</sup> and Polyethylene terephthalate (PET).<sup>[41]</sup> In particular, a first example of direct growth of graphene electrodes on silicon with excellent adhesion to a

silicon substrate could enable on-chip integration. The extra benefits of this approach include improved conductivity and device performance with the binder-free electrode.<sup>[42]</sup> Moreover, this approach could be extended to fabricate 3D electrode structures with a further enhancement of energy density.<sup>[28]</sup>

In this paper, as indicated by the schematic in **Figure 2**, we start with design considerations and performance metrics, followed by electrochemical performances of various graphene-based MSCs as well as an overview of fabrication methods. Finally, the upcoming challenges and perspectives for graphene-based planar MSCs will be discussed.

## 2. Design considerations and performance metrics for micro-supercapacitors

The electrochemical properties of supercapacitors depend on the combination of several components, which include electrodes, electrolytes, separators and current collectors. In addition, the final properties of each of those components also strongly depend on design of the device, the matching of each components and device assembly.<sup>[43]</sup> Therefore, the advancement of the properties of each individual component is not an appropriate strategy to optimize the properties of supercapacitors.<sup>[6, 36, 44-50]</sup> Many review papers have already been published discussing different aspects of advanced SCs. <sup>[1, 2, 5-7, 21]</sup> Here, architectural approaches and the parameters for benchmarking MSCs performance are the major focus.

### 2.1. Design considerations for MSCs

Initially, MSCs were fabricated in a sandwiched configuration, similar to the planar thin film micro-batteries or capacitors (**Figure 3a**). However, from the practical application standpoint, this 2D sandwich-like design brings several disadvantages, which include unwanted position displacement of the electrodes under the different environments of application. Also, there are

limitations in balancing both the energy and power performance to design superior performance MSCs in such a structure. Although thicker electrodes are in great demand to increase the mass loading and therefore enhance the energy density, the power density decreases as the thicker electrodes typically result in longer ion diffusion paths and higher electronic resistance.<sup>[17]</sup>

As illustrated in **Figure 3b**, in the planar interdigitated architecture, each electrode of the device contains a number of microelectrode fingers on a substrate. The electrode fabrication process typically follows the thin film fabrication techniques, which involve patterning of electrode. The planar interdigitated electrode design has many advantages over conventional sandwich-like configuration. For example, large number of open edges provided by the interdigitated electrode fingers can improve the diffusion of the electrolyte ions.<sup>[51]</sup> Another advantage is that the narrow interspaces between electrode fingers can be controlled by applying conventional microelectronic fabrication processes or other advanced patterning processes. Therefore, ultra-high power is obtained due to the reduced ionic diffusion distance between electrodes and small ion transport resistance.<sup>[38]</sup> In addition, planar interdigitated MSCs possess excellent electrical and mechanical properties because they are fabricated without any separators and binders. Furthermore, the planar architecture of the electrodes eases the fabrication and the integration of MSCs with other micro-devices, which is advantageous **for the full design of the microelectronic system, aiming at miniaturization.**

To obtain a high performance MSCs, some key parameters as shown in **Figure 3b** are of great importance, according to Liu et al..<sup>[51]</sup> As the ion conductivity of the electrolyte is constant,<sup>[52]</sup> the power density drops as the ion diffusion path and the ESR of the device increase if the distance of the gap between electrodes ( $W_g$ ) gets higher. Herein, to reduce the resistance and improve the energy/power density of the MSCs, it's important to increase the ratio of the width of the gap ( $W_g$ ) to the width of the electrodes ( $W_e$ ).<sup>[53]</sup> Apart from this, the energy density can be further improved via two simple approaches. One is to extend the length of the

finger electrodes (I), and another one is to build up a thicker electrode (t) to form a 3D structure. The latter allows for a higher areal mass loading of the active materials, so that the performance of the device per unit area increases.<sup>[54]</sup> In addition to the on-chip planar interdigitated design, there is also a helical structure as shown in **Figure 3c**.<sup>[55]</sup> Such a design may enhance the strength of the device.<sup>[56]</sup>

On the other hand, there is another important limitation regarding ion diffusion path specifically in layered 2D materials electrodes. In the traditional thin-film planar MSCs, ions can only diffuse into the interlayer of the electrodes from the edge, limiting the power performance seriously, even though the device is under optimized design. Therefore, the use of porous thin-film, which provides more ion diffusion channels, may help shorten the ion diffusion path greatly and increase the power density. Recently, to further improve the power density of the electrode, Yun et al. introduced a porous graphene film as the electrode of the MSC as shown in **Figure 3d**, this combination exhibits superior capacitance as well as power density, comparing with other carbon-based all-solid-state MSCs.<sup>[57]</sup>

The three-dimensional (3D) interdigitated architecture is one of other choices with highest potential for further improvement of energy density of MSCs. There are many studies have been the subject for the development of 3D configuration for micro-batteries.<sup>[58-60]</sup> The increased areal energy density of the device and the enhanced power density due to the reduced ion transportation distance of electrolyte ions are the major benefits of a 3D configuration for electrochemical energy storage systems. This architectural concept can be also beneficial for MSCs. If the electrode materials possess high electrical conductivity, the areal energy density significantly increases due to the increased length in the z direction of 3D architecture. Compared to micro batteries, this is more practical for micro-supercapacitors as the materials used in micro-supercapacitors are generally much more conductive.<sup>[17]</sup> Although 3D electrodes are preferred configuration for MSCs, only a few fabrication techniques for micro-supercapacitors with 3D architecture have been demonstrated.

1 Recently, a number of portable/wearable, flexible and miniaturized electronic devices  
2 including flexible sensors, artificial electronic skin and roll-up displays, have been reported,<sup>[61]</sup>  
3  
4 <sup>[62]</sup> which require thin, flexible and integrated high-performance MSCs.<sup>[63, 64]</sup> The fundamental  
5  
6 mechanical properties of the electrode materials, electrolytes, substrates, and their assembly  
7  
8 play a key role on the flexibility of MSCs.<sup>[65]</sup> Generally, flexible substrates, such as polymer  
9  
10 films and papers, which satisfy the requirements, are used to support MSCs. Meanwhile, gel  
11  
12 and solid-state electrolytes are the most appropriate types for integrated, rigid and flexible,  
13  
14 planar MSCs.  
15  
16  
17  
18  
19  
20  
21

## 22 **2.2. Performance metrics of micro-supercapacitors**

23  
24  
25  
26

27 The main figures of merit of a supercapacitor are related to how much energy stored and how  
28  
29 much power delivered per unit volume or weight. Gravimetric capacitance, energy and power  
30  
31 densities are the parameters that are generally used for assessing the performance of  
32  
33 supercapacitors against units of volume and weight. Note that the gravimetric performance of  
34  
35 supercapacitors depends on total mass, density and thickness of the electrodes and also weight  
36  
37 of other constituents. Thus, it is difficult to compare different micro-supercapacitors based on  
38  
39 gravimetric capacitance.<sup>[66]</sup> The gravimetric capacitance metrics is not appropriate for planar  
40  
41 MSCs, where the weight of the electrode materials is negligible and the volume and substrate  
42  
43 area of the device are always limited. Since the total mass loading of active materials is small  
44  
45 in MSCs, the volumetric and particularly the areal performances are more suitable as  
46  
47 benchmark of the electrochemical performance.  
48  
49  
50  
51

52 There are many reports showing that volumetric capacitances are mostly dependent on  
53  
54 properties of electrode materials. For thicker electrodes, the value of volumetric capacitance is  
55  
56 important. However, it is hard to achieve constant volumetric capacitance of a certain material  
57  
58 where the thickness of the electrodes is different. In particular, for EDLCs, if electrode is  
59  
60  
61  
62  
63  
64  
65

thicker and consists of complex internal pore structure the volumetric capacitance tends to decrease.<sup>[20]</sup> The volumetric capacitance also decreases for pseudo capacitive materials with inaccessible redox sites.<sup>[67]</sup> As the devices are supposed to integrate with miniaturised electronic devices with limited areas, performance assessment against the footprint area of MSCs is the key. Thus, areal capacitance, power and energy density are the more dependable parameters for MSCs benchmarking. Areal capacitance  $C_s$  (F cm<sup>-2</sup>), energy  $E_s$  (W h cm<sup>-2</sup>) and power densities  $P_s$  (W cm<sup>-2</sup>) can be calculated as per following equation:

$$C_s = Q/s\Delta V \quad (1)$$

$$E_s = \frac{0.5C\Delta V^2}{3600s} \quad (2)$$

$$P_s = \frac{\Delta V^2}{4ESR*s} \quad (3)$$

Where  $C_s$  is the areal capacitance,  $s$  indicates the total area of the microelectrode array, and  $\Delta V$  is the voltage range,  $E_s$  and  $P_s$  are the maximum energy and power densities. The capacitance and the voltage window can be indicated in circular voltametric (CV) method and galvanic charge/ discharge (GCD) method directly. The key to figure out the areal performance of the electrode is to measure the total area accurately.

### 2.2.1. Methods for evaluation the porosity of thin-film electrode

As mentioned earlier, the porosity and pore structure of MSC electrodes is a particularly important parameter linked to the accessibility of a maximum electrode area by the electrolyte. Therefore, the tailoring of porosity, pore size and connectivity of the electrode material to the chosen electrolyte is a key factor to maximise the total as well as the areal capacitance of an MSC, as well as its power densities. However, an accurate optimisation of the porosity of MSCs electrode materials has been held back so far by the fact that the pore characterisation for thin-film materials is more challenging as compared to bulk materials.

Traditional N<sub>2</sub> adsorption porosimetry [Barrett–Joyner–Halenda (BJH)] is widely used in the indication of porosity and surface area of porous materials. However, it's not applicable in the measurement of thin-film porosity, according to Maex and co-workers.<sup>[68]</sup> Several concerns are listed in their review. As the technique works by measuring the mass or volume of adsorbate condensed in the pores, samples on the substrate needs to be scrubbed off to collect enough powder like sample, in case the small amount fails to meet the sensitivity of the detector and induce large errors in the estimate of the total porous surface. The other drawback of the method is the extremely low temperature of the nitrogen. High pressure may be generated inside the thin film and result in swelling and cracking during cooling, especially when there are closed pores, inducing errors in the estimates. To enhance the accuracy of porosity evaluation, some advanced techniques, including positron annihilation lifetime spectroscopy,<sup>[23, 69]</sup> Positron annihilation spectroscopy,<sup>[70, 71]</sup> small-angle neutron scattering (SANS),<sup>[72]</sup> small angle x-ray scattering (SAXS)<sup>[73]</sup> and ellipsometric porosimetry (EP),<sup>[74-77]</sup> which have all been extensively developed for electronic thin-film materials such as low-k dielectrics,<sup>[68]</sup> will be introduced in the following sections.

#### Positron annihilation (lifetime) spectroscopy (PAS and PALS)

A focused positronium (Ps, a free electron-positron couple) beam is used as probe for voids within matter. The positronium has a short lifetime as it tends to annihilate or then decay via an electron bond in contact with electrons in the matter, PALS can collect the information of pore structure and size by detecting the lifetime of Ps, and PAS can provide porosity data through extracting information from the Ps annihilation reaction, as shown in **Figure 4**.<sup>[78, 79]</sup> And it's noteworthy that if there are all open pores which are interconnected, a capping layer should be deposited, to avoid Ps escaping to the vacuum and resulting in an inaccurate assessment.

In the PALS method, the Ps lifetime distribution curve can be obtained by recording the lifetime histogram. Assuming a known pore geometry, pore size can then be calculated using mathematical models.<sup>[69]</sup> For calculating the porosity of the sample, the PAS method is used. By detecting the amount of 2 $\gamma$  and 3 $\gamma$  photons that generate in annihilation reaction and comparing the 2 $\gamma$  (annihilation with a molecular electron<sup>[80]</sup> from the pore wall) and 3 $\gamma$  (self-annihilation) photon annihilation ratio of Ps, porosity can be calculated. As in PAS method, the ratio of 2 $\gamma$  photon reflects the collision frequency with pore walls, which affects the Ps lifetime, therefore, the porosity properties can be derived.<sup>[80]</sup> Tang et al. have used PALS method to explore the pore interconnectivity of porous silica thin film,<sup>[81]</sup> a frequently-used template for porous carbon electrodes.<sup>[82]</sup> The Ps 3 $\gamma$ -annihilation fraction was highly related to the diffusion of Ps, the diffusion of which was governed by the interconnectivity of the porous silica thin-film. Herein, the porous structure of silica was unravelled with PALS and showed good correlation to their cyclic voltammetry measurements.

#### Scattering techniques (SANS, SAXS)

A variation in the small-angle scattering lengths of neutrons (SANS) and X-Rays (SAXS) density occurs with the matter is observed when pores are present within the solid sample. The scattering concept for neutrons and X-rays is similar, but SANS and SAXS offer complementary information by comparing the interaction of a neutral particle to that of X-rays. In the scattering experiment setup as shown in **Figure 5a**, where the intensity is a function of  $2\Theta$ , the pore size is estimated as  $d \sim \lambda/2\Theta$ , where  $\lambda$  is the wavelength of the scattered radiation,<sup>[83]</sup> the angular distribution of scattered intensity can be measured and details of the porosity can be obtained. Combining with specular XRR and normalizing the XRR film density to the skeleton density, also the total porosity information can be calculated as shown in **Figure 5b**.<sup>[73]</sup> The pore size is accurately evaluated through the comparison of the

observed scattering intensity profile and the calculated profile, as in **Figure 5c**. This method has its limitations as only the mean pore size can be obtained.<sup>[73]</sup> Also, the sensitivity and the resolution of the scattering method is lower, due to the small volume of thin film, comparing with bulk samples.<sup>[72]</sup> Using in-situ SAXS, Prehal and co-workers managed to unravel the distribution of ions in microporous carbons. Moreover, the authors believe that the developed toolkit could be used to further understand the mechanism of EDLC and would be useful in the capacitive deionization field.<sup>[84]</sup>

### Ellipsometric porosimetry (EP)

This method is specifically developed for porous thin-film dielectrics or low-k films. Combining both the nonintrusive (wave propagation) and intrusive (adsorption) methods, and measuring the polarization state of a light beam reflected off a surface, two measured parameters of Ellipsometric porosimetry, the phase and amplitude ellipsometric angles  $\Delta$  and  $\Psi$  can be collected. The Fresnel reflection coefficients  $R_{\perp}$  and  $R_{\parallel}$  can be then calculated using equation 4:

$$\frac{R_{\parallel}}{R_{\perp}} = \tan(\Psi) \exp(i\Delta) \quad (4)$$

Then following the theory developed by Dubinin and Radushkevitch (DR),<sup>(85)</sup> the porous profile of the sample can be obtained, as shown in **Figure 6**.<sup>[68]</sup> The EP method is one of the simplest and more accurate for thin-films, however, the method is not reliable for films with thickness below ~10nm. Such a method was used by Kozbial and colleagues to study the hydrocarbon absorption onto the exfoliated highly ordered pyrolytic graphite (HOPG). The wettability of HOPG was explained on the basis of their EP data.<sup>[86]</sup>

All these methods have their advantages as well as drawbacks, which needs further detail study, especially when be applied to thin-film MSCs electrodes.

### 2.2.2 Efficiency of Micro-Supercapacitor

Multiple parameters should be used to accurately assess and benchmark the MSCs performance. The coulombic efficiency (CE; ratio of the cathodic and anodic capacity) is often used as a metric of the efficiency of energy storage. 100 % CE is desirable because it indicates that electrons are not lost to parasitic processes, such as electrolyte decomposition. A less-reported measure of energy storage performance is called energy efficiency, which captures the efficiency of both the capacity (CE) as well as the potential. The energy efficiency (E) is determined by taking the ratio of discharging energy and charging energy ( $E_{\text{discharge}}/E_{\text{charge}}$ ).<sup>[87, 88]</sup> The energy is calculated for the cathodic and anodic scan using Equation 5, where  $\Delta t$  is the charge/discharge time determined by the scan rates, and  $dv$  is the potential window.

$$E = \left( \int_{V_0}^{V_f} i dV \right) \Delta \quad (5)$$

### 2.2.3 Micro-Supercapacitor components and architectures

A broad range of electrode materials has been investigated to fabricate MSCs.<sup>[89-92]</sup> Among these electrode materials, two-dimensional (2D) graphene has received tremendous attention thanks to its superior electron mobility of  $15\,000\text{ cm}^2\text{ V}^{-1}\text{ s}^{-1}$  and large surface area of  $2630\text{ m}^2\text{ g}^{-1}$  with a outstanding theoretical capacitance of  $550\text{ F g}^{-1}$ .<sup>[70, 93]</sup> The integration of MSCs with other micro-devices could be facilitated by the 2D nature of graphene because of its analogy with thin-film materials as used in microelectronics. Additionally, the electrolyte and its tailoring to the chosen electrode material, is another vital factor for the electrochemical performance improvement of planar MSCs. It's worth mentioning that hydrated graphene

oxide (GO) shows the potential to work as solid-state electrolyte for graphene-based MSCs.

In section 3, we will review the graphene-based planar interdigitated MSCs.

Additionally, to date, a lot of electrode materials and feasible fabrication techniques have been reported for the assembly of MSCs. However, it is essential to understand the application purposes of the device before appropriate design. There are several parameters such as integrability, areal energy and power densities and cycling stability that are mostly desirable for the application of MSCs in an integrated self-powering system. The integrability strongly depends on the compatibility of electrode fabrication and the packaging of electrolytes. The energy and power densities also depend on the fabrication procedure as they determine what architectures to be constructed and what electrolyte and electrode material to be used for the device.<sup>[27]</sup> In section 4, we will talk about recent progress in the fabrication of graphene-based MSCs.

#### 2.2.4 Electrolytes for MSCs

The electrolyte is another key component of planar micro-supercapacitors. An ideal electrolyte should be electrochemically stable in a large voltage window, ionically conductive and electronically insulating, in addition to the requirements of low cost, low viscosity, low volatility, low toxicity and availability at high purity. The operando voltage of supercapacitors depends on the electrolyte decomposition voltage, which is a key factor to the maximum specific energy values. Meanwhile, the electrolyte conductivity influences the equivalent series resistance (ESR), which contributes to the power density of supercapacitors.

Electrolytes for SCs are classified into liquid electrolytes and solid electrolytes. The liquid electrolytes can be further categorised into aqueous electrolyte, organic electrolyte and ionic liquids.<sup>[94]</sup> Although liquid electrolytes have already been well developed for commercial supercapacitors, electrolyte leakage and difficult packaging hinder their application in

electronic systems. For MSCs, the use of solid-state or gel-type electrolytes is highly recommended, as they not only alleviate possible internal shorting and external electrolyte leakage issues, but also help reduce the device thickness by removing the need for a separator and extra encapsulation layers.<sup>[51]</sup> The development of solid-state electrolytes has been more recent in time and is still undergoing dramatic progress.

### Aqueous electrolytes

Aqueous electrolytes (such as  $\text{H}_2\text{SO}_4$ ,  $\text{KOH}$ ,  $\text{Na}_2\text{SO}_4$  etc.) have generally high ionic conductivity (up to  $1 \text{ S cm}^{-1}$ ) and low resistance, but limited voltage windows. For instance, Sugimoto and co-workers reported mesoporous  $\text{RuO}_2$  as the active material and  $0.5 \text{ M H}_2\text{SO}_4$  aqueous electrolyte for MSC with a gravimetric capacitance of  $400 \text{ F g}^{-1}$  and energy density of  $12.5 \text{ W h kg}^{-1}$ .<sup>[95]</sup> Recently, Bhawna et al. introduced the redox pair  $\text{I}^-/\text{I}_3^-$  into electrolytes by adding  $\text{KI}$  into  $\text{H}_2\text{SO}_4$  based electrolyte. The as-fabricated paper-based graphene MSC generated enhanced performance with an outstanding volumetric performance of  $29.6 \text{ mF cm}^{-3}$  under the current density of  $6.5 \text{ mA cm}^{-2}$ .<sup>[96]</sup> However, the energy stored is limited by the narrow working voltage range of about  $1 \text{ V}$  due to the low decomposition voltage of water ( $1.23 \text{ V}$ ).<sup>[97]</sup> In addition, the aqueous electrolytes are rather common as they can be prepared using relatively simple processes.

### Organic electrolytes

Organic electrolyte, a kind of mixture of salt and organic solvents, e.g. acetonitrile and propylene carbonate (PC), which provides a wide potential window as high as  $3 \text{ V}$ , increasing the energy performance of the MSC significantly.<sup>[98]</sup> With  $1 \text{ M}$  tetraethyl ammonium tetrafluoroborate ( $\text{NEt}_4\text{BF}_4$ ) in PC electrolyte, the obtained carbide-derived carbon based

MSC showed a voltage range of 2 V and a areal capacitance of  $1.5 \text{ mF cm}^{-2}$ , resulting in a energy density of  $3.0 \text{ J cm}^{-2}$ .<sup>[99]</sup> Further, Huang et al. reported a free-standing elastic carbon film based MSC with 2M EMI,  $\text{BF}_4$  in  $\text{CH}_3\text{CN}$  electrolyte showed a wide potential range of 3V and demonstrated a volumetric capacitance of  $160 \text{ F cm}^{-3}$  under a scan rate of  $20 \text{ mV s}^{-1}$ , resulting in an improved energy density.<sup>[100]</sup> However, the poor ionic conductivity limits the organic electrolyte application in high power performance MSCs.<sup>[98]</sup>

### Ionic liquids

Ionic liquids, which are usually molten salts at room temperature, have attracted considerable attention for application in MSCs. As a kind of electrolyte without solvents, ionic liquid is non-flammable and has a low vapour pressure that inhibiting the risk of explosion. Moreover, comparing with aqueous, ionic liquid provides a wider potential window.<sup>[101]</sup> Eustache and co-workers used 1-ethyl-3-methylimidazolium bis (trifluoromethylsulfonyl) imide (EMI-TFSI) ionic liquid working as electrolyte in the  $\text{MnO}_2$  thin-film based MSC. The operational voltage range of the as-obtained MSC was 1.5V, which was almost two times of the same combination with an aqueous electrolyte (0.8V). However, due to the low ionic conductivity of ionic liquid, the MSC with EMI-TFSI electrolyte demonstrated slightly lower energy density ( $>6.5 \text{ } \mu\text{Wh cm}^{-2}$ ) than the one using 0.5M  $\text{Na}_2\text{SO}_4$  electrolyte ( $>10 \text{ } \mu\text{Wh cm}^{-2}$ ) with a power density of  $1 \text{ mW cm}^{-2}$ .<sup>[102]</sup> Further development and improvement of ionic liquid by mixing ionic liquid with gel-electrolytes for application in integrated MSCs is an important direction of next generation MSCs.

### Solid state electrolytes

The main disadvantage of the electrolytes discussed above is their liquid nature, requiring an adequate and reliable encapsulation, which is often unpractical for miniaturization and flexible devices. Solid-state electrolytes are thus of particular interest for application in MSCs, and offer additional advantages for miniaturization and integration. For instance, the separator and electrolyte functions can be combined into a single layer.<sup>[103-105]</sup>

Solid electrolytes are commonly produced by mixing a polymer matrix with the additives, e.g. acids, salts or ionic liquids, in which the ionic conduction mainly takes place through voids or defects in the solid solution. Their performance nowadays compare well with liquid electrolytes.<sup>[31, 106]</sup> Researchers have developed different polymer matrixes, including poly(vinyl alcohol) (PVA), poly(vinylidene fluoride) (PVDF), polyacrylonitrile (PAN) and poly(vinylpyrrolidone). Among these matrixes, PVA is the most commonly used polymer. PVA/H<sub>2</sub>SO<sub>4</sub> and PVA/ H<sub>3</sub>PO<sub>4</sub> and PVA/lithium chloride have been extensively reported as solid-state electrolytes for planar MSCs.<sup>[25, 107-109]</sup> These solid-state electrolytes exhibit excellent mechanical properties, with good cyclability and low leakage current.<sup>[110]</sup> The ionic conductivity of PVA/H<sub>3</sub>PO<sub>4</sub> ranges from 10<sup>-5</sup> to 10<sup>-3</sup> S cm<sup>-1</sup>, while that of PVA/H<sub>2</sub>SO<sub>4</sub> has been reported as high as 7 × 10<sup>-3</sup> S cm<sup>-1</sup> at room temperature.<sup>[111, 112]</sup> Ionic liquid -based solid-state electrolytes (or ionic gels) have also demonstrated operation voltages above 2 V, improving substantially the energy density of MSCs. PVA/1-butyl-3 methyl imidazolium tetrafluoroborate (BMIBF<sub>4</sub>) and 1-ethyl-3-methylimidazolium bis (trifluoromethylsulfonyl) imide/fumed silica have also been successfully applied as non-aqueous gel electrolytes for micro-supercapacitors, showing a wide operation voltage range of 2.5 V, and excellent power performance.<sup>[113, 114]</sup>

However, as compared to liquid electrolytes, solid-state electrolytes typically exhibit lower ionic conductivities. Also, an adequate chemical stability of solid-state electrolytes is critical in order to ensure a large potential window and cyclability. In addition, as a requirement for flexible or stretchable MSCs, solid-state electrolytes need to guarantee mechanical flexibility

and often transparency.<sup>[105]</sup> Lu et al. have recently reported a 3D-graphene -based MSC using PVA/H<sub>2</sub>SO<sub>4</sub> as solid state electrolyte. The MSC exhibited a high power density of 14.4 mW cm<sup>-2</sup> with a reasonable energy density of 0.29 μWh cm<sup>-2</sup>, and a potential window of 1 V.<sup>[115]</sup>

### 3. Graphene-based Material in Planar Interdigitated Micro-supercapacitors

Given the advantages of planar interdigitated MSCs mentioned earlier,<sup>[20, 38]</sup> the fabrication of planar MSCs using various nanostructured carbon materials as electrodes has been extensively pursued, including activated carbon,<sup>[116]</sup> CNTs,<sup>[117]</sup> carbide-derived carbon,<sup>[20]</sup> onion-like carbon<sup>[38]</sup> and graphene<sup>[28]</sup>.

In particular, graphene, as a 2D carbon material with a high specific surface area, a remarkable Young's modulus as high as 1.0 TPa and high electrical conductivity, has attracted increasing research interest over the years among various fields of physics and materials science.<sup>[118]</sup> The following section reviews recent progress in the development of graphenic materials as electrodes for planar interdigitated MSCs.

#### 3.1. Graphenic materials as electrodes

##### 3.1.1 Graphene

The specific capacitance of EDLCs is strongly related to the specific surface area of the active materials. Graphene possesses an outstanding electronic conductivity and a large specific surface area, both important requirements for electrode materials. Synthetic graphene, as well as reduced graphene oxide, have been extensively evaluated in both rigid and flexible planar MSCs. For example, Yoo et al. compared a monolayer graphene synthesized by a CVD method to a multilayer reduced graphene oxide (RGO) films as electrodes for ultrathin planar

**supercapacitor.** The areal capacitance of monolayer graphene-based device is around  $80 \mu\text{F cm}^{-2}$ , while the value of multilayer RGO film is  $394 \mu\text{F cm}^{-2}$ .<sup>[48]</sup>

Niu et al. obtained an ultrathin, compact, flexible all-solid-state reduced graphene oxide (RGO) interdigitated microelectrode-based MSC by conventional photolithography along with electrophoretic methods as shown in **Figure 7**.<sup>[90]</sup> With  $\text{H}_3\text{PO}_4$ / PVA gel electrolyte, the fabricated MSC delivered a superior capacitance of  $462 \mu\text{F cm}^{-2}$  with a high coulombic efficiency of 98%.

With advancements in the fields of thin film fabrication and device design, the electrochemical performance of graphene-based MSCs has been significantly boosted in terms of capacity, energy and power performance. Wu et al. have developed graphene-based planar interdigitated MSCs on both rigid and flexible substrates with outstanding performance through micro patterning of graphene films reduced by methane plasma.<sup>[19]</sup> As shown in **Figure 8a-d**, a graphene oxide solution was dispersed by spin-coating, treated with oxygen plasma, and then reduced by methane ( $\text{CH}_4$ ) plasma. Following the fabrication of the interdigitated current collectors, the exposed graphene on Si wafer was subject to oxidative etching to form the interdigitated microelectrodes. The obtained all solid-state MSCs with PVA/  $\text{H}_2\text{SO}_4$  electrolyte demonstrated a power density of  $495 \text{ W cm}^{-3}$  with an energy density of  $2.5 \text{ mW h cm}^{-3}$ . The MSC still possessed an outstanding cycling stability and ~98 % capacitance retained even after 100000 cycles at the scan rate of  $50 \text{ V s}^{-1}$ . Wu et al. have reported improved electrochemical performance by the reduction of the width of the finger and space between them for interdigitated electrodes.<sup>[119]</sup> The MSCs presented an enhanced specific capacitance of  $116 \text{ mF cm}^{-2}$  with a power density of  $1270 \text{ W cm}^{-3}$ . This work highlighted the consequence of reduced widths of fingers, space between the adjacent fingers and number of fingers, in the design of high-performance MSCs.

Wang et al. have also used a thin film based technique to grow SiC-derived graphene directly on the silicon substrates through the use of epitaxial silicon carbide to fabricate all-solid state supercapacitors.<sup>[39]</sup>

In addition, Xiong et al designed a superior graphitic petal (GP) electrode based symmetric MSCs by combining microwave plasma chemical vapour deposition (MPCVD) and electrochemical oxidation steps. Firstly, the GP layer was grown on the substrate using MPCVD, and then the current collector was coated onto the GP surface via electron-beam evaporator. Later, the pattern was formed by plasma etching. After an electrochemical oxidation treatment in a three-electrode system, the GP-based MSC demonstrated a high volumetric capacitance of  $\sim 68 \text{ F cm}^{-3}$ , due to the improved surface wettability and the larger amount of oxidation functional group. Compared to commercial devices, the devices by Xiong et al exhibited a superior energy density of up to  $10 \text{ mWh cm}^{-3}$ .<sup>[120]</sup>

To further enhance the areal and volumetric performance of the device, Z-S Wu et al designed a binder-free activated graphene (AG) compact film via altering deposition of AG and electrochemical exfoliated graphene (EG) onto the PTFE membrane with the help of vacuum filtration, then the film was dried and transferred to Si wafer, following by oxygen plasma etching as shown in **Figure 9**.<sup>[121]</sup> The MSC fabricated with the AG-EG film output a specific capacitance of  $147 \text{ F cm}^{-3}$  at the scan rate of  $10 \text{ mV s}^{-1}$  and  $19.3 \text{ F cm}^{-3}$  even with an scan rate of  $10 \text{ V s}^{-1}$ .

Nickel-assisted graphitization process also introduced to prepare highly conductive graphenic nano-carbon with significantly increased accessible surface area. The graphene thin film based all solid-state supercapacitors demonstrated promising performance and capacitance retention upon long-term cycling. The process they described and materials and equipment they used for the fabrication of graphene that are used in semiconductor technologies. This also indicates that thousands of micro-devices can be produced on large wafer by wafer-scale lithography in a single step.<sup>[122, 123]</sup>

### 3.1.2 Graphene quantum dots

Next to graphene sheets, graphene quantum dot (GQD) is another promising class of graphenic materials showings novel physical and chemical properties including nanometre-sized sheets, chemical stability, exceptional electrical conductivity, and many edge defects.<sup>[124]</sup> Liu et al. developed an electrophoretic deposition GQD-based planar symmetric MSC (**Figure 10**).<sup>[125]</sup> With a high scan rate of  $1000 \text{ V s}^{-1}$ , the obtained MSC showed an ultrafast frequency response with  $\tau_0 = 103.6 \text{ }\mu\text{s}$  in  $0.5 \text{ M Na}_2\text{SO}_4$  electrolyte. Its operational voltage window was expanded to  $2.7 \text{ V}$  with the use of ionic liquid electrolyte. Thanks to the numerous edge defects in the GDQ, the electrolyte accessibility and ionic diffusion through the graphene layers are highly enhanced, leading to a remarkable electrochemical performance.

### 3.1.3 Heteroatom-doped Graphene

The capacitance of graphene-based supercapacitors can be improved via heteroatom doping, e.g. nitrogen,<sup>[126]</sup> boron,<sup>[127]</sup> phosphor<sup>[128]</sup> and sulphur.<sup>[129]</sup> However, the preparation of homogeneously doped graphene films for MSCs over a large scale is challenging.

Combining spray-coating with thermal treatment, Mullen et al. have synthesised homogeneous and continuous sulphur-doped graphene (SG) ultrathin films derived from a sulphur-decorated graphene using a bottom-up, wafer-scale approach (**Figure 11**).<sup>[130]</sup> The described process provides a new strategy for the preparation of high performance MSCs based on uniform doping and highly conductive large area graphene films. The SG-MSCs delivered exceptional specific capacitance of  $553 \text{ }\mu\text{F cm}^{-2}$  under the scan rate of  $10 \text{ mV s}^{-1}$

and superior rate performance with an areal capacitance of  $8.1 \mu\text{F cm}^{-2}$  at the even higher scan rate of  $2000 \text{ V s}^{-1}$ . Even at  $200 \text{ V s}^{-1}$ , 95 % capacitance was retained after 10000 cycles (Figure 11 j).

Nevertheless, boron-doped graphene reported by Peng et al is shown in Figure 12.<sup>[131]</sup> To obtain the boron-doped light induction graphene film (B-LIG), PAA solution in N-methylpyrrolidone was added into  $\text{H}_3\text{BO}_3$  and mixed as a precursor solution. Then a solid PAA/ $\text{H}_3\text{BO}_3$  sheet was synthesized by pouring the precursor solution onto an aluminium dish and dried under vacuum. After that, PI/ $\text{H}_3\text{BO}_3$  film was obtained via dehydrated the previous sheet. Following this, the PI/ $\text{H}_3\text{BO}_3$  film turned into B-LIG film under laser induction process. Both areal capacitance and volumetric energy density at various power densities were enhanced significantly by boron-doping.

Also, N-doped graphene is also a kind of widely studied materials. A fibre electrode based high performance wearable MSC with nitrogen-doped graphene was reported by G. Wu et al. recently.<sup>[132]</sup> As presented in Figure 13 a-c, the well-dispersed GO and urea mixing solution was injected into a micro reactor. During the first step heat treatment, self-assembly 3D-network amino-GO was formed. Further reduction and N-doping of the graphene took place in second step heating. To fabricate the MSC, gel-electrolyte was added between two pieces of N-doped graphene fibre. The fibre is ultra-flexible and can be assembled in cloth as shown in fig.10d. Thanks to the high electronic conductivity, large specific surface area, and uniform pore distribution of the fibre, the as-obtained MSC delivered a high areal capacitance of  $1132 \text{ mF cm}^{-2}$ , and excellent stability under cycling as well as bending with the  $\text{H}_3\text{PO}_4/\text{PVA}$  electrolyte.

As a combination, nitrogen and boron co-doped graphene-based planar interdigitated MSCs were fabricated using conventional photolithography and a layer by layer assembly.<sup>[133]</sup> The co-doping with dual heteroatoms improved the electrode/ electrolyte interface wettability and provided additional pseudocapacitive contributions to the overall capacitance, leading to a

specific capacitance of  $488 \text{ F cm}^{-3}$ , and high cycle stability even under the high scan rate of  $2000 \text{ V s}^{-1}$ , which indicates that heteroatom-doped graphene electrodes may be a promising alternate avenue for MSCs.

### 3.2. Graphene-based composites and heterostructure

As discussed, the accessibility of electrolyte ions through all graphene layers is the key to improving the overall performance of MSCs. The performance of planar MSCs can be further enhanced by the addition of electroactive components as spacers, including carbon nanotubes (CNTs), electrically conductive polymers and nanostructured metal oxides between the graphene layers.<sup>[134]</sup> Assisting by the electroactive components, the agglomeration of the graphene sheets could be avoided, hence enhancing the accessible surface area of the electrode material, aiming at an overall improved electrochemical performance.<sup>[135, 136]</sup>

#### 3.2.1. Graphene/CNTs

Wang and co-worker's developed a binder-free RGO/CNT hybrid interdigitated microelectrodes with the width of  $100 \mu\text{m}$  and the interspace  $50 \mu\text{m}$  through electrostatic spray deposition (ESD) and photolithography methods (**Figure 14**).<sup>[36]</sup> As mentioned before, the accessible surface area for effective diffusion of electrolyte ions was enlarged by CNT. The interdigitated MSC demonstrated an energy density of  $0.68 \text{ mW h cm}^{-3}$  with a power density of  $77 \text{ W cm}^{-3}$ , which is superior to that of MSCs made from individual RGO or CNTs. By optimising both the material design and fabrication step, using CNTs as spacers to enhance the active material/ electrolyte interface area, the obtained MSC shows superior performance to conventional designs.

Ultrafast charge transport pathways and low interfacial resistance between the electrodes and current collectors are two factors to increase the frequency response of MSCs. For this purpose, a 3D graphene-CNT carpet (G-CNTC) based hybrid MSC on nickel substrate was reported by Lin et al. by introducing vertically aligned CNT on few-layer graphene.<sup>[137]</sup> At a frequency of 120 Hz, the fabricated G-CNTC-MSCs demonstrated an impedance phase angle of  $-81.5^\circ$ . Thanks to the advanced structure, the as-obtained device exhibited a remarkable power density of  $115 \text{ W cm}^{-3}$  with the energy density of  $2.42 \text{ m Wh cm}^{-3}$  in ionic liquid electrolyte (1 M BMIM-BF<sub>4</sub>).

Similarly, X. Mao successfully designed a multi wall carbon nanotube (MWCNT)/ graphene electrode as shown in **Figure 15**.<sup>[138]</sup> MWCNT was firstly oxidized to o-MWCNT with H<sub>2</sub>SO<sub>4</sub> and HNO<sub>3</sub>. Then o-MWCNT was mixed with GO under ultrasonic to form a homogeneous solution and sprayed onto PET substrate. After dried, laser treating was applied to reduce the GO into RGO and the electrode pattern was printed either. PVA/ H<sub>3</sub>PO<sub>4</sub> gel electrolyte was prepared for electrolyte. The fabricated MSCs presented an outstanding specific capacitance, energy density and power density as high as  $46.6 \text{ F cm}^{-3}$ ,  $6.47 \text{ mW h cm}^{-3}$  and  $10 \text{ mW cm}^{-3}$  at a current density of  $20 \text{ mA cm}^{-3}$ , and excellent cycling reliability.

In addition, a highly stretchable tandem MSC based on graphene/carbon nanotube/cross-linked PH1000 film (GCP) is reported lately by H. Xiao et al. as shown in **Figure 16**.<sup>[139]</sup> Firstly the exfoliated graphene (EG), carbon nanotube (CNT) and cross-linked PH1000 were mixed in ethanol/ DI water, following by vacuum filtration through a PTFE membrane. Then H<sub>2</sub>SO<sub>4</sub> was deposited on each side with the assistance of the interdigitated mask. After that, the film was transferred to the surface of a 230% pre-stretched rubber substrate, which was brushed with PVA aqueous solution. Finally, the GCP-based MSC is fabricated. The device showed specific capacitances of  $15.2 \text{ mF cm}^{-2}$  at  $500 \text{ mV s}^{-1}$  and  $4.4 \text{ mF cm}^{-2}$  at a high scan rate of  $2 \text{ V s}^{-1}$ . Also, even with 200% strain rate, the MSC device still shows similar performance, comparing with 0% strain rate. Moreover, after 2000 cycles test for each strain

states repeated from 200% to 0%, the MSC still had impressive cycle stability of 93.2% initial capacitance retention rate.

### 3.2.2. Graphene/Conducting polymers

The addition of pseudo-capacitive materials to graphene electrodes has also been shown as an effective option to provide extra capacitance, originating from Faradaic redox reactions which take place at the electrode-electrolyte interface. Recently, a micromolding with capillary method to form patterned RGO microelectrodes with vertically aligned PANI nanorod arrays was reported by Xue et al.<sup>[140]</sup> Under the current density of  $2.5 \text{ A g}^{-1}$ , the RGO/PANI delivered the gravimetric capacitance of  $937 \text{ F g}^{-1}$ . The reversible nature of the redox transitions was indicated by cyclic voltammetry, and the authors reported that the charge transfer efficiency was tunable by adjusting the density and dimensions of the PANI rod arrays.

The homogeneous dispersion of the active materials or their precursors is critical for devising thin-film MSCs based on graphene. Song et al. developed a RGO/sulfonated PANI (RG/SP)-based electrode, prepared via spin-coating onto a flexible Kapton tape.<sup>[91]</sup> Mask -assisted oxygen plasma etching was introduced to form the patterns with the gold current collector. Thanks to the strong  $\pi$ - $\pi$  interaction between RGO and SPANI, the SPANI intercalates uniformly into graphene layers. Because of the unique nanostructure and excellent conductivity of the thin film, the as-obtained device presented a high volumetric capacitance of  $16.55 \text{ F cm}^{-3}$ , referring to the energy density of  $1.51 \text{ mW h cm}^{-3}$  in  $\text{H}_2\text{SO}_4/\text{PVA}$  gel electrolyte. Apart from this, the volume expansion during redox reactions can be prevented by the SPANI in the robust graphene network, resulting in good cycling performance (85.4% capacitance retained after 10000 cycles).

To further improve the performance, it's essential to explore the pseudocapacitive layer to the electrolyte. In this regard, X. Tian et al designed a holey-graphene/ PANI composite as electrode of MSC as shown in **Figure 17a**. The GO suspension was obtained via a modified Hummers' method and diluted. Then 70% concentrated HNO<sub>3</sub> solution was added and mixed with stirring as well as sonication to synthesize holey-graphene. Later, the photoresist material was spin-coated on the SiO<sub>2</sub> substrate. After baking, the interdigital patterns and Ti/Au current collectors are produced using lithography and physical vapour deposition. As next step, the holey-GO was deposited on the current collector and reduced. Finally, PANI was electro-polymerized on the holey-graphene intermediate layer, so that the ions from the electrolyte can diffuse to the inter PANI layer, resulting in superior performance.<sup>[141]</sup>

Oppositely, mesoporous PANI was introduced into graphene/PANI system by Z. Liu et al as shown in **Figure 17b**.<sup>[142]</sup> 1-pyrenesulfonic acid sodium salt (PSA) functionalized exfoliated graphene (EG) was fabricated first. Then amphiphilic block copolymer polystyrene-b-poly(ethylene oxide) (PS<sub>146</sub>-b-PEO<sub>117</sub>) mono-micelles were prepared and introduced onto the surface of the as-prepared EG. Later, mesoporous PANI (mPANI) was formed on both sides of the EG. At last, the PS<sub>146</sub>-b-PEO<sub>117</sub> templates were removed and EG-mPANI was obtained. The combination of electron-double-layer capacitive graphene and pseudocapacitive mesoporous-PANI resulted in an impressive performance and high power density of up to 600 W cm<sup>-3</sup>, as described by the authors.

Additionally, poly pyrrole is also a part of graphene/ conducting polymers (mPPy@RGO-POM, mPGM). Template-based mesoporous poly pyrrole-graphene sheet MSC was reported by J. Qin et al, as presented in **Figure 17c**.<sup>[143]</sup> The obtained mPGM-MSC, containing a combination of mPPy@RGO-POM and EG nanosheets, delivered a specific capacitance of 115 mF cm<sup>-2</sup>, with excellent mechanical flexibility, and excellent integration capabilities.

### 3.2.3. Graphene/Metal oxide

As pseudocapacitive materials, transition metal oxides can also be used in MSCs.<sup>[37]</sup> As reported by Peng et al., a MnO<sub>2</sub>/graphene integrated electrode-based all-solid-state MSC demonstrated a gravimetric capacitance of 267 F g<sup>-1</sup> under the current density of 0.2 A g<sup>-1</sup> and also stable cycling performance (92 % capacitance retained after 7000 cycles) (Figure 18).<sup>[144]</sup> In the design of this hybrid thin -film system, the integration of MnO<sub>2</sub> with graphene provided extra active surfaces as well as created more interface paths between graphene sheets, facilitating charge transport.

To enhance the performance of graphene/MnO<sub>2</sub> electrodes, silver nanowires were introduced by W. Liu et al as shown in Figure 19. The graphene/ MnO<sub>2</sub>/Ag-nanowire film was prepared by the vacuum filtration of GMA suspension and transferred to the ammonia substrate first. With thin gold layer thermally evaporated onto the surface of the film assisted by a mask, the pattern was created by oxygen plasma etching. After being annealed, the MSC was assembled and demonstrated a specific energy densities of 2.3 mW h cm<sup>-3</sup> with a power density of 162.0 mW cm<sup>-3</sup> in an ionic liquid gel electrolyte.<sup>[145]</sup>

With similar purpose, P. Hu put forward an RGO/MnO<sub>2</sub> wire-in-scroll electrode design.<sup>[40]</sup> As the ion can only diffuse through the gap between graphene layer and MnO<sub>2</sub> nanowire as shown in Figure 20a, porous graphene (pGO)/MnO<sub>2</sub> nanowire was developed to shorten the ion diffusion path. Under a scan rate of 20 mV/s, the device based on MnO<sub>2</sub>/pGO presented a 4 -fold improvement in capacitance as compared to the MnO<sub>2</sub>/RGO nanowire device. Plus, the capacitance contribution was calculated under various scan rates as presented in Figure 20c. The result indicated that the rate performance was seriously limited by ion diffusion step and explained the outstanding rate capability of the MnO<sub>2</sub>/ pGO design.

Additionally, MnO<sub>2</sub> was replaced by Fe<sub>2</sub>O<sub>3</sub> in the work from S. Gu et al.<sup>[146]</sup> Firstly, the graphene oxide solution was mixed with FeCl<sub>3</sub> under ultrasonic. Following by hydrothermal

1 treatment, the resulting graphene/Fe<sub>2</sub>O<sub>3</sub> product was filtered and washed. During MSC  
2 assembly step, PVA/KOH gel electrolyte was used. The fabricated device delivered a specific  
3 capacitance of 11.57 F cm<sup>-3</sup> at a high scan rate of 200mV s<sup>-1</sup>.  
4  
5  
6  
7  
8

#### 9 3.2.4 Graphene/Phosphorene 10

11  
12 In spite of those traditional pseudocapacitive components, a recently discovered 2-  
13 dimensional compound, phosphorene, was mixed with graphene working as electrode for  
14 MSCs by H. Xiao et al..<sup>[147]</sup> The graphene/phosphorene film was prepared via a two-step  
15 vacuum filtration method. Then the pattern of the electrode was etching by plasma. To avoid  
16 the irreversible reaction of phosphorene with moisture, an ionic liquid was used as electrolyte.  
17 The device showed advantages of not only outstanding flexibility and wide potential range of  
18 3V, but also output impressive areal capacitance of 9.8 mF cm<sup>-2</sup> at a scan rate of 5 mV s<sup>-1</sup>, as  
19 shown in **Figure 21**.  
20  
21  
22  
23  
24  
25  
26  
27  
28  
29  
30  
31  
32  
33  
34  
35  
36  
37  
38  
39  
40  
41  
42  
43  
44  
45

### 46 3.3 Graphene-based asymmetric MSCs 47

48  
49 Asymmetric supercapacitors have recently been proposed, aiming to expand the voltage  
50 window and enhance the energy density with the combination of both EDLC and  
51 pseudocapacitive materials.<sup>[148]</sup> Some typical hybrid MSCs will be discussed in this section.  
52  
53  
54  
55  
56  
57  
58  
59  
60  
61  
62  
63  
64  
65

### 3.3.1 Graphene // MXene hybrid device

Albeit one of the most recently discovered family of 2-dimensional materials, MXenes have been widely applied as electrodes for supercapacitors over the last years. C. Couly et al introduced MXene ( $\text{Ti}_3\text{C}_2\text{T}_x$ ) into the graphene-based flexible interdigitated asymmetric MSC as presented in **Figure 22**.<sup>[149]</sup> To obtain such a device, ink-like MXene and RGO suspension were prepared separately first. Then the material was applied via spray coating using a Kapton mask, to produce the finger electrodes. And PVA/ $\text{H}_2\text{SO}_4$  gel electrolyte was used during MSC assembly. The optimal and SEM images of RGO//MXene MSC were shown in **Figure 22a-d**. The inter-finger spacing is 400  $\mu\text{m}$  and a finger width is 900  $\mu\text{m}$ , while the thickness is around 300 nm. **Figure 22e, f** showed the superior flexibility of the MSC. Moreover, comparing with the all MXene based MSCs, the asymmetric design had a wider voltage window of 1V. The MXene//graphene MSC exhibited an energy density of 8.6  $\text{mW h cm}^{-3}$  at a power density of 0.2  $\text{W cm}^{-3}$ .

### 3.3.2 Graphene//Metallic compounds

To enhance the energy density of the device, introducing pseudocapacitive materials into the system, e.g. metal oxide, is a common method.<sup>[125]</sup> Also, despite of 2-dimensionsal materials, the use of traditional carbon materials in MSCs is also widely studied.<sup>[150-152]</sup> D. Yu et al developed an N-doped RGO/single-walled nanotube (SWCNT)// $\text{MnO}_2$ -coated RGO/SWCNT asymmetric micro supercapacitor as shown in **Figure 23a**.<sup>[153]</sup> The SWCNT shows high electronic conductivity but limited surface absorption area, but the RGO shows significantly larger surface area but worse electronic conductivity. Combining both the advantages of these two carbon materials, and also enhancing the electrode performance through coating the pseudocapacitive  $\text{MnO}_2$  layer on the surface or doping nitrogen atom into graphene, the

asymmetric MSC delivered a high volumetric energy density of  $5 \text{ mWh cm}^{-3}$ . Moreover, the device was used to power a ZnO based UV photodetector in this study.

Nevertheless, the GQDs//MnO<sub>2</sub> nano-needle -based MSC designed by Liu et al. delivered an energy density twice as high as that of GQD-based symmetric MSCs.<sup>[125]</sup>

In addition, an all-solid-state asymmetric MSC on a polyimide flexible substrate based on a two-step deposition laser-induced graphene (LIG) and metal oxide/hydroxide has been reported by Li et al.<sup>[37]</sup> In this work, LIG-FeOOH and LIG-MnO<sub>2</sub> were used as negative and positive electrodes, respectively. The asymmetric device demonstrated a capacitance of  $5.4 \text{ F cm}^{-3}$  in LiCl/PVA gel electrolyte with a working voltage of  $1.8 \text{ V}$ , along with good cycling and mechanical stability.

To meet the demand of high performance MSCs, S. Zheng developed a printable MSC based on all-in-one monolithic stacked--layer MnO<sub>2</sub>/poly (3,4-ethylenedioxythiophene) poly (styrene sulfonate) nanosheets as positive electrode, exfoliated graphene (EG) as negative electrode and boron nitride nanosheets as separator, PVA/LiCl gel as electrolyte. Such a fabrication (**Figure 24**) has a wide operational voltage window of  $1.8 \text{ V}$  and comparative volumetric energy density of  $8.6 \text{ mW h cm}^{-3}$  as well as flexibility.<sup>[154]</sup>

Additionally, MoS<sub>2</sub>, another functional material in supercapacitors, can also be applied onto graphene-based MSCs. H. Pan reported a bio-inspired MoS<sub>2</sub>/ graphene-based nanofiber application in asymmetric MSC.<sup>[155]</sup> As shown in **Figure 25 a, b and g**, the bio-inspired fibre was prepared via a fabrication sequence including centrifugation, prototyping, oxygen plasma treatment, spinning and carbonization. The MSC was assembled with RGO-CNC and RGO-MoS<sub>2</sub> as electrodes and PVA/H<sub>3</sub>PO<sub>4</sub> gel electrolyte. The microfibers showed an ultrahigh conductivity ( $3.12 \times 10^4 \text{ S m}^{-1}$  for RGO-CNC and  $3.27 \times 10^4 \text{ S m}^{-1}$  for RGO-MoS<sub>2</sub>), which is superior to other RGO-based fibres.<sup>[156-158]</sup> Besides, the asymmetric MSC had a wide voltage window up to  $1.5 \text{ V}$ . With the nanofiber structure, which enhances the power density and the assistance of carbon/ MoS<sub>2</sub>, which improves the energy density, the fabricated device

showed both excellent power/ energy performance, with a specific energy density of  $\sim 100 \mu\text{W h cm}^{-2}$  and a power density of  $\sim 102 \text{ mW h cm}^{-2}$ .

### 3.4 Role of hydrated Graphene oxide (h-GO)

Although graphene oxide usually works as the precursor of RGO in the development of graphene-based MSC, the hydrated GO can be a part of electrolyte or membrane as reported previously.<sup>[55, 157, 159-162]</sup>

M. F. El-Kady et al reported a design of GO-membrane based on-chip MSC with electrolyte over-coating as shown in **Figure 26**.<sup>[157]</sup> Prepared with a modified Hummer's method first, GO was dispersed into aqueous suspension. Meanwhile, a PET layer was attached onto the surface of a DVD disc. Then the GO solution was dropped onto the PET surface and dried. The laser subscribed graphene (LSG) pattern was reduced with a computer optical drive as shown in **Figure 26a**. The optical image of the LSG electrode and the GO membrane under a microscope was presented in **Figure 26b**, whereas the black side is LSG and the golden part is GO. Also, in the SEM image of GO/LSG interface, it's clear that the GO and LSG are well contacted. The electronic conductivity of GO and LSG was tested and compared, which indicated that GO layer could play the role of membrane with low conductivity. With electrolyte over-coating, the obtained MSC delivered a volumetric capacitance of  $2.35 \text{ F cm}^{-3}$  under a current density of  $16.8 \text{ mA cm}^{-3}$ . Even when being charged/ discharged with a high current density of  $1.84 \times 10^4 \text{ mA cm}^{-3}$ , the device retained a capacitance of  $1.40 \text{ F cm}^{-3}$ , as described by the authors.

Additionally, two works focus on planar sandwich structure MSC are also worth mentioning.

S. Zheng et al compared the performance of exfoliated graphene (EG)-based MSCs with

(denoted as PG-PSSs) / without (denoted as PG-CSSs) NGO (nanosized graphene oxide) as separator as shown in **Figure 27a-c**.<sup>[162]</sup> The EG and NGO layers were prepared via a simple spray method. PVA/H<sub>2</sub>SO<sub>4</sub> gel electrolyte was used in MSC assembly process. From the data presented in **Figure 27e-h**, the NGO contained MSC, with a specific capacitance of 94 F cm<sup>-3</sup>, which showed better performance than the PG-CSSs. The enhanced capacitance was attributed by the authors to the synergetic effect of the electric field and the charged NGO sheets, assisting the H<sup>+</sup> and H<sub>3</sub>O<sup>+</sup> diffusion through the sandwiched EG layers.<sup>[161]</sup>

To further investigate the function of GO especially hydrated GO in the graphene-based MSCs, Y. Gao et al designed three different graphene-based capacitors, including graphene//graphene, hydrated graphene oxide//hydrated graphene oxide and hydrated graphene oxide//graphene as shown in **Figure 28a-d**.<sup>[55]</sup> Considering charge distribution ( $\rho$ ) and atomic density inside the gaps between GO and RGO layers and their dependence on several factors including electric field ( $E_0$ ), gap spacing ( $d_0$ ), functional groups (-O and -OH) on the graphene, the amount of water molecules, and defects, the charge storage mechanism in the hydrated GO contained system can be referred to the polarized water molecules, which shows the same conclusion of S. Zheng's work. Besides, the authors also called for the interdigitated or scrolled design for the RGO-GO-RGO MSC design, which would enhance the capacitance couple times, comparing the sandwich structure in their work.

Apart from these functions, Wang et al. for the first time proposed to assemble a water-dielectric capacitor by using the h-GO membrane in which the graphene oxide sheets shield the water intercalate from being leached with metal ions.<sup>[163]</sup> Wang proposed a new mechanism that utilized the dielectric property of two-dimensional confined water layer as the man-sized dielectric for capacitors. In this work, the voltage stability window of h-GO film was determined on stainless steel electrodes. It was found that the h-GO could be reduced at voltages above 3V. In fact, most of the papers that used h-GO as solid electrolyte cannot exceed 1V voltage. This work also correlated the capacitive behaviour with the de-hydrated

GO films showing the dependence of capacitive and resistive currents on the water content. The optimized h-GO film exhibited areal capacitances ranging from 100 to 800  $\mu\text{F cm}^{-2}$  as a function of the applied voltage, which was 5 to 40 times higher than the double layer capacitance of activated carbon, as shown in **Figure 29**.

#### 4. Fabrication of Graphene-based planar interdigitated MSCs

Graphene with different qualities and in different quantities have been prepared through chemical vapour deposition (CVD),<sup>[164-167]</sup> chemical exfoliation,<sup>[168-170]</sup> micromechanical cleavage,<sup>[118]</sup> bottom-up organic synthesis,<sup>[171]</sup> electrochemical exfoliation,<sup>[172]</sup> and epitaxial growth.<sup>[173, 174]</sup> It also successfully applied in dye-sensitized solar cells,<sup>[175]</sup> catalysts,<sup>[176]</sup> sensors,<sup>[177]</sup> electronics,<sup>[178]</sup> field emission,<sup>[179]</sup> polymer hybrids,<sup>[180]</sup> batteries<sup>[181, 182]</sup> and supercapacitors.<sup>[183, 184]</sup>

Planar MSCs is capable of fabrication of electrodes and integration into miniaturized electronic devices on the same plane. In MSCs, internal resistance can be further decreased reducing the space between neighbouring interdigitated electrodes.<sup>[185]</sup>

In 2003, the first prototype planar MSC was reported by Sung et al..<sup>[186]</sup> They fabricated interdigitated conducting polymer based MSC by using conventional photolithography and electrochemical polymerization methods. Initially, platinum or gold micro-electrode array was prepared on a silicon substrate by using photolithography followed by wet etching method. After that, poly-(3-phenylthiophene) (PPT) and polypyrrole (PPy) were deposited on the microelectrodes through electrochemical polymerization. The conducting polymer interdigitated MSCs contains 50 parallel microelectrodes where the distance between the electrodes and width are of 50  $\mu\text{m}$ . The conducting polymer (PPy or PPT) interdigitated MSC delivered the cell capacitance of 14 mF at the cell potential between 0.6 and 1.4V with organic electrolyte.

However, in practical applications, the possibility of leakage of liquid electrolytes must be considered to construct devices. Thus, solid materials are required to develop all-solid-state MSCs. Sung et al. successfully implemented an all-solid-state MSC on SiO<sub>2</sub>/Si using a new gel-polymer electrolyte, to avoid material leakage.<sup>[187]</sup> Subsequently, the same group designed and fabricated flexible all-solid-state MSCs in 2006, using a PVA/H<sub>3</sub>PO<sub>4</sub> gel electrolyte layer as the substrate and using electrochemical polymerization of PPy on microelectrode arrays. The resulting MSC is uniquely composed of polymeric materials, which is flexible, small and lightweight. The device can be bent and rolled-up without with good reliability.

Further device miniaturization accompanied by a route towards large-scale fabrication is essential for MSCs. Larger-scale fabrication of graphene-based MSCs has been explored by several groups either using photolithography or a direct writing technique, or a combination of both. Besides, some other techniques are developed recently.

#### 4.1 Photolithographic process

To achieve the goals of high efficiency, low cost, tunable reduction degree, flexible patterning, and superior integration of graphene-based micro devices, UV irradiation with various catalysts, e.g. TiO<sub>2</sub>, ZnO, WO<sub>3</sub> and H<sub>3</sub>PWO<sub>40</sub>,<sup>[164, 188-191]</sup> to photo chemically reduce GO, comes into MSCs application. Wang and co-worker's established a photocatalytic strategy to produce GO-TiO<sub>2</sub> hybrid films for high-performance graphene-based MSCs.<sup>[192]</sup> They used a photomask-assisted photo-reduction to pattern the GO-TiO<sub>2</sub> film under UV at room temperature. Remarkably, the MSC exhibited high specific capacitance of 233.0 F cm<sup>-3</sup> in PVA/H<sub>2</sub>SO<sub>4</sub> with exceptional flexibility. The obtained MSC also demonstrated a volumetric energy density of 7.7 mW h cm<sup>-3</sup> with a power density of 312 W cm<sup>-3</sup>. More importantly, the device showed outstanding cyclability that no capacitance loss after 10000 cycles.

Another simple, fast and low cost photonic reduction method was designed by S. H. Kang et al as shown in **Figure 30c-d**.<sup>[41]</sup> Once coated on the PET film, the GO solution was dried. A stainless steel mask was then used to generate interdigitated patterns. Comparing with those UV-reduction processes, the exposure time of this method can be as short as few milliseconds. And the condition of the reduced electrode can be optimized by the voltage, pulse width, exposure energy, as well as exposure time of the lamp, accordingly. Gel electrolyte PVA/H<sub>2</sub>SO<sub>4</sub> was also use in this case. The MSC exhibited high specific capacitance of 36.90 mF cm<sup>-2</sup> using a current of 0.2 mA cm<sup>-2</sup>.

## 4.2 Laser writing

Compared to photolithographic processes, direct laser writing of MSCs provides a less-process intensive fabrication and more versatile route, although limited by its serial writing mode.<sup>[193, 194]</sup> Some parameters, including laser power and scanning speed, would have influence on the performance of the resulted RGO, e.g. electronic conductivity.<sup>[195]</sup> In this regard, El-Kady and Kaner reported planar MSCs by a relatively fast direct laser writing on GO films using a LightScribe DVD burner.<sup>[28]</sup> Their fabrication process is described in **Figure 31**. A graphene interdigitated capacitor pattern is obtained by selectively reducing a GO film coated onto a DVD disc, leading to thin and flexible devices. They have used a hydrogel-polymer electrolyte (H<sub>2</sub>SO<sub>4</sub>/PVA) as well as a ionic liquid-based gel electroly and demonstrated a working voltage up to 2.5 V, with a power density of around 200 W cm<sup>-3</sup>.

Gao et al. described a versatile approach to MSC fabrication, still based on direct laser writing on the GO films to form graphene electrodes, but where GO is also used as an electrolyte and separator.<sup>[196]</sup> The GO near the surfaces is reduced by the laser, so that sandwiched RGO–GO–RGO patterns are obtained to form a planar MSC with excellent electrochemical performance.

Xie et al. have also fabricated flexible laser-processed graphene (LPG) based MSCs through tuning the output laser power, the reduction and patterning of LPG electrode arrays.<sup>[197]</sup> The LPG-MSCs showed excellent rate performance, high specific energy density of 0.98 mW h cm<sup>-3</sup> in LiCl-PVA electrolyte and 5.7 mW h cm<sup>-3</sup> in ionic electrolyte. The LPG-MSCs also presented superior cycling stability and 93 % of capacitance still retained after 20000 cycles.

To simplify the electrode preparation procedure and enhance the performance, a one-step RGO/ gold current collector synthesis method was reported by R. Z. Li et al as presented in **Figure 32**.<sup>[198]</sup> The aqueous GO dispersion was prepared and mixed with HAuCl<sub>4</sub>. After that, being spread onto a photo paper, the mixture was dried under room temperature. The laser beam was introduced into an upright microscope system and conducted onto the hybrid GO film (**Figure 32a-b**). The scanning speed was provided by a computer-controlled 2-axis motorized platform. The unreacted HAuCl<sub>4</sub> was removed by DI water rinsing (**Figure 32c**). Finally, the MSC was assembled with PVA/ H<sub>2</sub>SO<sub>4</sub> as electrolyte (**Figure 32e**). This novel strategy led to two orders of magnitude increase in electrode conductivities, providing excellent rate capability, and areal capacitances of 0.46 mF cm<sup>-2</sup> at a scan rate of 100V s<sup>-1</sup>.

Shen et al have proposed a combination of direct writing and controllable microdroplet transfer method shown in **Figure 33**.<sup>[199]</sup> The GO suspension was first prepared and being drop casted onto the SiO<sub>2</sub> substrate forming a continuous GO-film. Then laser was applied to reduce the GO with prograded pattern. After that, a PVA/H<sub>2</sub>SO<sub>4</sub> gel electrolyte -coated glass was placed above the as-prepared RGO electrodes. The fs laser pulses were focused through the glass onto the gel layer to generate single microdrops containing electrolyte. The device delivered a specific capacitance of 2.14 mF cm<sup>-2</sup> at 5 mA cm<sup>-2</sup> and 78% of capacitance maintained when being operated at an ultrahigh current density of 50 mA cm<sup>-2</sup>. The accessibility of the inter surface of fsRGO to the electrolyte results in very little impediment to ion transport.

### 4.3 Focused ion beam

It is also worth mentioning that Lobo and co-workers have developed a focused ion beam (FIB) technology to pattern RGO with 1  $\mu\text{m}$  spacing,<sup>[200]</sup> as shown in **Figure 34**. **The technique reduces GO via exposure to an ion beam.** In addition to the advanced capabilities for miniaturization given by this approach, the authors have indicated that the small electrode spacing can alter the ionic diffusion kinetics such to obtain superior frequency response. The FIB-RGO MSC had a high capacitance of 102  $\text{mF cm}^{-2}$ , and a stable cyclability at an ultra-large current density of 45  $\text{mA cm}^{-2}$ .

### 4.4 Printing

The as-mentioned MSCs fabrication techniques show difficulties in large scale commercial applications. Therefore, to overcome this drawback, direct printing techniques, including spray deposition and inkjet printing, which offer a promising protocol for future roll-to-roll production of MSC arrays, are widely developed.<sup>[201]</sup> In this section, we would like to talk about some advanced printing technologies.

#### 4.4.1 *Spraying, Ink-jet printing, Screen printing and 3D printing*

S. S. Delekta et al introduced a highly transparent and flexible graphene-based MSC using a direct inkjet printing method.<sup>[202]</sup> As presented in **Figure 35a-f**, a large-area and uniform thin film of graphene flakes was firstly printed on the glass substrate, and then an interdigitated hard mask was printed with silver ink in the inner region of the graphene film. After that, the whole structure was subsequently etched using  $\text{O}_2$  plasma and the uncovered graphene was removed. Lately, the silver mask was also removed with  $\text{HNO}_3$  solution. The PVA/ $\text{H}_3\text{PO}_4$  gel

electrolyte was deposited when assembling the MSC. The thickness and the transmittance of the electrode can be tuned by the amount of spraying solution. This MSC exhibited remarkable performance versus transparency (ranging from a single-electrode areal capacitance of  $16 \mu\text{F cm}^{-2}$  at transmittance of 90% to a capacitance of  $99 \mu\text{F cm}^{-2}$  at transmittance of 71%), which provides the possibility to work as the energy storage system of the solar cell or being applied onto wearable devices.

In contrast to the inkjet printing and dry etching method, J. Li reported a mask-assisted full inkjet-printed MSCs fabrication strategy (**Figure 35g-h**).<sup>[203]</sup> Firstly, the electrochemically exfoliated graphene (EEG) was prepared and dispersed in DMF. Later, the EEG-ink was formulated with the centrifugation-assisted solvent exchange technique. On the other hand, the polyelectrolyte, poly (4-styrenesulfonic acid) (PSSH), was synthesized. Then the MSCs arrays were printed in 3 steps: EEG printing, EEG annealing, and PSSH electrolyte printing using a commercial piezoelectric Dimatix Materials printer. The fully printed graphene-based MSC output the highest areal capacitance of  $0.7 \text{ mF/cm}^2$ . When more than 100 devices were connected to form large-scale MSC arrays, it could be charged to 12V with 8 months retention.

Z. Liu and colleagues fabricated planar MSCs using a patterned-mask assisted spraying method. The electrochemically exfoliated graphene solution was printed onto the paper substrate via spray gun to form a homogeneous thin-film. The as-prepared MSC with PVA/H<sub>2</sub>SO<sub>4</sub> gel-electrolyte achieved a volumetric capacitance of  $800 \mu\text{F cm}^{-2}$  under a scan rate of  $1 \text{ mV s}^{-1}$ .<sup>[201]</sup>

In addition, screen printing, a photolithographic and chemical etching steps free method, is also used for MSCs electrode patterning.<sup>[204]</sup> Woo Jin Hyun and co-workers reported a high resolution screen printing method in preparing graphene-based MSC, shown in **Figure 36**.<sup>[205]</sup> A thin silicon stencil is first prepared via photolithography and reactive ion etching, as described in **Figure.36a**. Later, the stencil is applied onto the polyimide substrate using

spacers and the graphene structures are then printed using a high -definition squeegee. The thickness of the graphene lines is controlled by the thickness of the spacer, while the width is adjustable by applying graphene inks with different viscosities.

In addition to the 2-dimensional printing above, Z. Wang et al successfully introduced 3D printing technique into the graphene-based MSCs fabrication as shown in **Figure 37**.<sup>[206]</sup> Firstly, GO dispersion was mixed with PANI-NMP solution to form GO/ PANI gel. Then the gel was filled in a syringe and the extrusion pressure was provided by an air-powered fluid dispenser. The gel was deposited on a 3-dimensional moving substrate, software-controlled to obtain the desired shape (**Figure 37a-b**). Also, PVA/H<sub>2</sub>SO<sub>4</sub> gel electrolyte was printed in the gap between the electrode fingers. The prepared device demonstrated a high areal capacitance of 1.255 F cm<sup>-2</sup> at a current density of 4.2 mA cm<sup>-2</sup>. And the capacitance retention rate was around 75% after 1000 cycles under the current density of 50mA cm<sup>-2</sup> (**Figure 37c-f**).

#### 4.4.2 Gravure printing and Stamping

Hard-printing/ stamping and gravure, typically roll-to-roll, have been also pursued as a method for graphene -based electrode preparation. W. J Hyun combined the stamping method with a Xenon lamp reduction technique to obtain the patterned graphene-based MSCs as shown in **Figure 38a-e**.<sup>[207]</sup> The polydimethylsiloxane (PDMS) stamp was first fabricated onto a pre-treated Si wafer: a mixture of PDMS monomer and its curing agent was poured onto the master mold and cured in an oven. The PDMS stamp was peeled off and post cured in an oven. Then a UV-curable polymer was poured on a PET film that was plasma-treated and pressed by the PDMS stamp. After the polymer being exposed to the UV light for a constant time, the stamp was removed. The as-prepared GO ink was inkjet-printed onto the holder and exposed to the Xenon lamp for reduction. Later, ion gel was also inkjet-printed

onto the electrolyte receiver to assemble the MSCs. The obtained device exhibited a specific capacitance of  $268 \mu\text{F cm}^{-2}$  at a CV scan rate of  $10 \text{ mV s}^{-1}$ .

Meanwhile, rotary gravure printing has also been used to fabricate MSCs. Ethan et al. have developed a gravure printing method using a flooding-doctoring-printing approach for large-area fabrication of graphene-based flexible electronics, as shown in **Figure 39**.<sup>[208]</sup> Firstly, in flooding step, the gravure printing cell is filled with graphene-ink. In the doctoring step, the extra ink on the surface is removed. Finally, the ink is transferred (printing step). The resolution of the graphene line is determined by the size of the cell.

Similarly, an advanced mask-less, photoresist-free technology for patterning graphene based on roll-based manufacturing technique was reported by S. Kim et al.<sup>[209]</sup> Firstly, graphene was grown onto Cu substrate using the CVD method. Then the highly durable Ni stamps were used to pattern the graphene at room temperature using a roll-to-plate transfer machine. Later, a carrier film was attached to the patterned CVD graphene and the Cu foil was removed by etching in ammonium persulfate (APS) solution. Finally, the patterned graphene was transferred to the target substrate. PVA/  $\text{H}_2\text{SO}_4$  gel electrolyte was added as electrolyte by drop-casting method in this MSC. The area-specific capacitance value was  $5.0 \mu\text{F cm}^{-2}$  (at a scan rate of  $0.05 \text{ V s}^{-1}$ ). This novel technique provides a viable roll-based technology for patterning CVD graphene, which was one of the most challenging issues in the roll-to-roll manufacturing of graphene electrodes.

## 5. Summary and Perspectives

The main aim for planar MSCs is their miniaturization and integration with functional devices within a microsystem in an efficient and manufacturable fashion, while maximizing their areal energy, power density and life span to meet the energy consumption requirements of microelectronic devices. Planar, interdigitated MSCs have seen an accelerated recent

development (**Figure 40**). A summary of the current best electrochemical performances from the literature of graphene-based MSCs is provided in Table 1. Note that since the device data is related to a range of various supercapacitor geometries, thicknesses, and is often reported using different specific metrics of performance and cyclability, clear-cut comparisons are generally challenging. Overall, as the comparison of performance in Ragone plot indicates in **Figure 41**, advanced graphene-based planar MSCs exhibit superior power performance accompanied by energy densities competitive with commercial lithium thin-film batteries. It is important to note that as the lab-fabricated MSCs may not be fully packaged as the commercial devices, the volume of package may be excluded in the calculation of energy/power density in literatures. According to Gogotsi and Simon, the volumetric density of a well-packed carbon-based device would be just around 1/5 of the electrode-based density.<sup>[210]</sup> Nevertheless, even taking into consideration a package correction factor of 20%, graphene-based MSCs are still competitive with commercial lithium thin-film battery under high current density thanks to their extraordinary rate performance. MSCs are particularly suitable for fast and repetitive charging/discharging at large currents, while such an operation could damage micro-batteries.

We have already discussed how benefits of a planar interdigitated electrode design result in a simplified integration of MSCs into miniaturized systems. Additionally, interdigital electrodes with microscale gap sizes dramatically decrease the ionic diffusion distance, leading to improved electrochemical performance including higher charge-discharge rates and frequency response as compared to sandwich-type supercapacitors.<sup>[211]</sup> We also remind that Lobo et al.<sup>[200]</sup> assessed interdigitated MSCs with electrode spacing of only 1  $\mu\text{m}$ , delivering an extraordinarily high areal capacitance of 102  $\text{mF cm}^{-2}$ . In interdigitated MSCs, the width and number of electrode fingers are another important factor to increase the overall performance. For example, Mullen et al have compared the performance of different numbers of electrode fingers maintaining the same total surface for their MSCs on a silicon substrate.<sup>[119]</sup> The

performance was found to greatly improve as the number of the finger electrodes increased while the finger width and gap were scaled down to occupy the same area. Such results are encouraging, as they all indicate that smaller geometries and feature sizes tend to improve electrochemical performance. The optimization of geometric parameters has hence an influence on the final performance that goes beyond the purely geometric capacitance to include enhanced ionic and electronic transport phenomena, which is of great interest for miniaturisation.

In addition, the porous electrode approach shows ultra-excellent performance due to the shorter ion diffusion path and high specific area, e.g. the porous graphene film reported by X. Yun showed a high energy density of  $1.45 \text{ mWh cm}^{-3}$  at the current density of  $0.6 \text{ mA cm}^{-2}$ , which is superior other non-porous graphene-based MSCs, accordingly.<sup>[57]</sup> The engineering of porosity in the electrode material could be therefore an important enhancement going forward. However, as discussed in section 2, BET may not be an appropriate method to access the porosity and pore size in thin films.<sup>[68]</sup> The latter characteristics are crucial when optimizing the performance of MSCs, since the choice of electrolytes need to be tailored to the porous structure of the electrodes for maximum performance and efficiency.<sup>[212-216]</sup>

In terms of specific electrode material, we note that reduced graphene oxide (RGO) is by far the most common type of graphene used in highly-performant MSCs, likely due to its ease of synthesis, including in large quantities, ease of patterning through selective reduction through either direct writing or photolithography, low-cost and good electrochemical performance.<sup>[217]</sup> Graphene-based composite materials, especially those with heterostructure, such as graphene/carbon, a combination of two EDLC type materials which expand the gap between RGO sheets and enlarge the surface area between active materials and electrolyte shows both higher capacitance and faster ion diffusion rate, comparing with bulk graphene/ RGO. Apart from RGO/ MWCNT based MSC reported by X. Mao et al.,<sup>[138]</sup> carbide derived carbon (CDC) is also reported as a function of nano-spacer between RGO sheets in SCs application

by M. Alhabeb et al.<sup>[218]</sup> The as-reported RGO/ CDC free standing film was prepared via vacuum filtration method and exhibited superior capacitance of  $200 \text{ F g}^{-1}$  at a high scan rate of  $100 \text{ mV s}^{-1}$  as well as 94% capacitance retention rate after 10000 cycles at  $10 \text{ A g}^{-1}$ . Such a hybrid electrode may be fabricated in the MSCs with mask-assisted method or laser scribing techniques. Additionally, onion-like carbon, reported by D. Petch et al.,<sup>[219]</sup> with a diameter of 6-7 nm and was able to be cycled under a high scan rate of  $200 \text{ V s}^{-1}$ , also shows the possibility to play the role of nano-spacer in graphene-based MSC electrodes. Therefore, the design of carbon-based, nano-spacer-pillared 2-D structural graphene film would be able to push the development of next generation high performance graphene-based planar interdigitated MSCs. The particle size, surface area, power/ energy density and cycle stability are some critical parameters in nano-spacer selection.

Another type of hetero-structured graphene-based material, combining the EDLC type graphene/ RGO and pseudocapacitive materials, e.g. graphene/conducting polymers and graphene/metal oxides, has also been explored for implementation in MSCs to enhance the energy density. Except the examples listed in this review, there are also some graphene-based hybrid electrodes applied in SCs, showing the potential to be introduced into MSCs. X. Xu reported a 3-D RGO/metal organic framework (MOF) derived composite aerogel based flexible all-solid-state SC with a high areal capacitance of  $250 \text{ mF cm}^{-3}$  at  $6.4 \text{ mA cm}^{-3}$  and a capacity retention of 96.3% after 5000 cycles at  $50.4 \text{ mA cm}^{-3}$  as well as superior flexibility.<sup>[220]</sup> Such a material design provides a new possible strategy for introducing various metal oxides into graphene-based MSCs.

Notably, for those graphene and pseudocapacitive material hybrid electrodes, it is significant to expose the intermedia electrochemical active layer to the electrolyte as shown in the design of holey-graphene/PANI and holey-PANI/ graphene and etc..<sup>[141, 142]</sup> Or the power density of the electrode would be significantly limited as the ions could only diffuse to the active material surface through the gap between two layers. Therefore, there is still a long road and

potential towards the selection of composite electrodes, optimization of structure designs and fabrication methods for the development of graphene/pseudocapacitive material hybrid electrodes based MSCs.

Additionally, to further improve the energy density of the MSCs, asymmetric fabrication, which could widen the operational voltage window, would be a promising option. Some asymmetric designs, including graphene//Mxene and graphene//MoS<sub>2</sub>, are discussed in section 4. Other electroactive materials, e.g. the newly reported tungstate acid-link polyaniline,<sup>[221]</sup> which exhibit high areal capacitance and high cut-off voltage, are also potential candidates in high performance graphene-based asymmetric MSCs.

In spite of these, the possible application of hydrated GO would be one of the direction of graphene-based MSCs development. Recently, the capacitance enhancement function of hydrated GO in RGO-based MSCs was reported and the concept of polarized water molecule was introduced as the possible mechanism. With the increasing electric field, the intercalation water molecule rotate from the randomly distribution to the status with positive charged hydrogen atoms heading the negative electrode and negative charged oxygen atoms facing positive electrode. The ordered water molecular in the GO layer stores energy under the effect of electric field.<sup>[55, 157, 162]</sup> However, a detailed understanding, including of the relationship between the amount of water molecule intercalation and the capacitance enhancement, is still to be obtained. Besides, is it possible to design an electrolyte-free hydrated-GO planar graphene-based MSC? Could the hydrated-GO be applied to asymmetric designs? Also, are there any other solvents that would have a comparable behaviour when intercalated into the GO layer? There is still plenty of understanding to be pursued regarding hydrated-GO.

Going beyond the usual metrics, the possibility for a high-voltage window is an additional desirable parameter for MSCs in some of the integrated applications, such as sensors and actuators.<sup>[222]</sup> To improve the voltage output in device level, Shi et al. fabricated a new class of planar graphene-based linear tandem MSCs (LTMSs) on various substrates with both

symmetric and asymmetric configuration.<sup>[223]</sup> Graphene-based LTMSs contains 10 MSCs, which presented high-voltage window of 8.0 V. The areal capacitance of LTMSs can be further improved up to 7.6  $\mu\text{F cm}^{-2}$  by the combining polyaniline-based pseudo-capacitive material into the graphene electrodes.

Finally, Xiao et al reported a novel design of highly stretchable graphene-based interconnected tandem MSC as mentioned in section 3. With three serially-interconnected single cells, the voltage can be extended to 2.4V, comparing with 0.8V of the single cell.<sup>[139]</sup>

Further improvements in MSCs will draw from a plethora of very different fundamental and technical domains. Firstly, the fundamental understanding of the complex relationships among the architecture, the electrolyte ion transport, the electrical transport in the electrode material and capacitive performance is a still a very open research question encompassing mechanisms from the nano to the micro and macro-scale which will be key to advancing the design of high-performance and reliable graphene-based MSCs. Further findings in this area will determine among others future geometries of planar interdigitated MSCs with improved energy and power densities.

From a specific electrode material point of view, future research in the graphene-based MSCs will likely emphasize graphenic material designed to get a larger and more readily-accessible specific surface area, including 3D structures and holey hetero-structural composites, with a controlled porosity and defective structure. The fundamental understanding of physical and chemical defects and their role in the electrochemical performance will be key for further advances.<sup>[123]</sup> An important challenge to be addressed in this regard is the unambiguous benchmarking and adequate/quantifiable characterisation of the material system, including its porous volume structure. This may be a particularly challenging task for planar/thin-film electrodes. As mentioned, there is a whole body of literature about characterisation of thin film porosity available from microelectronics research that may be useful in this respect.<sup>[68]</sup>

1 Finally, another key area mature for further development is the integrability of the  
2 supercapacitors, focusing on electrode manufacturing technologies which can realize large-  
3  
4 scale production of planar interdigitated electrodes on arbitrary substrates. While there  
5  
6 appears to be plenty of approaches on flexible substrates (most of the examples in Table 1),  
7  
8 there are only few options that are compatible with semiconductor technologies.<sup>[39]</sup>  
9  
10

11 In this paper, we have reviewed the advances and breadth of designs and approaches for the  
12  
13 exploitation of graphenic material in electrodes for planar interdigitated MSCs. The usual  
14  
15 metrics for benchmarking planar supercapacitors are their energy and power densities,  
16  
17 particularly in terms of their specific areal densities, their cyclability, and their integrability in  
18  
19 a microsystem. Those parameters are determined by the often combined effect of electrode  
20  
21 and electrolyte properties, adopted geometries and architectures, and their fabrication methods.  
22  
23 Because of those combined effects, the ability of making direct comparisons among the  
24  
25 literature results is usually constrained. Also, important properties such as current leakage,  
26  
27 output window, coulombic efficiency, mechanical stability and cycle life, etc., are often  
28  
29 overlooked or not reported using comparable protocols.  
30  
31  
32  
33  
34  
35

36 Nevertheless, the recent body of literature indicates that, thanks to its 2D and highly  
37  
38 conductive nature, graphene demonstrates superior versatility and compatibility for  
39  
40 integration on both rigid and flexible planar substrates, which is of great promise for  
41  
42 integrated power sources for example in a wide variety of sensors for the Internet of  
43  
44 Everything. A wide range of graphene-based MSCs have been reported with high energy and  
45  
46 power densities by using vastly different fabrication processes, some of which are extremely  
47  
48 promising, and we have here grouped and compared in an extensive table.  
49  
50  
51  
52

53 In spite of recent advances, research and development of graphene-based MSCs is still at an  
54  
55 immature stage and has a vast scope for further advances, from the understanding of  
56  
57 fundamental electrochemistry and transport mechanisms to the more technological fabrication  
58  
59 and integration aspects. In addition, graphene's 2D nature also poses some limitations as to  
60  
61  
62  
63  
64  
65

the optimization of the accessible surface area of the electrodes, co-tailoring electrode porosity and electrolyte ions, and certainly the next few years will show more advances in this respect.

To achieve high-performance graphene-based MSCs it is indispensable to optimize thin-film fabrication and characterisation techniques, microelectrode design, active electrode materials (including porosity and defect engineering), and selection of the electrolytes and interfacial integrity of the key components. On the other hand, graphene offers undisputed advantages in terms of high conductivity, robustness and ultimate miniaturisation thanks to its 2D nature. In addition, graphene and graphenic materials are relatively low-cost and they can be synthesized, patterned, functionalized and engineered through a plethora of fabrication techniques, covering from small to large-area, from flexible to rigid substrates.

As their energy densities trend is catching up with thin-film batteries, we believe that further advances of graphene-based MSCs may greatly contribute to small-scale energy storage devices in the future, for both silicon and organic-based semiconductor microsystems. Cooperative interdisciplinary research is mandatory to achieve the full integration of MSCs with energy harvesters and other microelectronic components. Such advances towards truly autonomous systems could underpin a self-powered and sustainable Internet of Everything.

## Acknowledgements

D.Wang acknowledges the support by the Australian Research Council Discovery through the project DP160103244. F.Iacopi would like to acknowledge the financial support by the AFOSR through the Grant No. AOARD 17IOA027, as well as the support by the Australian National Fabrication Facility (ANFF).

Received: ((will be filled in by the editorial staff))  
 Revised: ((will be filled in by the editorial staff))  
 Published online: ((will be filled in by the editorial staff))

## References

1. Simon P, Gogotsi Y. Materials for electrochemical capacitors. *Nat. Mater.* 2008;7:845.
2. Miller JR, Simon P. Electrochemical capacitors for energy management. *Science Magazine.* 2008;321(5889):651-2.
3. Liu C, Li F, Ma LP, Cheng HM. Advanced materials for energy storage. *Adv. Mater.* 2010;22(8).
4. Simon P, Gogotsi Y, Dunn B. Where do batteries end and supercapacitors begin? *Science.* 2014;343(6176):1210-1.
5. Wang Y, Xia Y. Recent progress in supercapacitors: from materials design to system construction. *Adv. Mater.* 2013;25(37):5336-42.
6. Frackowiak E, Beguin F. Carbon materials for the electrochemical storage of energy in capacitors. *Carbon.* 2001;39(6):937-50.
7. Han Y, Lai Z, Wang Z, Yu M, Tong Y, Lu X. Designing Carbon Based Supercapacitors with High Energy Density: A Summary of Recent Progress. *Chem. Eur. J.* 2018.
8. Wang F, Wu X, Yuan X, Liu Z, Zhang Y, Fu L, et al. Latest advances in supercapacitors: from new electrode materials to novel device designs. *Chem Soc Rev.* 2017;46(22):6816-54.
9. Lee J, Yoon S, Hyeon T, Oh SM, Kim KB. Synthesis of a new mesoporous carbon and its application to electrochemical double-layer capacitors. *Chem. Commun.* 1999(21):2177-8.
10. Miller JR, Outlaw RA, Holloway BC. Graphene double-layer capacitor with ac line-filtering performance. *Science.* 2010;329(5999):1637-9.
11. Wang R, Wang S, Jin D, Zhang Y, Cai Y, Ma J, Zhang L. Engineering layer structure of MoS<sub>2</sub>-graphene composites with robust and fast lithium storage for high-performance Li-ion capacitors. *Energy Storage Materials.* 2017;9:195-205.

12. Song MY, Kim NR, Yoon HJ, Cho SY, Jin HJ, Yun YS. Long-Lasting Nb<sub>2</sub>O<sub>5</sub>-Based Nanocomposite Materials for Li-Ion Storage. *ACS Appl. Mater. Interfaces*. 2017;9(3):2267-74.
13. Wang ZL. Toward self-powered sensor networks. *Nano Today*. 2010;5(6):512-4.
14. Wang ZL. Self - powered nanosensors and nanosystems. *Adv. Mater.* 2012;24(2):280-5.
15. Saadon S, Sidek O. Micro-electro-mechanical system (MEMS)-based piezoelectric energy harvester for ambient vibrations. *Procedia-Social and Behavioral Sciences*. 2015;195:2353-62.
16. Wang ZL, Wu W. Nanotechnology-enabled energy harvesting for self-powered micro- / nanosystems. *Angew. Chem., Int. Ed.* 2012;51(47):11700-21.
17. Beidaghi M, Gogotsi Y. Capacitive energy storage in micro-scale devices: recent advances in design and fabrication of micro-supercapacitors. *Energy Environ. Sci.* 2014;7(3):867.
18. Arthur TS, Bates DJ, Cirigliano N, Johnson DC, Malati P, Mosby JM, Perre E, Rawls MT, Prieto AL, Duun B. Three-dimensional electrodes and battery architectures. *Mrs Bulletin*. 2011;36(7):523-31.
19. Wu ZS, Parvez K, Feng X, Müllen K. Graphene-based in-plane micro-supercapacitors with high power and energy densities. *Nat. Commun.* 2013;4.
20. Chmiola J, Largeot C, Taberna P-L, Simon P, Gogotsi Y. Monolithic carbide-derived carbon films for micro-supercapacitors. *Science*. 2010;328(5977):480-3.
21. Shen C, Xu S, Xie Y, Sanghadasa M, Wang X, Lin L. A Review of On-Chip Micro Supercapacitors for Integrated Self-Powering Systems. *J. Microelectromech. Syst.* 2017;26(5):949-65.
22. Aradilla D, Gentile P, Bidan G, Ruiz V, Gómez-Romero P, Schubert TJ, Sahin H, Frackowiak E, Sadki S. High performance of symmetric micro-supercapacitors based on

silicon nanowires using N-methyl-N-propylpyrrolidinium bis (trifluoromethylsulfonyl) imide as electrolyte. *Nano Energy*. 2014;9:273-81.

23. Zheng B, Huang T, Kou L, Zhao X, Gopalsamy K, Gao C. Graphene fiber-based asymmetric micro-supercapacitors. *J. Mater. Chem. A*. 2014;2(25):9736-43.
24. Yu D, Goh K, Zhang Q, Wei L, Wang H, Jiang W, Chen Y. Controlled Functionalization of Carbonaceous Fibers for Asymmetric Solid - State Micro - Supercapacitors with High Volumetric Energy Density. *Adv. Mater.* 2014;26(39):6790-7.
25. Meng C, Maeng J, John SW, Irazoqui PP. Ultrasmall Integrated 3D Micro - Supercapacitors Solve Energy Storage for Miniature Devices. *Adv. Energy Mater.* 2014;4(7).
26. Kim SK, Koo HJ, Lee A, Braun PV. Selective Wetting - Induced Micro - Electrode Patterning for Flexible Micro - Supercapacitors. *Adv. Mater.* 2014;26(30):5108-12.
27. Wu Z-S, Feng X, Cheng H-M. Recent advances in graphene-based planar micro-supercapacitors for on-chip energy storage. *Natl. Sci. Rev.* 2014;1(2):277-92.
28. El-Kady MF, Kaner RB. Scalable fabrication of high-power graphene micro-supercapacitors for flexible and on-chip energy storage. *Nat. Commun.* 2013;4:1475.
29. Gu S, Lou Z, Li L, Chen Z, Ma X, Shen G. Fabrication of flexible reduced graphene oxide/Fe<sub>2</sub>O<sub>3</sub> hollow nanospheres based on-chip micro-supercapacitors for integrated photodetecting applications. *Nano Res.* 2016;9(2):424-34.
30. Huang P, Pech D, Lin R, McDonough JK, Brunet M, Taberna P-L, et al. On-chip micro-supercapacitors for operation in a wide temperature range. *Electrochem. Commun.* 2013;36:53-6.
31. Yoo JJ, Balakrishnan K, Huang J, Meunier V, Sumpter BG, Srivastava A, et al. Ultrathin planar graphene supercapacitors. *Nano Lett.* 2011;11(4):1423-7.

32. Reina A, Jia X, Ho J, Nezich D, Son H, Bulovic V, Dresselhaus MS, Kong J. Large area, few-layer graphene films on arbitrary substrates by chemical vapor deposition. *Nano Lett.* 2008;9(1):30-5.
33. Dreyer DR, Park S, Bielawski CW, Ruoff RS. The chemistry of graphene oxide. *Chem. Soc. Rev.* 2010;39(1):228-40.
34. Lu X, Li L, Song B, Moon K-s, Hu N, Liao G, Shi T, Wong C. Mechanistic investigation of the graphene functionalization using p-phenylenediamine and its application for supercapacitors. *Nano Energy.* 2015;17:160-70.
35. Pei S, Cheng H-M. The reduction of graphene oxide. *Carbon.* 2012;50(9):3210-28.
36. Beidaghi M, Wang C. Micro - supercapacitors based on interdigital electrodes of reduced graphene oxide and carbon nanotube composites with ultrahigh power handling performance. *Adv. Funct. Mater.* 2012;22(21):4501-10.
37. Li L, Zhang J, Peng Z, Li Y, Gao C, Ji Y, Ye R, Kim N, Zhong Q, Yang Y, Fei H, Ruan G, Tour JM. High - Performance Pseudocapacitive Microsupercapacitors from Laser - Induced Graphene. *Adv. Mater.* 2016;28(5):838-45.
38. Pech D, Brunet M, Durou H, Huang P, Mochalin V, Gogotsi Y, Taberna P.L, Simon P. Ultrahigh-power micrometre-sized supercapacitors based on onion-like carbon. *Nat. Nanotechnol.* 2010;5(9):651-4.
39. Wang B, Ahmed M, Wood B, Iacopi F. All-solid-state supercapacitors on silicon using graphene from silicon carbide. *Appl. Phys. Lett.* 2016;108(18):183903.
40. Hu P, Yan M, Wang X, Han C, He L, Wei X, Niu C, Zhao K, Tian X, Wei Q, Li Z, Mai L. Single-Nanowire Electrochemical Probe Detection for Internally Optimized Mechanism of Porous Graphene in Electrochemical Devices. *Nano Lett.* 2016;16(3):1523-9.

41. Kang SH, Kim IG, Kim B-N, Sul JH, Kim YS, You I-K. Facile Fabrication of Flexible In-Plane Graphene Micro-Supercapacitor via Flash Reduction. *ETRI Journal*. 2018;40(2):275-82.
42. Iacopi F, Mishra N, Cunnning BV, Goding D, Dimitrijevic S, Brock R, Reinhold H. D, Barry W, John B. A catalytic alloy approach for graphene on epitaxial SiC on silicon wafers. *J. Mater. Res.* 2015;30(5):609-16.
43. Pandolfo A, Hollenkamp A. Carbon properties and their role in supercapacitors. *J. Power Sources*. 2006;157(1):11-27.
44. Ghosh A, Lee YH. Carbon - based electrochemical capacitors. *ChemSusChem*. 2012;5(3):480-99.
45. Simon P, Gogotsi Y. Materials for electrochemical capacitors. *Nat. Mater.* 2008;7(11):845-54.
46. Dai L, Chang DW, Baek JB, Lu W. Carbon nanomaterials for advanced energy conversion and storage. *small*. 2012;8(8):1130-66.
47. Futaba DN, Hata K, Yamada T, Hiraoka T, Hayamizu Y, Kakudate Y, Tanaike O, Hatori H, Yumura M, Iijima S. Shape-engineerable and highly densely packed single-walled carbon nanotubes and their application as super-capacitor electrodes. *Nat. Mater.* 2006;5(12):987.
48. Yoo JJ, Balakrishnan K, Huang J, Meunier V, Sumpter BG, Srivastava A, Conway M, Reddy. A. L, Yu. J, Vajtai, R, Ajayan. P. M. Ultrathin planar graphene supercapacitors. *Nano Lett.* 2011;11(4):1423-7.
49. Simon P, Gogotsi Y. Capacitive energy storage in nanostructured carbon–electrolyte systems. *Acc. Chem. Res.* 2012;46(5):1094-103.

50. Chmiola J, Yushin G, Gogotsi Y, Portet C, Simon P, Taberna P-L. Anomalous increase in carbon capacitance at pore sizes less than 1 nanometer. *Science*. 2006;313(5794):1760-3.
51. Liu NS, Gao YH. Recent Progress in Micro-Supercapacitors with In-Plane Interdigital Electrode Architecture. *Small*. 2017;13(45).
52. Kotz R, Carlen M. Principles and applications of electrochemical capacitors. *Electrochim. Acta*. 2000;45(15-16):2483-98.
53. Shen CW, Wang XH, Zhang WF, Kang FY. A high-performance three-dimensional micro supercapacitor based on self-supporting composite materials. *J Power Sources*. 2011;196(23):10465-71.
54. Liu L, Niu Z, Chen J. Design and integration of flexible planar micro-supercapacitors. *Nano Res*. 2017;10(5):1524-44.
55. Gao Y, Wan YY, Wei BQ, Xia ZH. Capacitive Enhancement Mechanisms and Design Principles of High-Performance Graphene Oxide-Based All-Solid-State Supercapacitors. *Adv Funct Mater*. 2018;28(17):1706721.
56. Liu P, Jin Z, Katsukis G, Draushuk LW, Shimizu S, Shih CJ, Wetzel, E. D, Taggart-Scarff. J. K, Qing. B, Van Vliet. K. J, Li. R, Wardle. B. L, Strano. M. S. Layered and scrolled nanocomposites with aligned semi-infinite graphene inclusions at the platelet limit. *Science*. 2016;353(6297):364-7.
57. Yun XW, Xiong ZY, Tu L, Bai LQ, Wang XG. Hierarchical porous graphene film: An ideal material for laser-carving fabrication of flexible micro-supercapacitors with high specific capacitance. *Carbon*. 2017;125:308-17.
58. Long JW, Dunn B, Rolison DR, White HS. Three-dimensional battery architectures. *Chem. Rev*. 2004;104(10):4463-92.

59. Long JW, Rolison DR. Architectural design, interior decoration, and three-dimensional plumbing en route to multifunctional nanoarchitectures. *Acc. Chem. Res.* 2007;40(9):854-62.
60. Rolison DR, Long JW, Lytle JC, Fischer AE, Rhodes CP, McEvoy TM, Bourg ME, Lubers AM. Multifunctional 3D nanoarchitectures for energy storage and conversion. *Chem. Soc. Rev.* 2009;38(1):226-52.
61. Hammock ML, Chortos A, Tee BCK, Tok JBH, Bao Z. 25th anniversary article: the evolution of electronic skin (e - skin): a brief history, design considerations, and recent progress. *Adv. Mater.* 2013;25(42):5997-6038.
62. Wang X, Lu X, Liu B, Chen D, Tong Y, Shen G. Flexible Energy - Storage Devices: Design Consideration and Recent Progress. *Adv. Mater.* 2014;26(28):4763-82.
63. Wang X, Shi G. Flexible graphene devices related to energy conversion and storage. *Energy Environ. Sci.* 2015;8(3):790-823.
64. Shao Y, El-Kady MF, Wang LJ, Zhang Q, Li Y, Wang H, Mousavi MF, Kaner RB. Graphene-based materials for flexible supercapacitors. *Chem. Soc. Rev.* 2015;44(11):3639-65.
65. Niu Z, Liu L, Zhang L, Zhou W, Chen X, Xie S. Programmable Nanocarbon - Based Architectures for Flexible Supercapacitors. *Adv. Energy Mater.* 2015;5(23).
66. Gogotsi Y, Simon P. True performance metrics in electrochemical energy storage. *Science.* 2011;334(6058):917-8.
67. Toupin M, Brousse T, Bélanger D. Charge storage mechanism of MnO<sub>2</sub> electrode used in aqueous electrochemical capacitor. *Chem. Mater.* 2004;16(16):3184-90.
68. Maex K, Baklanov MR, Shamiryan D, Iacopi F, Brongersma SH, Yanovitskaya ZS. Low dielectric constant materials for microelectronics. *J. Appl. Phys.* 2003;93(11):8793-841.

69.     Gidley DW, Frieze WE, Dull TL, Sun J, Yee AF, Nguyen CV, Yoon DY.  
Determination of pore-size distribution in low-dielectric thin films. *Appl Phys Lett*.  
2000;76(10):1282-4.
70.     Raccichini R, Varzi A, Passerini S, Scrosati B. The role of graphene for  
electrochemical energy storage. *Nat. Mater*. 2015;14(3):271-9.
71.     Petkov MP, Weer MH, Lynn KG, Rodbell KP, Cohen SA. Doppler broadening  
positron annihilation spectroscopy: A technique for measuring open-volume defects in  
silsesquioxane spin-on glass films. *Appl Phys Lett*. 1999;74(15):2146-8.
72.     Wu WL, Wallace WE, Lin EK, Lynn GW, Glinka CJ, Ryan ET, Ho HM. Properties of  
nanoporous silica thin films determined by high-resolution x-ray reflectivity and small-angle  
neutron scattering. *J. Appl. Phys*. 2000;87(3):1193-200.
73.     S. Kawamura TO, K. Omote, Y. Ito, R. Suzuki, and T. Ohdara, editor New  
measurement technique of pore size distribution of porous low-k film. *Proceeding IITC'2001*;  
2001.
74.     Dultsev FN, Baklanov MR. Nondestructive determination of pore size distribution in  
thin films deposited on solid substrates. *Electrochem Solid St*. 1999;2(4):192-4.
75.     Baklanov MR, Mogilnikov KP, Polovinkin VG, Dultsev FN. Determination of pore  
size distribution in thin films by ellipsometric porosimetry. *J Vac Sci Technol B*.  
2000;18(3):1385-91.
76.     Baklanov MR, Mogilnikov KP. Characterization of porous dielectric films by  
ellipsometric porosimetry. *Opt Appl*. 2000;30(4):491-6.
77.     C.Wongmanerod SZ, H.Arwin. Determination of pore size distribution and surface  
area of thin porous silicon layers by spectroscopic ellipsometry. *Appl. Surf. Sci*.  
2001;172:117-25.
78.     D. W. Gidley WEF, T. L. Dull, J. N. Sun, and A. F. Yee. Probing Pore Characteristics  
in Low-K Thin Films Using Positronium Annihilation Lifetime Spectroscopy. *Mater*

Res Soc Symp Proc. 2000;612.

79. Sun JN, Gidley DW, Dull TL, Frieze WE, Yee AF, Ryan ET, Lin S, Wetzel J. Probing diffusion barrier integrity on porous silica low-k thin films using positron annihilation lifetime spectroscopy. *J. Appl. Phys.* 2001;89(9):5138-44.
80. Petkov MP, Weber MH, Lynn KG, Rodbell KP. Porosity characterization by beam-based three-photon positron annihilation spectroscopy. *Appl Phys Lett.* 2001;79(23):3884-6.
81. Tang X, Xiong B, Li Q, Mao W, Xiao W, Fang P, He C. Development of pore interconnectivity/morphology in porous silica films investigated by cyclic voltammetry and slow positron annihilation spectroscopy. *Electrochim. Acta.* 2015;168:365-9.
82. Leyva-García S, Lozano-Castelló D, Morallón E, Cazorla-Amorós D. Silica-templated ordered mesoporous carbon thin films as electrodes for micro-capacitors. *J. Mater. Chem. A.* 2016;4(12):4570-9.
83. Ramsay JDF. Characterization of the pore structure of membranes. *Mrs Bull.* 1999;24(3):36-40.
84. Prehal C, Koczwar C, Jäckel N, Schreiber A, Burian M, Amenitsch H, Hartmann MA, Presser V, Paris O. Quantification of ion confinement and desolvation in nanoporous carbon supercapacitors with modelling and in situ X-ray scattering. *Nat. Energy.* 2017;2:16215.
85. Dubinin MMar, L.V., editor *Equation of the Characteristic Curve of Activated Charcoal.* the Academy of Sciences of the USSR; 1947.
86. Kozbial A, Li Z, Sun J, Gong X, Zhou F, Wang Y, Xu H, Liu H, Li L. Understanding the intrinsic water wettability of graphite. *Carbon.* 2014;74:218-25.
87. Mitchell JB, Lo WC, Genc A, LeBeau J, Augustyn V. Transition from Battery to Pseudocapacitor Behavior via Structural Water in Tungsten Oxide. *Chem. Mater.* 2017;29(9):3928-37.

88. Miller JR, Burke AF. Electrochemical capacitors: challenges and opportunities for real-world applications. *Electrochem. Soc. Interface*. 2008;17(1):53.
89. Hsia B, Marschewski J, Wang S, In JB, Carraro C, Poulidakos D, Grigoropoulos CP, Maboudian R. Highly flexible, all solid-state micro-supercapacitors from vertically aligned carbon nanotubes. *Nanotechnology*. 2014;25(5):055401.
90. Niu Z, Zhang L, Liu L, Zhu B, Dong H, Chen X. All - solid - state flexible ultrathin micro - supercapacitors based on graphene. *Adv. Mater.* 2013;25(29):4035-42.
91. Song B, Li L, Lin Z, Wu Z-K, Moon K-s, Wong C-P. Water-dispersible graphene/polyaniline composites for flexible micro-supercapacitors with high energy densities. *Nano Energy*. 2015;16:470-8.
92. Shen C, Wang X, Li S, Zhang W, Kang F. A high-energy-density micro supercapacitor of asymmetric MnO<sub>2</sub>-carbon configuration by using micro-fabrication technologies. *J. Power Sources*. 2013;234:302-9.
93. Ivanovskii AL. Graphene-based and graphene-like materials. *Russian Chem. Rev.* 2012;81(7):571.
94. Wang G, Zhang L, Zhang J. A review of electrode materials for electrochemical supercapacitors. *Chem Soc Rev*. 2012;41(2):797-828.
95. Makino S, Yamauchi Y, Sugimoto W. Synthesis of electro-deposited ordered mesoporous RuO<sub>x</sub> using lyotropic liquid crystal and application toward micro-supercapacitors. *J Power Sources*. 2013;227:153-60.
96. Nagar B, Dubal DP, Pires L, Merkoci A, Gomez-Romero P. Design and Fabrication of Printed Paper-Based Hybrid Micro-Supercapacitor by using Graphene and Redox-Active Electrolyte. *ChemSusChem*. 2018;11(11):1849-56.
97. Pandolfo AG, Hollenkamp AF. Carbon properties and their role in supercapacitors. *J Power Sources*. 2006;157(1):11-27.

98. Qi D, Liu Y, Liu Z, Zhang L, Chen X. Design of Architectures and Materials in In-Plane Micro-supercapacitors: Current Status and Future Challenges. *Adv Mater.* 2017;29(5).
99. Huang P, Heon M, Pech D, Brunet M, Taberna P-L, Gogotsi Y, Lofland S, Hettinger JD, Simon P. Micro-supercapacitors from carbide derived carbon (CDC) films on silicon chips. *J Power Sources.* 2013;225:240-4.
100. Huang P, Lethien C, Pinaud S, Brousse K, Laloo R, Turq V, Respaud, M. Demortiere A, Daffos B, Taberna P. L, Chaudret B. Gogotsi Y. Simon P. On-chip and freestanding elastic carbon films for micro-supercapacitors. *Science.* 2016;351(6274):691-5.
101. Lahiri A, Endres F. Review—Electrodeposition of Nanostructured Materials from Aqueous, Organic and Ionic Liquid Electrolytes for Li-Ion and Na-Ion Batteries: A Comparative Review. *J. Electrochem. Soc.* 2017;164(9):D597-D612.
102. Eustache E, Douard C, Demortière A, De Andrade V, Brachet M, Le Bideau J, Brousse T, Lethien C. High Areal Energy 3D-Interdigitated Micro-Supercapacitors in Aqueous and Ionic Liquid Electrolytes. *Adv. Mater Technologies.* 2017;2(10):1700126.
103. Meng C, Liu C, Fan S. Flexible carbon nanotube/polyaniline paper-like films and their enhanced electrochemical properties. *Electrochem. Commun.* 2009;11(1):186-9.
104. Meng C, Liu C, Chen L, Hu C, Fan S. Highly flexible and all-solid-state paperlike polymer supercapacitors. *Nano Lett.* 2010;10(10):4025-31.
105. Manuel Stephan A. Review on gel polymer electrolytes for lithium batteries. *Eur. Polym. J.* 2006;42(1):21-42.
106. Morita M, Qiao J-L, Yoshimoto N, Ishikawa M. Application of proton conducting polymeric electrolytes to electrochemical capacitors. *Electrochim. Acta.* 2004;50(2-3):837-41.
107. In JB, Hsia B, Yoo J-H, Hyun S, Carraro C, Maboudian R, Grigoropoulos CP. Facile fabrication of flexible all solid-state micro-supercapacitor by direct laser writing of porous carbon in polyimide. *Carbon.* 2015;83:144-51.

108. Kai W, Wenjun Z, Baogang Q, Aifang Y, Haiping W, Peng J, Zhixiang W. An All-Solid-State Flexible Micro-supercapacitor on a Chip. *Adv. Energy Mater.* 2011;1(6):1068-72.
109. Yang P, Xiao X, Li Y, Ding Y, Qiang P, Tan X, Mai W, Lin Z, Wu W, Li T, Jin H, Liu P, Zhou J, Wong C. P, Wang Z. L. Hydrogenated ZnO core-shell nanocables for flexible supercapacitors and self-powered systems. *ACS Nano.* 2013;7(3):2617-26.
110. Hashmi SA, Suematsu S, Naoi K. All solid-state redox supercapacitors based on supramolecular 1,5-diaminoanthraquinone oligomeric electrode and polymeric electrolytes. *J Power Sources.* 2004;137(1):145-51.
111. Ma G, Dong M, Sun K, Feng E, Peng H, Lei Z. A redox mediator doped gel polymer as an electrolyte and separator for a high performance solid state supercapacitor. *J. Mater. Chem. A.* 2015;3(7):4035-41.
112. Prajapati GK, Roshan R, Gupta PN. Effect of plasticizer on ionic transport and dielectric properties of PVA–H<sub>3</sub>PO<sub>4</sub> proton conducting polymeric electrolytes. *J. Phys. Chem. Solids.* 2010;71(12):1717-23.
113. Wang S, Hsia B, Carraro C, Maboudian R. High-performance all solid-state micro-supercapacitor based on patterned photoresist-derived porous carbon electrodes and an ionogel electrolyte. *J. Mater. Chem. A.* 2014;2(21):7997-8002.
114. Feng J, Sun X, Wu C, Peng L, Lin C, Hu S, Yang J, Xie Y. Metallic few-layered VS<sub>2</sub> ultrathin nanosheets: high two-dimensional conductivity for in-plane supercapacitors. *J Am Chem Soc.* 2011;133(44):17832-8.
115. Zhang L, DeArmond D, Alvarez NT, Malik R, Oslin N, McConnell C, Adusei P, K Hsieh Y. Y, Shanov V. Flexible Micro-Supercapacitor Based on Graphene with 3D Structure. *Small.* 2017;13(10).

116. Durou H, Pech D, Colin D, Simon P, Taberna P-L, Brunet M. Wafer-level fabrication process for fully encapsulated micro-supercapacitors with high specific energy. *Microsyst. Technol.* 2012;18(4):467-73.
117. Jiang Y, Zhou Q, Lin L, editors. *IEEE 22nd International Conference on Micro Electro Mechanical Systems. MEMS*; 2009.
118. Novoselov KS, Geim AK, Morozov SV, Jiang D, Zhang Y, Dubonos SV, Grigorieva IV, Firsov AA. Electric field effect in atomically thin carbon films. *Science*. 2004;306(5696):666-9.
119. Wu Z-S, Parvez K, Feng X, Müllen K. Photolithographic fabrication of high-performance all-solid-state graphene-based planar micro-supercapacitors with different interdigital fingers. *J. Mater. Chem. A*. 2014;2(22):8288-93.
120. Xiong G, Meng C, Reifengerger RG, Irazoqui PP, Fisher TS. Graphitic Petal Micro-Supercapacitor Electrodes for Ultra-High Power Density. *Energy Technol.* 2014;2(11):897-905.
121. Wu Z-S, Yang S, Zhang L, Wagner JB, Feng X, Müllen K. Binder-free activated graphene compact films for all-solid-state micro-supercapacitors with high areal and volumetric capacitances. *Energy Storage Materials*. 2015;1:119-26.
122. Cunnig BV, Ahmed M, Mishra N, Kermany AR, Wood B, Iacopi F. Graphitized silicon carbide microbeams: wafer-level, self-aligned graphene on silicon wafers. *Nanotechnology*. 2014;25(32):325301.
123. Ahmed M, Wang B, Gupta B, Boeckl JJ, Motta N, Iacopi F. On-Silicon Supercapacitors with Enhanced Storage Performance. *J. Electrochem. Soc.* 2017;164(4):A638-A44.
124. Zhang Z, Zhang J, Chen N, Qu L. Graphene quantum dots: an emerging material for energy-related applications and beyond. *Energy Environ. Sci.* 2012;5(10):8869-90.

125. Liu WW, Feng YQ, Yan XB, Chen JT, Xue QJ. Superior Micro - Supercapacitors Based on Graphene Quantum Dots. *Adv. Funct. Mater.* 2013;23(33):4111-22.
126. Xie H, Tang S, Li D, Vongehr S, Meng X. Flexible Asymmetric Supercapacitors Based on Nitrogen-Doped Graphene Hydrogels with Embedded Nickel Hydroxide Nanoplates. *ChemSusChem.* 2017;10(10):2301-8.
127. Santhosh R, Raman SRS, Krishna SM, Ravuri Ss, Sandhya V, Ghosh S, Sahu NK, Punniyakoti S, Karthik M, Kollu P, Jeong SK, Grace AN. Heteroatom doped graphene based hybrid electrode materials for supercapacitor applications. *Electrochim. Acta.* 2018;276:284-92.
128. Xia K, Huang Z, Zheng L, Han B, Gao Q, Zhou C, Wang J, Wu J. Facile and controllable synthesis of N/P co-doped graphene for high-performance supercapacitors. *J Power Sources.* 2017;365:380-8.
129. Islam MM, Subramaniam CM, Akhter T, Faisal SN, Minett AI, Liu HK, Konstantinov K, Dou SX. Three dimensional cellular architecture of sulfur doped graphene: self-standing electrode for flexible supercapacitors, lithium ion and sodium ion batteries. *J Mater. Chem. A.* 2017;5(11):5290-302.
130. Wu Z-S, Tan Y-Z, Zheng S, Wang S, Parvez K, Qin J, Shi X, Sun C, Bao X, Feng X, Müllen K. Bottom-Up Fabrication of Sulfur-Doped Graphene Films Derived from Sulfur-Annulated Nanographene for Ultrahigh Volumetric Capacitance Micro-Supercapacitors. *J. Am. Chem. Soc.* 2017;139(12):4506-12.
131. Peng Z, Ye R, Mann JA, Zakhidov D, Li Y, Smalley PR, Lin J, Tour AM. Flexible Boron-Doped Laser-Induced Graphene Microsupercapacitors. *ACS Nano.* 2015;9(6):5868-75.
132. Wu G, Tan PF, Wu XJ, Peng L, Cheng HY, Wang CF, Chen W, Yu ZY, Chen S. High-Performance Wearable Micro-Supercapacitors Based on Microfluidic-Directed Nitrogen-Doped Graphene Fiber Electrodes. *Adv Funct Mater.* 2017;27(36).

133. Wu ZS, Parvez K, Winter A, Vieker H, Liu X, Han S, Turchanin A, Feng X, Müllen K. Layer - by - Layer Assembled Heteroatom - Doped Graphene Films with Ultrahigh Volumetric Capacitance and Rate Capability for Micro - Supercapacitors. *Adv. Mater.* 2014;26(26):4552-8.
134. Cheng Q, Tang J, Ma J, Zhang H, Shinya N, Qin L-C. Graphene and carbon nanotube composite electrodes for supercapacitors with ultra-high energy density. *Phys. Chem. Chem. Phys.* 2011;13(39):17615-24.
135. Luo J, Jang HD, Huang J. Effect of sheet morphology on the scalability of graphene-based ultracapacitors. *Acs Nano.* 2013;7(2):1464-71.
136. Wu Z-S, Zhou G, Yin L-C, Ren W, Li F, Cheng H-M. Graphene/metal oxide composite electrode materials for energy storage. *Nano Energy.* 2012;1(1):107-31.
137. Lin J, Zhang C, Yan Z, Zhu Y, Peng Z, Hauge RH, Natelson D, Tour JM. 3-dimensional graphene carbon nanotube carpet-based microsupercapacitors with high electrochemical performance. *Nano Lett.* 2012;13(1):72-8.
138. Mao X, Xu J, He X, Yang W, Yang Y, Xu L, Zhao Y, Zhou Y. All-solid-state flexible microsupercapacitors based on reduced graphene oxide/multi-walled carbon nanotube composite electrodes. *Appl. Surf. Sci.* 2018;435:1228-36.
139. Xiao H, Wu Z-S, Zhou F, Zheng S, Sui D, Chen Y, Bao X. Stretchable tandem micro-supercapacitors with high voltage output and exceptional mechanical robustness. *Energy Storage Materials.* 2018;13:233-40.
140. Xue M, Li F, Zhu J, Song H, Zhang M, Cao T. Structure - Based Enhanced Capacitance: In Situ Growth of Highly Ordered Polyaniline Nanorods on Reduced Graphene Oxide Patterns. *Adv. Funct. Mater.* 2012;22(6):1284-90.

141. Tian X, Xiao B, Xu X, Xu L, Liu Z, Wang Z, Yan M, Wei Q, Mai L. Vertically stacked holey graphene/polyaniline heterostructures with enhanced energy storage for on-chip micro-supercapacitors. *Nano Res.* 2016;9(4):1012-21.
142. Liu Z, Liu S, Dong R, Yang S, Lu H, Narita A, Feng X, Müllen K. High Power In-Plane Micro-Supercapacitors Based on Mesoporous Polyaniline Patterned Graphene. *Small.* 2017;13(14).
143. Qin J, Zhou F, Xiao H, Ren R, Wu Z-S. Mesoporous polypyrrole-based graphene nanosheets anchoring redox polyoxometalate for all-solid-state micro-supercapacitors with enhanced volumetric capacitance. *Sci. China Mater.* 2017;61(2):233-42.
144. Peng L, Peng X, Liu B, Wu C, Xie Y, Yu G. Ultrathin two-dimensional MnO<sub>2</sub>/graphene hybrid nanostructures for high-performance, flexible planar supercapacitors. *Nano Lett.* 2013;13(5):2151-7.
145. Liu W, Lu C, Wang X, Tay RY, Tay BK. High-performance microsupercapacitors based on two-dimensional graphene/manganese dioxide/silver nanowire ternary hybrid film. *ACS Nano.* 2015;9(2):1528-42.
146. Gu S, Lou Z, Li L, Chen Z, Ma X, Shen G. Fabrication of flexible reduced graphene oxide/Fe<sub>2</sub>O<sub>3</sub> hollow nanospheres based on-chip micro-supercapacitors for integrated photodetecting applications. *Nano Res.* 2015;9(2):424-34.
147. Xiao H, Wu ZS, Chen L, Zhou F, Zheng S, Ren W, Cheng HM, Bao X. One-Step Device Fabrication of Phosphorene and Graphene Interdigital Micro-Supercapacitors with High Energy Density. *ACS Nano.* 2017;11(7):7284-92.
148. Yan J, Fan Z, Sun W, Ning G, Wei T, Zhang Q, Zhang R, Zhi L, Wei F. Advanced asymmetric supercapacitors based on Ni (OH)<sub>2</sub>/graphene and porous graphene electrodes with high energy density. *Adv. Funct. Mater.* 2012;22(12):2632-41.

149. Couly C, Alhabeb M, Van Aken KL, Kurra N, Gomes L, Navarro-Suárez AM, Anasori B, Alshareef HN, Gogotsi Y. Asymmetric Flexible MXene-Reduced Graphene Oxide Micro-Supercapacitor. *Adv. Electron. Mater.* 2018;4(1):1700339.
150. Bae J, Song MK, Park YJ, Kim JM, Liu M, Wang ZL. Fiber supercapacitors made of nanowire-fiber hybrid structures for wearable/flexible energy storage. *Angew Chem Int Ed Engl.* 2011;50(7):1683-7.
151. Fu Y, Cai X, Wu H, Lv Z, Hou S, Peng M, Yu X, Zou D. Fiber supercapacitors utilizing pen ink for flexible/wearable energy storage. *Adv Mater.* 2012;24(42):5713-8.
152. Meng Y, Zhao Y, Hu C, Cheng H, Hu Y, Zhang Z, Shi G, Qu L. All-graphene core-sheath microfibers for all-solid-state, stretchable fibriform supercapacitors and wearable electronic textiles. *Adv Mater.* 2013;25(16):2326-31.
153. Yu D, Goh K, Zhang Q, Wei L, Wang H, Jiang W, Chen Y. Controlled functionalization of carbonaceous fibers for asymmetric solid-state micro-supercapacitors with high volumetric energy density. *Adv Mater.* 2014;26(39):6790-7.
154. Zheng S, Lei W, Qin J, Wu Z-S, Zhou F, Wang S, Shi X, Sun C, Chen Y, Bao X. All-solid-state high-energy planar asymmetric supercapacitors based on all-in-one monolithic film using boron nitride nanosheets as separator. *Energy Storage Materials.* 2018;10:24-31.
155. Pan H, Wang D, Peng Q, Ma J, Meng X, Zhang Y, Ma Y, Zhang S, Zhu D. High-Performance Microsupercapacitors Based on Bioinspired Graphene Microfibers. *ACS Appl. Mater. Interfaces.* 2018;10(12):10157-64.
156. Xin G, Yao T, Sun H, Scott SM, Shao D, Wang G, Lian J. Highly thermally conductive and mechanically strong graphene fibers. *Science.* 2015;349(6252):1083-7.
157. El-Kady MF, Kaner RB. Scalable fabrication of high-power graphene micro-supercapacitors for flexible and on-chip energy storage. *Nat Commun.* 2013;4:1475.

158. Chen S, Ma W, Cheng Y, Weng Z, Sun B, Wang L, Chen W, Li F, Zhu M, Cheng H-M. Scalable non-liquid-crystal spinning of locally aligned graphene fibers for high-performance wearable supercapacitors. *Nano Energy*. 2015;15:642-53.
159. Gao W, Singh N, Song L, Liu Z, Reddy AL, Ci L, Vajtai R, Zhang Q, Wei B, Ajayan PM. Direct laser writing of micro-supercapacitors on hydrated graphite oxide films. *Nat Nanotechnol*. 2011;6(8):496-500.
160. El-Kady MF, Strong V, Dubin S, Kaner RB. Laser scribing of high-performance and flexible graphene-based electrochemical capacitors. *Science*. 2012;335(6074):1326-30.
161. Zhang Q, Scrafford K, Li M, Cao Z, Xia Z, Ajayan PM, Wei B. Anomalous capacitive behaviors of graphene oxide based solid-state supercapacitors. *Nano Lett*. 2014;14(4):1938-43.
162. Zheng S, Tang X, Wu ZS, Tan YZ, Wang S, Sun C, Cheng H-M, Bao X. Arbitrary-Shaped Graphene-Based Planar Sandwich Supercapacitors on One Substrate with Enhanced Flexibility and Integration. *ACS Nano*. 2017;11(2):2171-9.
163. Wang D-W, Du A, Taran E, Lu GQ, Gentle IR. A water-dielectric capacitor using hydrated graphene oxide film. *J. Mater. Chem*. 2012;22(39):21085.
164. Qin J, Cao M, Li N, Hu C. Graphene-wrapped WO<sub>3</sub> nanoparticles with improved performances in electrical conductivity and gas sensing properties. *J. Mater. Chem*. 2011;21(43):17167.
165. Li X, Cai W, An J, Kim S, Nah J, Yang D, Richard P, Aruna V, Inhwa J, Emanuel T, Sanjay K. B, Luigi C, Rodney S. R. Large-area synthesis of high-quality and uniform graphene films on copper foils. *Science*. 2009;324(5932):1312-4.
166. Li X, Magnuson CW, Venugopal A, An J, Suk JW, Han B, Mark B, Cai W, Aruna V, Zhu Y, Fu L, Eric M. V, Edgar V, Luigi C, Rodney S. R. Graphene films with large domain size by a two-step chemical vapor deposition process. *Nano Lett*. 2010;10(11):4328-34.

167. Chen Z, Ren W, Gao L, Liu B, Pei S, Cheng H-M. Three-dimensional flexible and conductive interconnected graphene networks grown by chemical vapour deposition. *Nat. Mater.* 2011;10(6):424-8.
168. Wu Z-S, Ren W, Gao L, Liu B, Jiang C, Cheng H-M. Synthesis of high-quality graphene with a pre-determined number of layers. *Carbon.* 2009;47(2):493-9.
169. Park S, Ruoff RS. Chemical methods for the production of graphenes. *Nat. Nanotechnol.* 2009;4(4):217-24.
170. Wu Z-S, Ren W, Gao L, Zhao J, Chen Z, Liu B, Tang D, Yu B, Jiang C, Cheng H-M. Synthesis of graphene sheets with high electrical conductivity and good thermal stability by hydrogen arc discharge exfoliation. *ACS nano.* 2009;3(2):411-7.
171. Zhi L, Müllen K. A bottom-up approach from molecular nanographenes to unconventional carbon materials. *J. Mater. Chem.* 2008;18(13):1472-84.
172. Parvez K, Li R, Puniredd SR, Hernandez Y, Hinkel F, Wang S, Feng X, Müllen K. Electrochemically exfoliated graphene as solution-processable, highly conductive electrodes for organic electronics. 2013; 7(4): 3598–3606.
173. Berger C, Song Z, Li X, Wu X, Brown N, Naud C, Mayou D, Li T, Hass J, Marchenkov AN, Conrad EH, First PN, de Heer WA. Electronic confinement and coherence in patterned epitaxial graphene. *Science.* 2006;312(5777):1191-6.
174. Berger C, Song Z, Li T, Li X, Ogbazghi AY, Feng R, Zhenting D, Marchenkov AN, Conrad EH, First PN, de Heer WA. Ultrathin epitaxial graphite: 2D electron gas properties and a route toward graphene-based nanoelectronics. *J. Phys. Chem. B.* 2004;108(52):19912-6.
175. Wang X, Zhi L, Müllen K. Transparent, conductive graphene electrodes for dye-sensitized solar cells. *Nano Lett.* 2008;8(1):323-7.
176. Wu Z-S, Yang S, Sun Y, Parvez K, Feng X, Müllen K. 3D nitrogen-doped graphene aerogel-supported Fe<sub>3</sub>O<sub>4</sub> nanoparticles as efficient electrocatalysts for the oxygen reduction reaction. *J. Am. Chem. Soc.* 2012;134(22):9082-5.

177. Yavari F, Chen Z, Thomas AV, Ren W, Cheng H-M, Koratkar N. High sensitivity gas detection using a macroscopic three-dimensional graphene foam network. *Sci. Rep.* 2011;1.
178. Pang S, Hernandez Y, Feng X, Müllen K. Graphene as transparent electrode material for organic electronics. *Adv. Mater.* 2011;23(25):2779-95.
179. Wu ZS, Pei S, Ren W, Tang D, Gao L, Liu B, Li F, Liu C, Cheng H-M. Field emission of single - layer graphene films prepared by electrophoretic deposition. *Adv. Mater.* 2009;21(17):1756-60.
180. Stankovich S, Dikin DA, Dommett GH, Kohlhaas KM, Zimney EJ, Stach EA, Piner RD, Nguyen ST, Ruoff RS. Graphene-based composite materials. *Nature.* 2006;442(7100):282-6.
181. Wu Z-S, Ren W, Xu L, Li F, Cheng H-M. Doped graphene sheets as anode materials with superhigh rate and large capacity for lithium ion batteries. *ACS nano.* 2011;5(7):5463-71.
182. Wang G, Shen X, Yao J, Park J. Graphene nanosheets for enhanced lithium storage in lithium ion batteries. *Carbon.* 2009;47(8):2049-53.
183. Liu C, Yu Z, Neff D, Zhamu A, Jang BZ. Graphene-based supercapacitor with an ultrahigh energy density. *Nano Lett.* 2010;10(12):4863-8.
184. Zhang LL, Zhou R, Zhao X. Graphene-based materials as supercapacitor electrodes. *J. Mater. Chem.* 2010;20(29):5983-92.
185. Pech D, Brunet M, Dinh TM, Armstrong K, Gaudet J, Guay D. Influence of the configuration in planar interdigitated electrochemical micro-capacitors. *J. Power Sources.* 2013;230:230-5.
186. Sung J-H, Kim S-J, Lee K-H. Fabrication of microcapacitors using conducting polymer microelectrodes. *J. Power Sources.* 2003;124(1):343-50.
187. Sung J-H, Kim S-J, Lee K-H. Fabrication of all-solid-state electrochemical microcapacitors. *J. Power Sources.* 2004;133(2):312-9.

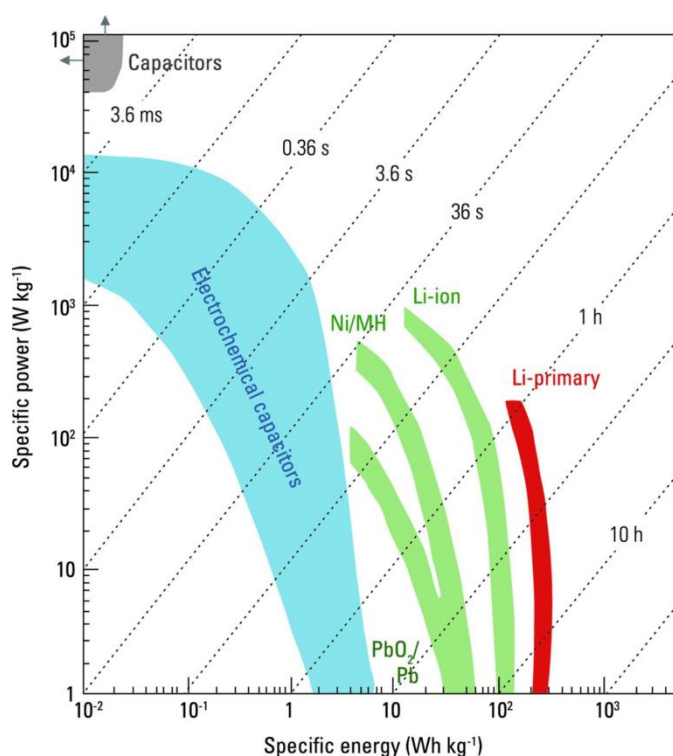
188. Akhavan O. Photocatalytic reduction of graphene oxides hybridized by ZnO nanoparticles in ethanol. *Carbon*. 2011;49(1):11-8.
189. Williams G, Seger B, Kamat PV. TiO<sub>2</sub>-graphene nanocomposites. UV-assisted photocatalytic reduction of graphene oxide. *ACS Nano*. 2008;2(7):1487-91.
190. Li H, Pang S, Wu S, Feng X, Mullen K, Bubeck C. Layer-by-layer assembly and UV photoreduction of graphene-polyoxometalate composite films for electronics. *J Am Chem Soc*. 2011;133(24):9423-9.
191. Zhang Y-L, Guo L, Xia H, Chen Q-D, Feng J, Sun H-B. Photoreduction of Graphene Oxides: Methods, Properties, and Applications. *Adv. Opt. Mater*. 2014;2(1):10-28.
192. Wang S, Wu Z-S, Zheng S, Zhou F, Sun C, Cheng H-M, Bao X. Scalable fabrication of photochemically reduced graphene-based monolithic micro-supercapacitors with superior energy and power densities. *ACS nano*. 2017;11(4):4283-91.
193. Wang F, Wang K, Zheng B, Dong X, Mei X, Lv J, Duan W, Wang W. Laser-induced graphene: preparation, functionalization and applications. *MATER TECHNOL*. 2018;33(5):340-56.
194. Wan Z, Streed EW, Lobino M, Wang S, Sang RT, Cole IS, Thiel DV, Li Q. Laser-Reduced Graphene: Synthesis, Properties, and Applications. *Adv. Mater. Technol*. 2018;3(4):1700315.
195. Kumar R, Savu R, Joanni E, Vaz AR, Canesqui MA, Singh RK, Timm RA, Kubota LT, Moshkalev SA. Fabrication of interdigitated micro-supercapacitor devices by direct laser writing onto ultra-thin, flexible and free-standing graphite oxide films. *RSC Adv*. 2016;6(88):84769-76.
196. Gao W, Singh N, Song L, Liu Z, Reddy ALM, Ci L, Vajtai R, Zhang Q, Wei B. Ajayan P. M. Direct laser writing of micro-supercapacitors on hydrated graphite oxide films. *Nat. Nanotechnol*. 2011;6(8):496-500.

197. Xie B, Wang Y, Lai W, Lin W, Lin Z, Zhang Z, Zou P, Xu Y, Zhou S, Yang C, Kang F, Wong C-P. Laser-processed graphene based micro-supercapacitors for ultrathin, rollable, compact and designable energy storage components. *Nano Energy*. 2016;26:276-85.
198. Li RZ, Peng R, Kihm KD, Bai S, Bridges D, Tumuluri U, Wu Z, Zhang T, Compagnini G, Feng Z, Hu A. High-rate in-plane micro-supercapacitors scribed onto photo paper using in situ femtolaser-reduced graphene oxide/Au nanoparticle microelectrodes. *Energy Environ. Sci*. 2016;9(4):1458-67.
199. Shen D, Zou G, Liu L, Zhao W, Wu A, Duley WW, Zhou YN. Scalable High-Performance Ultraminiature Graphene Micro-Supercapacitors by a Hybrid Technique Combining Direct Writing and Controllable Microdroplet Transfer. *ACS Appl. Mater. Interfaces*. 2018;10(6):5404-12.
200. Lobo DE, Banerjee PC, Easton CD, Majumder M. Miniaturized supercapacitors: Focused ion beam reduced graphene oxide supercapacitors with enhanced performance metrics. *Adv. Energy Mater*. 2015;5(19).
201. Liu Z, Wu ZS, Yang S, Dong R, Feng X, Mullen K. Ultraflexible In-Plane Micro-Supercapacitors by Direct Printing of Solution-Processable Electrochemically Exfoliated Graphene. *Adv Mater*. 2016;28(11):2217-22.
202. Sollami Delekta S, Smith AD, Li J, Ostling M. Inkjet printed highly transparent and flexible graphene micro-supercapacitors. *Nanoscale*. 2017;9(21):6998-7005.
203. Li J, Sollami Delekta S, Zhang P, Yang S, Lohe MR, Zhuang X, Feng X, Ostling M. Scalable Fabrication and Integration of Graphene Microsupercapacitors through Full Inkjet Printing. *ACS Nano*. 2017;11(8):8249-56.
204. Zeng W, Shu L, Li Q, Chen S, Wang F, Tao XM. Fiber-based wearable electronics: a review of materials, fabrication, devices, and applications. *Adv Mater*. 2014;26(31):5310-36.

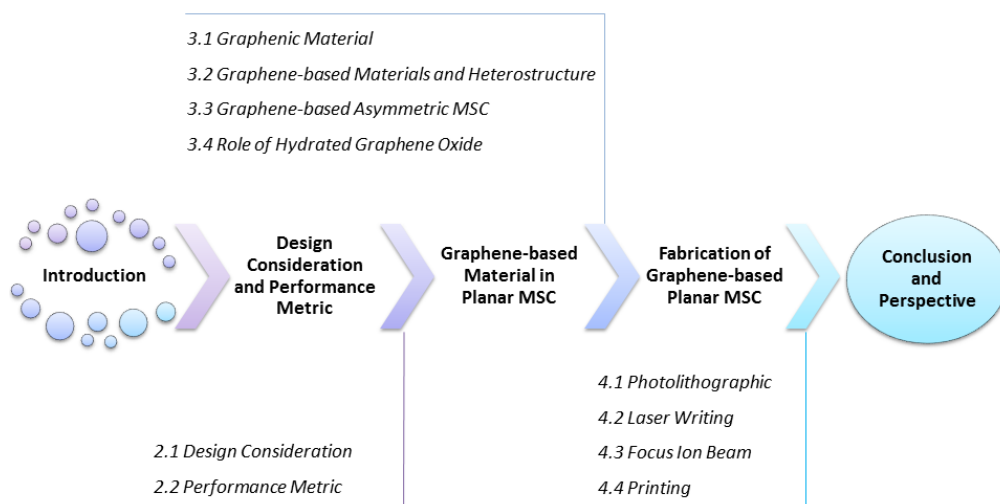
205. Hyun WJ, Secor EB, Hersam MC, Frisbie CD, Francis LF. High-resolution patterning of graphene by screen printing with a silicon stencil for highly flexible printed electronics. *Adv Mater.* 2015;27(1):109-15.
206. Wang Z, Zhang QE, Long S, Luo Y, Yu P, Tan Z, Bai J, Qu B, Yang Y, Shi J, Zhou H, Xiao Z. Y, Hong W, Bai H. Three-Dimensional Printing of Polyaniline/Reduced Graphene Oxide Composite for High-Performance Planar Supercapacitor. *ACS Appl. Mater. Interfaces.* 2018;10(12):10437-44.
207. Hyun WJ, Secor EB, Kim C-H, Hersam MC, Francis LF, Frisbie CD. Scalable, Self-Aligned Printing of Flexible Graphene Micro-Supercapacitors. *Adv. Energy Mater.* 2017;7(17):1700285.
208. Secor EB, Lim S, Zhang H, Frisbie CD, Francis LF, Hersam MC. Gravure printing of graphene for large-area flexible electronics. *Adv Mater.* 2014;26(26):4533-8.
209. Kim S-M, Jang B, Jo K, Kim D, Lee J, Kim K-S, Lee S-M, Lee H-J, Han S, Kim J-H. Mechanics-driven patterning of CVD graphene for roll-based manufacturing process. *2D Mater.* 2017;4(2):024003.
210. Gogotsi Y, Simon P. True Performance Metrics in Electrochemical Energy Storage. *Science.* 2011;334(6058):917-8.
211. Wang S, Wu ZS, Zheng S, Zhou F, Sun C, Cheng HM, Bao X. Scalable Fabrication of Photochemically Reduced Graphene-Based Monolithic Micro-Supercapacitors with Superior Energy and Power Densities. *ACS Nano.* 2017;11(4):4283-91.
212. Largeot C, Portet C, Chmiola J, Taberna PL, Gogotsi Y, Simon P. Relation between the ion size and pore size for an electric double-layer capacitor. *J Am Chem Soc.* 2008;130(9):2730-1.

213. Lin R, Huang P, Ségalini J, Largeot C, Taberna PL, Chmiola J, Gogotsi Y, Simon P. Solvent effect on the ion adsorption from ionic liquid electrolyte into sub-nanometer carbon pores. *Electrochim. Acta*. 2009;54(27):7025-32.
214. Lin R, Taberna PL, Chmiola J, Guay D, Gogotsi Y, Simon P. Microelectrode Study of Pore Size, Ion Size, and Solvent Effects on the Charge/Discharge Behavior of Microporous Carbons for Electrical Double-Layer Capacitors. *J. Electrochem. Soc.* 2009;156(1):A7.
215. Simon P, Gogotsi Y. Capacitive energy storage in nanostructured carbon-electrolyte systems. *Acc Chem Res*. 2013;46(5):1094-103.
216. Borchardt L, Oschatz M, Kaskel S. Tailoring porosity in carbon materials for supercapacitor applications. *Mater Horiz*. 2014;1(2):157-68.
217. Xiong G, Meng C, Reifemberger RG, Irazoqui PP, Fisher TS. A review of graphene - based electrochemical microsupercapacitors. *Electroanalysis*. 2014;26(1):30-51.
218. Alhabeb M, Beidaghi M, Van Aken KL, Dyatkin B, Gogotsi Y. High-density freestanding graphene/carbide-derived carbon film electrodes for electrochemical capacitors. *Carbon*. 2017;118:642-9.
219. Pech D, Brunet M, Durou H, Huang P, Mochalin V, Gogotsi Y, Taberna P. L, Simon P. Ultrahigh-power micrometre-sized supercapacitors based on onion-like carbon. *Nat Nanotechnol*. 2010;5(9):651-4.
220. Xu X, Shi W, Li P, Ye S, Ye C, Ye H, Lu, T, Zheng A, Zhu J, Xu L, Zhong M, Cao X. Facile Fabrication of Three-Dimensional Graphene and Metal–Organic Framework Composites and Their Derivatives for Flexible All-Solid-State Supercapacitors. *Chem. Mater*. 2017;29(14):6058-65.
221. Xiao K, Jiang D, Amal R, Wang DW. A 2D Conductive Organic-Inorganic Hybrid with Extraordinary Volumetric Capacitance at Minimal Swelling. *Adv Mater*. 2018:e1800400.

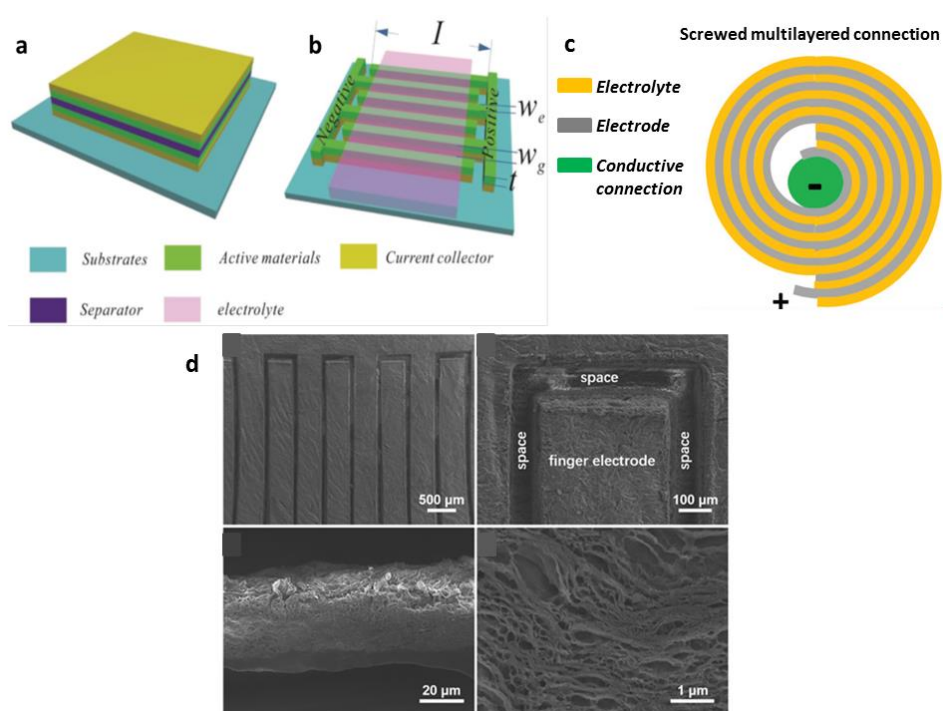
222. Li X, Cui Y, Qi M, Wu H, Xie Y, Zang X, Wen D, Teh KS, Ye J, Zhou Z, Huang Q-A, Cai W, Lin L. editors. A 1000-Volt planar micro-supercapacitor by direct-write laser engraving of polymers. Micro Electro Mechanical Systems (MEMS), 2017 IEEE 30th International Conference on; 2017: IEEE.
223. Shi X, Wu ZS, Qin J, Zheng S, Wang S, Zhou F, Sun C, Bao X. Graphene - Based Linear Tandem Micro - Supercapacitors with Metal - Free Current Collectors and High - Voltage Output. Adv. Mater. 2017;29(44).
224. Sun G, An J, Chua CK, Pang H, Zhang J, Chen P. Layer-by-layer printing of laminated graphene-based interdigitated microelectrodes for flexible planar micro-supercapacitors. Electrochem. Commun. 2015;51:33-6.



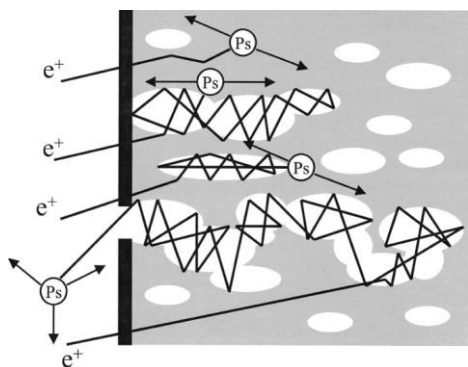
**Figure 1.** Ragone plot associated with specific energy and power for various electrochemical energy storage systems. Reproduced with permission.<sup>[1]</sup> Copyright 2008, Macmillan Publishers Limited.



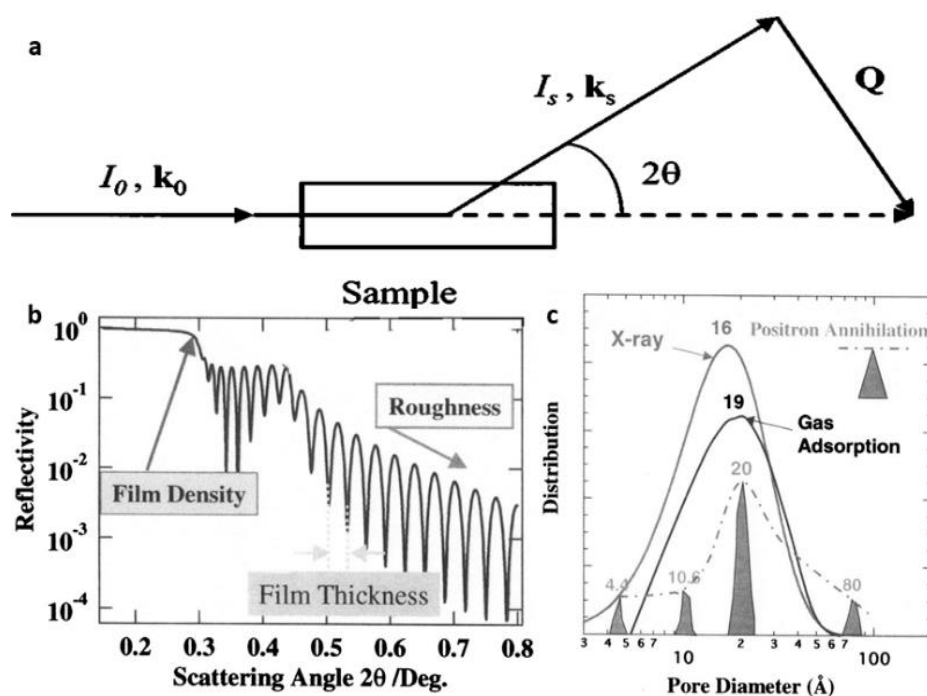
**Figure 2.** Schematic of contents covered in this review.



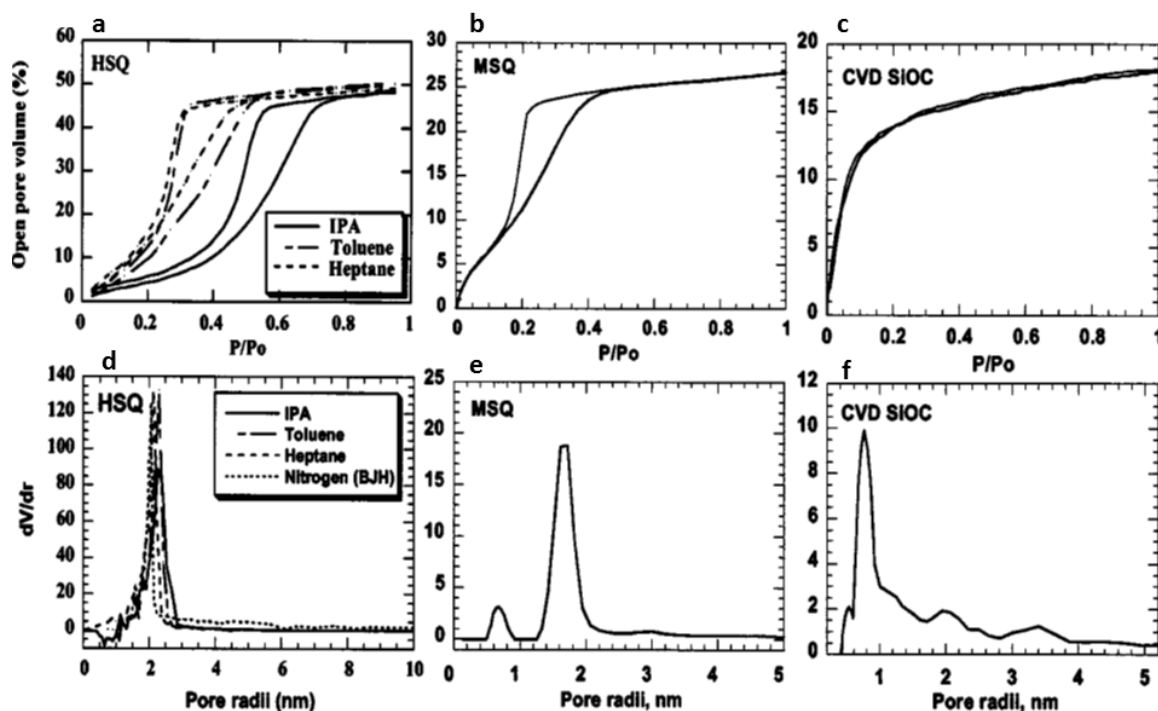
**Figure 3.** a) Schematic diagrams of conventional sandwich supercapacitor and b) MSC with in-plane interdigital electrode architecture. Reproduced with permission.<sup>[51]</sup> Copyright 2017 WILEY-VCH. c) screwed multilayer connection. Reproduced with permission.<sup>[55]</sup> Copyright 2018 WILEY-VCH Verlag GmbH & Co. d) SEM images of the Laser-carved porous RGO film electrode. Reproduced with permission.<sup>[57]</sup> Copyright 2017 Elsevier Ltd.



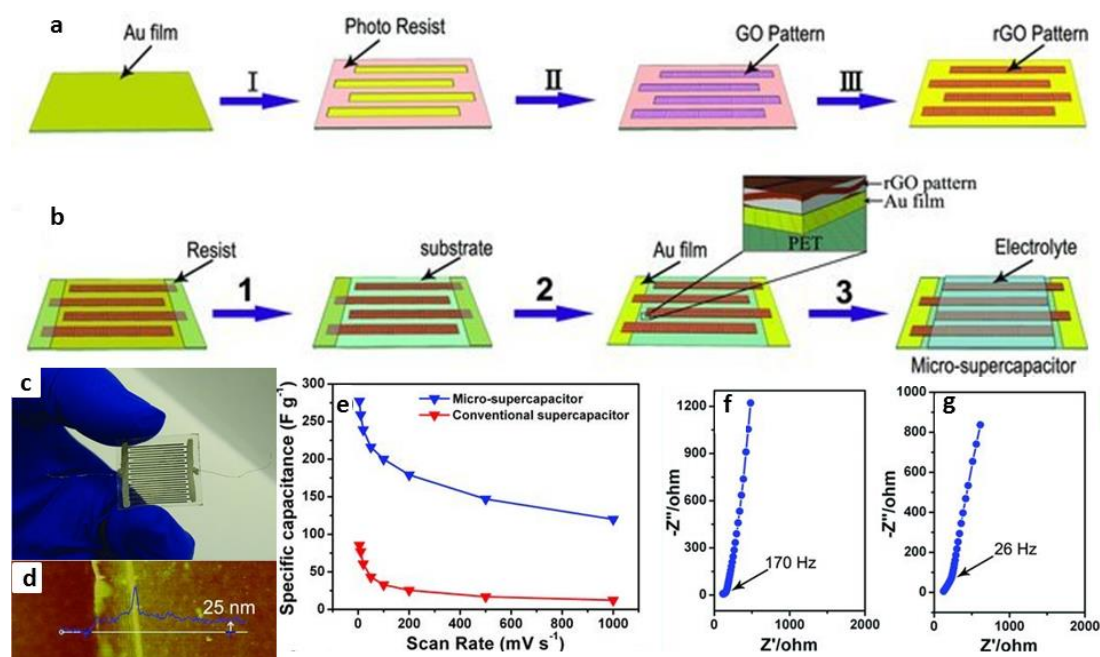
**Figure 4.** Formation and diffusion of positronium (Ps) in a porous material containing both open and closed pores. Reproduced with permission.<sup>[79]</sup> Copyright 2001 American Institute of Physics.



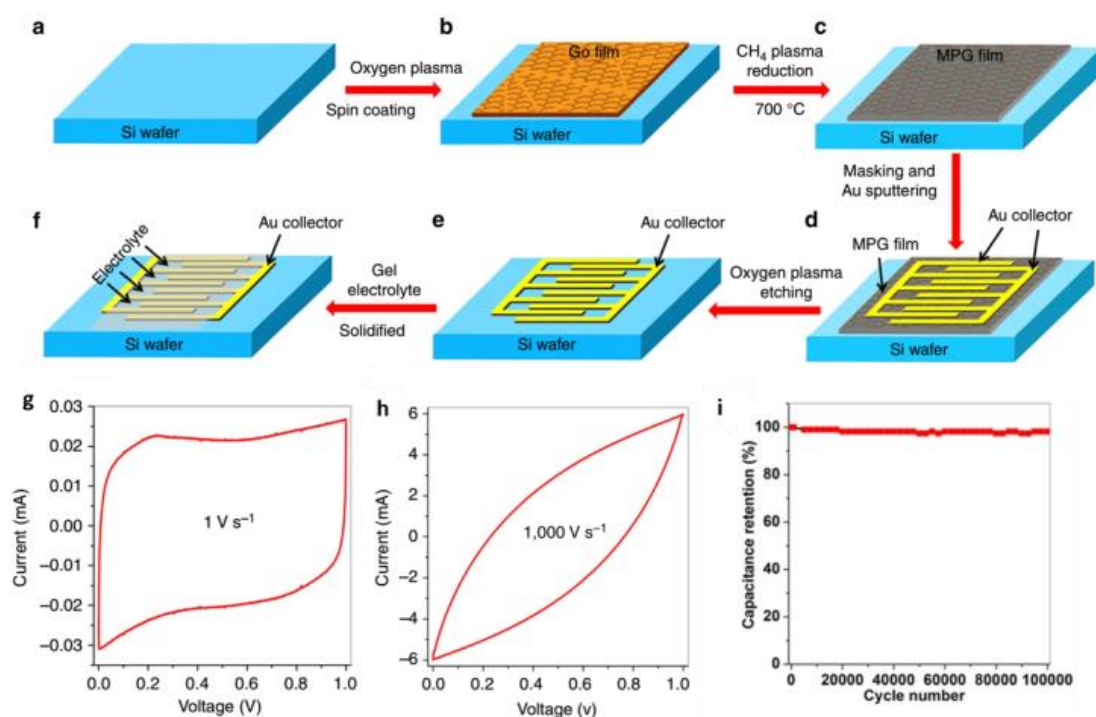
**Figure 5.** a) Schematic representation of the incident and scattered beams in a small angle scattering experiment. b) Determination of the film density and thickness from x-ray reflectivity. c) Pore size distribution as estimated by x-ray scattering, nitrogen porosimetry, and PALS. Reproduced with permission.<sup>[79]</sup> Copyright 2001 IEEE.



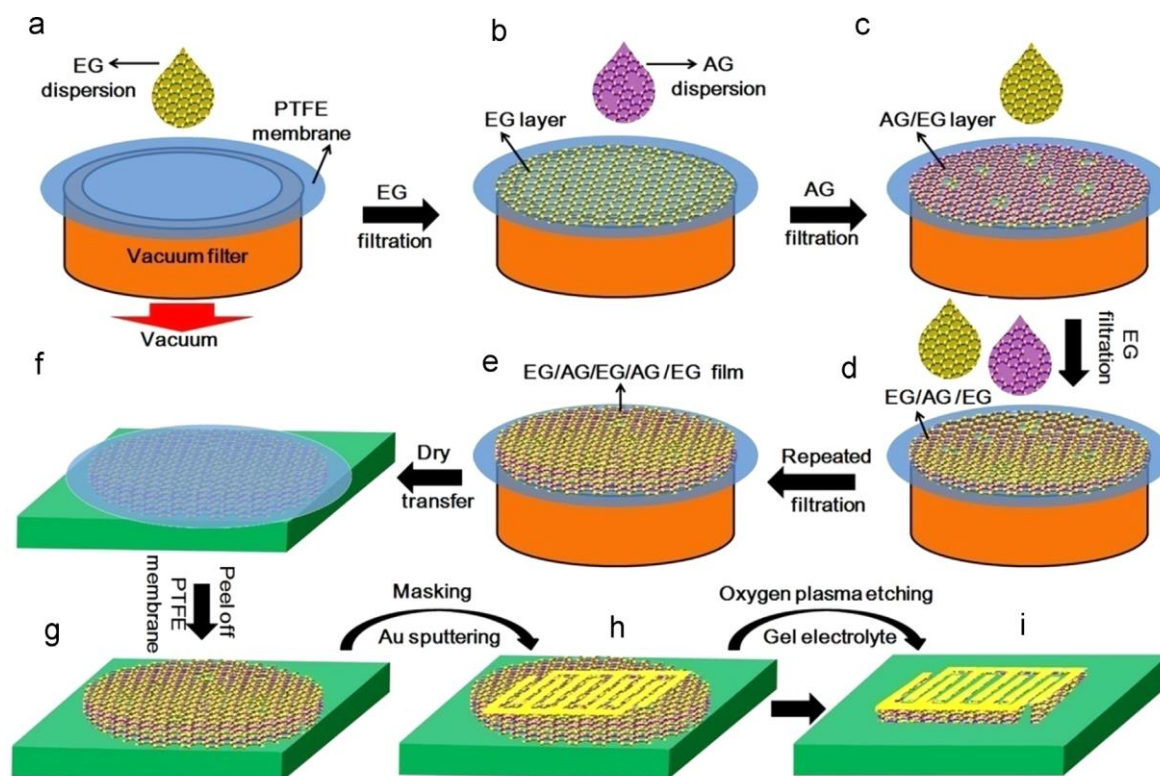
**Figure 6.** Ellipsometric porosimetry data for typical low-k films (a) mesoporous HSQ based material. This graph demonstrates good agreement of pore size calculated with different adsorptive and nitrogen (BJH) porosimetry, (b) MSQ based film with bi-modal porosity and (c) a carbon doped microporous silica film. In the last two cases adsorptive is toluene. Reproduced with permission.<sup>[68]</sup> Copyright 2003 American Institute of Physics.



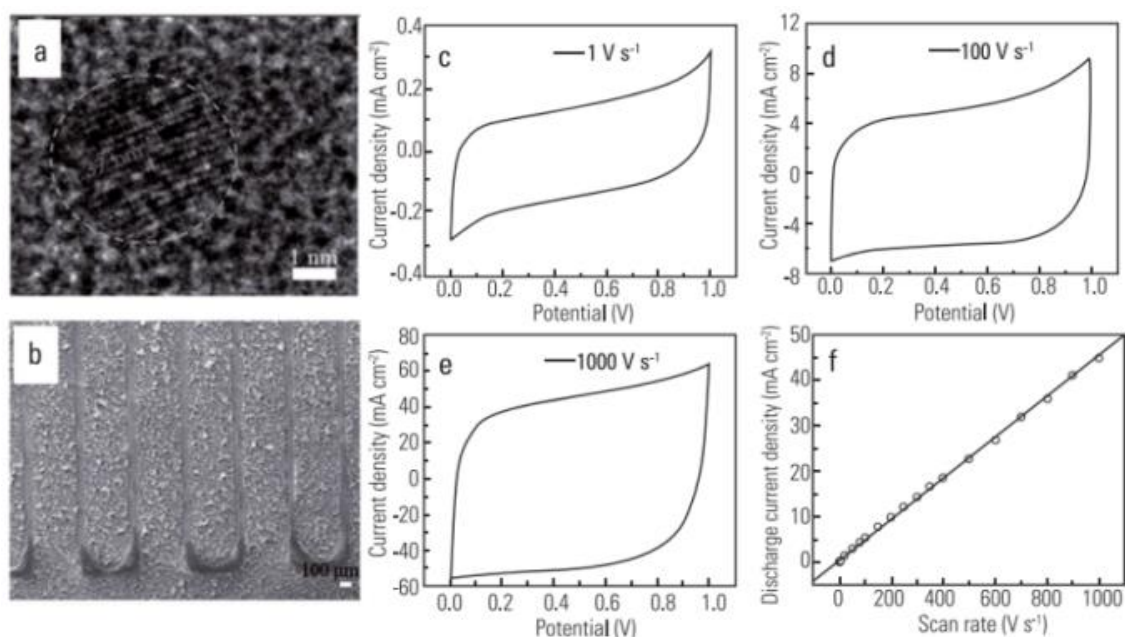
**Figure 7.** (a) and (b) Schematic process of ultrathin RGO-based MSC preparation. (c) Optical image of MSC on polyethylene terephthalate substrate. (d) AFM image with the average thickness of the electrodes. (e) The specific capacitance of the RGO MSC and conventional supercapacitor at various scan rates. The Nyquist plot of (f) RGO MSC and (g) conventional supercapacitor. Reproduced with permission.<sup>[90]</sup> Copyright 2013 WILEY-VCH Verlag GmbH & Co.



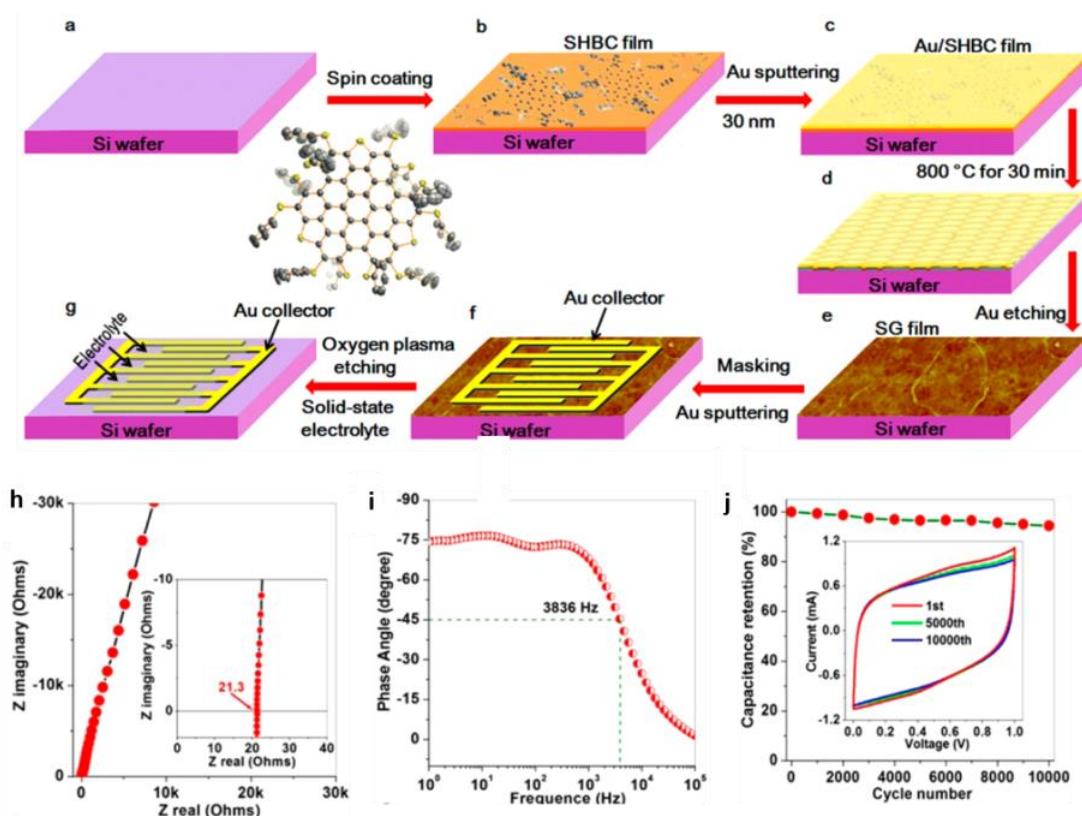
**Figure 8.** (a-f) Schematic fabrication illustration of MSC with RGO via plasma reduction. (g), (h) CV curves at scan rates of 1 and 1000 V s<sup>-1</sup>. (i) The capacitance retention versus cycle number. Reproduced with permission.<sup>[19]</sup> Copyright 2013 Macmillan Publishers Limited.



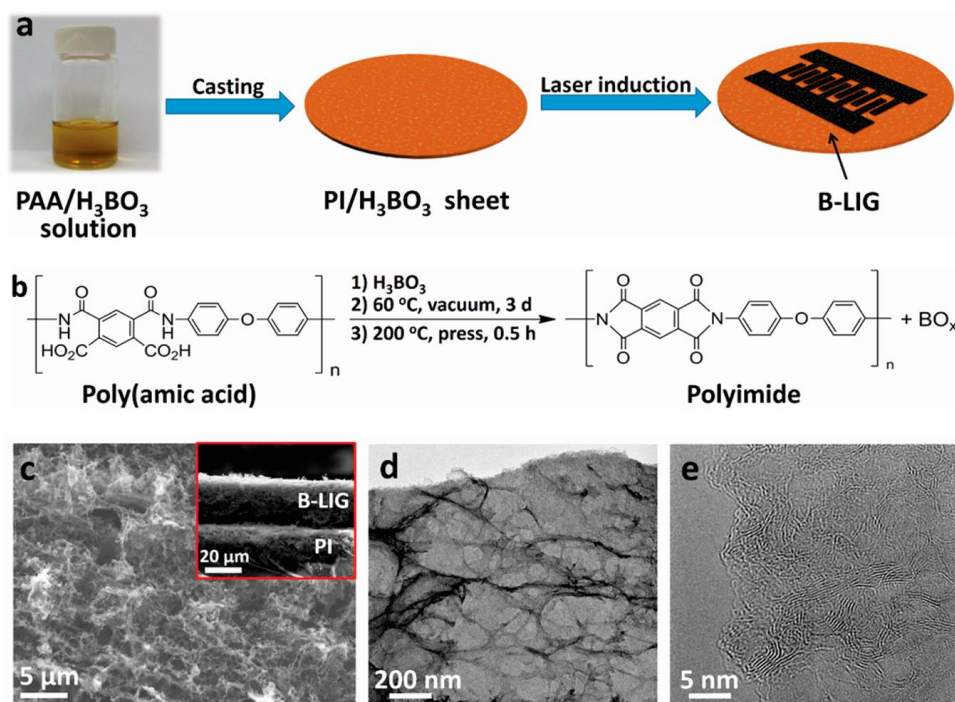
**Figure 9.** Schematic illustration of binder-free AG compact films for in-plane MSCs. (a) Vacuum filtration of EG dispersion on a PTFE membrane filter. (b) Vacuum filtration of AG dispersion on the top of EG film. (c) Vacuum filtration of EG dispersion on the top of an AG/EG film. (d) Repeated filtration of the AG layer and EG layer on the EG/AG/EG film. (e) Dry transfer of the alternating deposited AG film (EG/AG/EG/AG/EG) on the surface of SiO<sub>2</sub>/Si wafer under high pressure. (f) A compressed AG film on SiO<sub>2</sub>/Si wafer after peeling off the PTFE membrane. (g) Thermally evaporation of gold micro patterns as current collector. (h) Oxygen plasma etching and drop-casting of gel electrolyte on interdigital electrodes. (i) An all-solid-state AG-MSC achieved. Reproduced with permission.<sup>[121]</sup> Copyright 2015 Elsevier B.V.



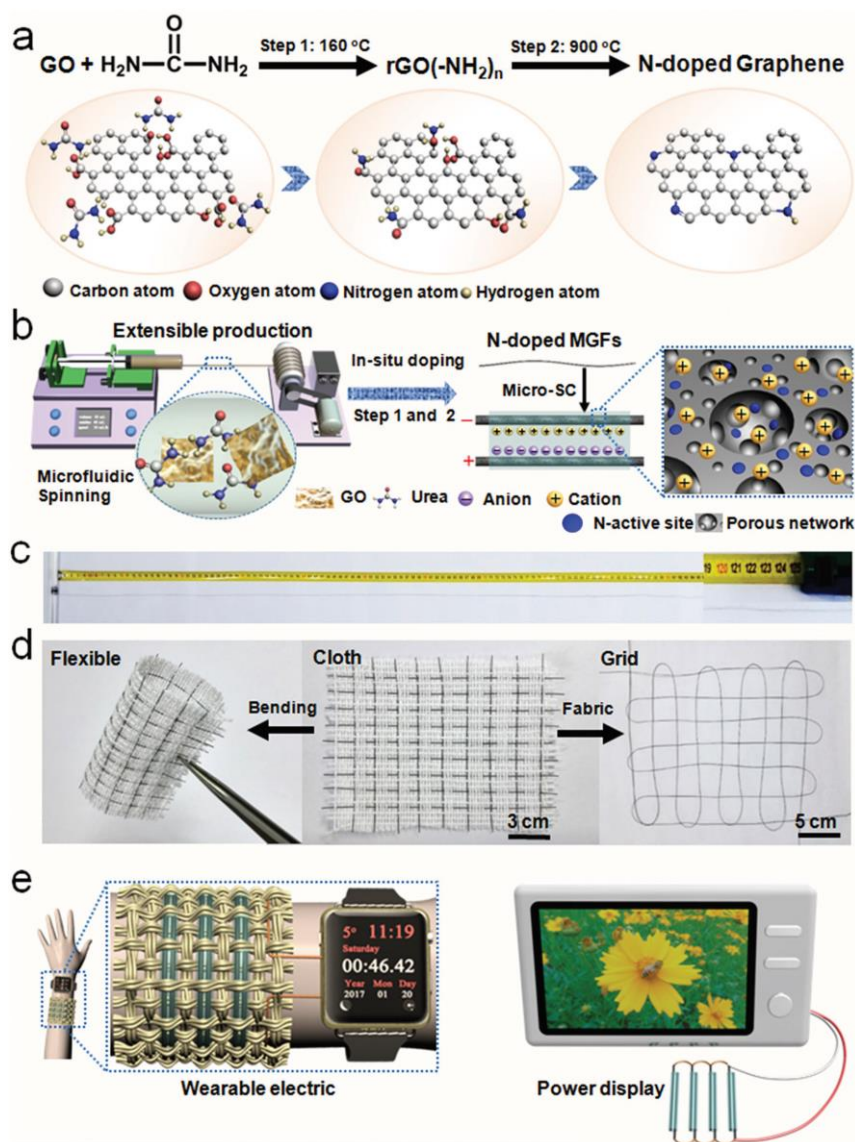
**Figure 10.** Graphene quantum dots (GQDs) as electrode material (a) TEM and (b) SEM of Au interdigitated electrodes with GQDs and (c-e) electrochemical performance using a 0.5 M Na<sub>2</sub>SO<sub>4</sub> electrolyte. (f) The discharge current density of GQD-MSCs as a function of scan rate. Reproduced with permission.<sup>[125]</sup> Copyright 2013 WILEY-VCH Verlag GmbH & Co.



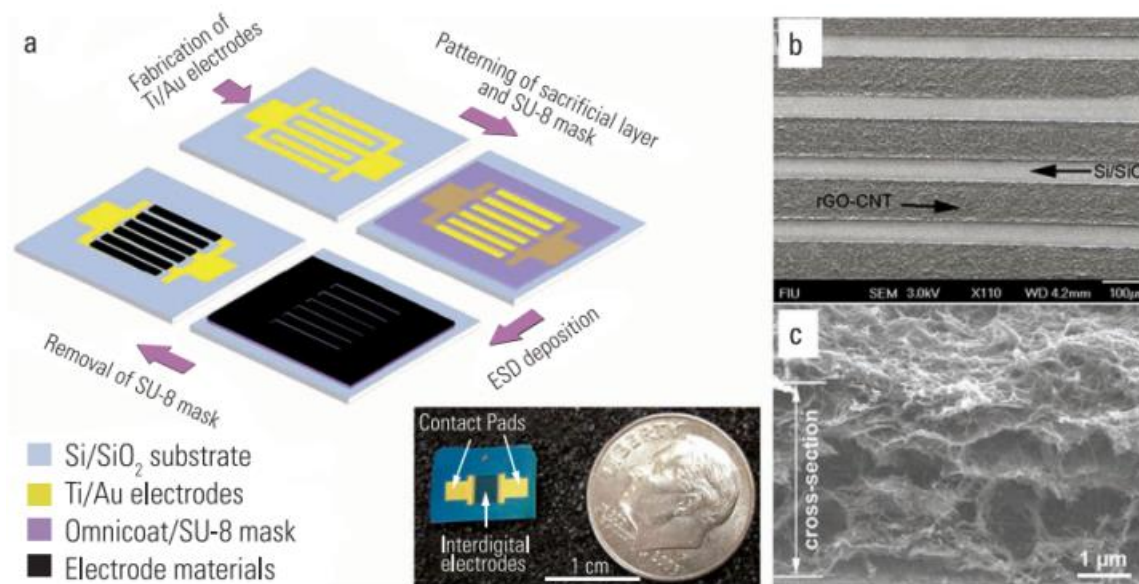
**Figure 11.** (a-g) Schematic illustration SHBC-derived SG films for planar MSC on a Si-SiO<sub>2</sub> wafer. (h) The impedance of SG-MSCs. Insert: Magnified plot of the high-frequency region. (i) Phase angle as a function of frequency of SG-MSCs. (j) Cycling stability of SGMSCs. Insert: 1st, 5000th, and 10000th CV curves of SG-MSCs tested at 200 V s<sup>-1</sup>. Reproduced with permission.<sup>[130]</sup> Copyright 2017 American Chemical Society.



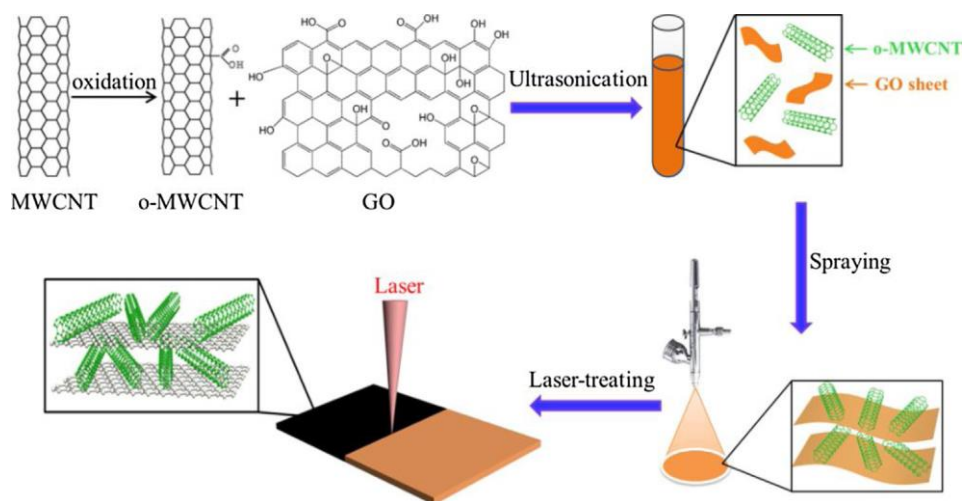
**Figure 12.** (a) Synthetic scheme for the preparation of B-LIG and fabrication of the B-LIG-MSC. (b) Scheme of the dehydration reaction from PAA to a PI film during the curing process. (c) SEM images of 5B-LIG. The insert is the cross sectional SEM image. (d) TEM image and (e) HRTEM image of 5B-LIG. Reproduced with permission.<sup>[131]</sup> Copyright 2015 American Chemical Society.



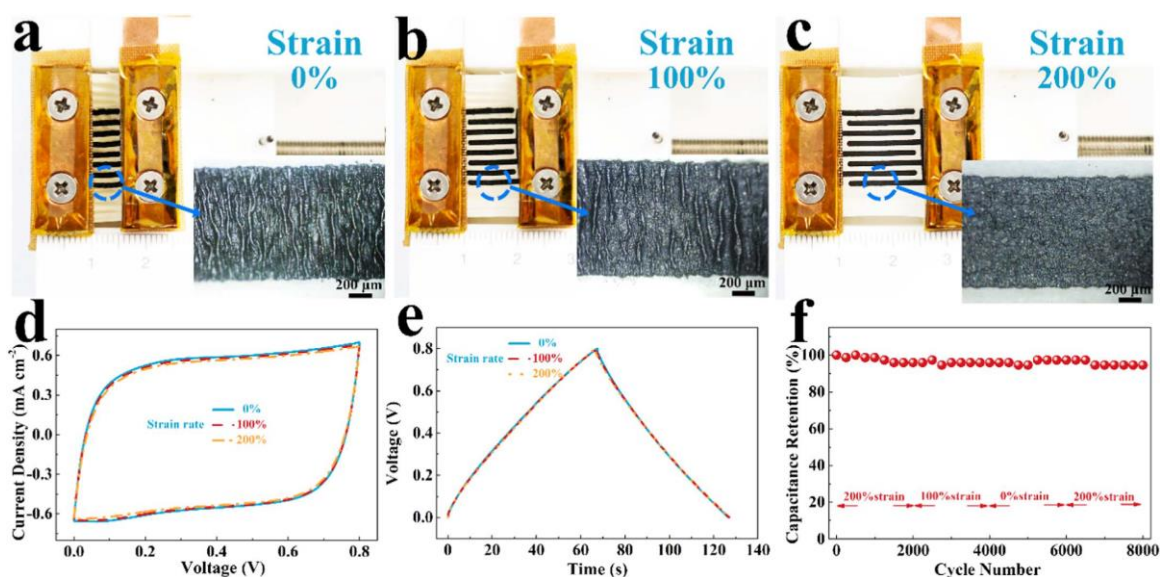
**Figure 13.** a) Schematic illustration of N-doped mechanism in graphene. b) Schematic illustration of the preparation of N-doped MGF. c) Photograph of N-doped MGF wrapped on a glass rod. d) Photograph of N-doped MGF being woven in cotton fabric, bending process of cotton fabric, and cloth woven by two individual fibers. e) The schematic illustration of fiber-based MSC integrated into miniaturized flexible and fabric substrate to powered electronics. Reproduced with permission.<sup>[132]</sup> Copyright 2017 WILEY-VCH Verlag GmbH & Co.



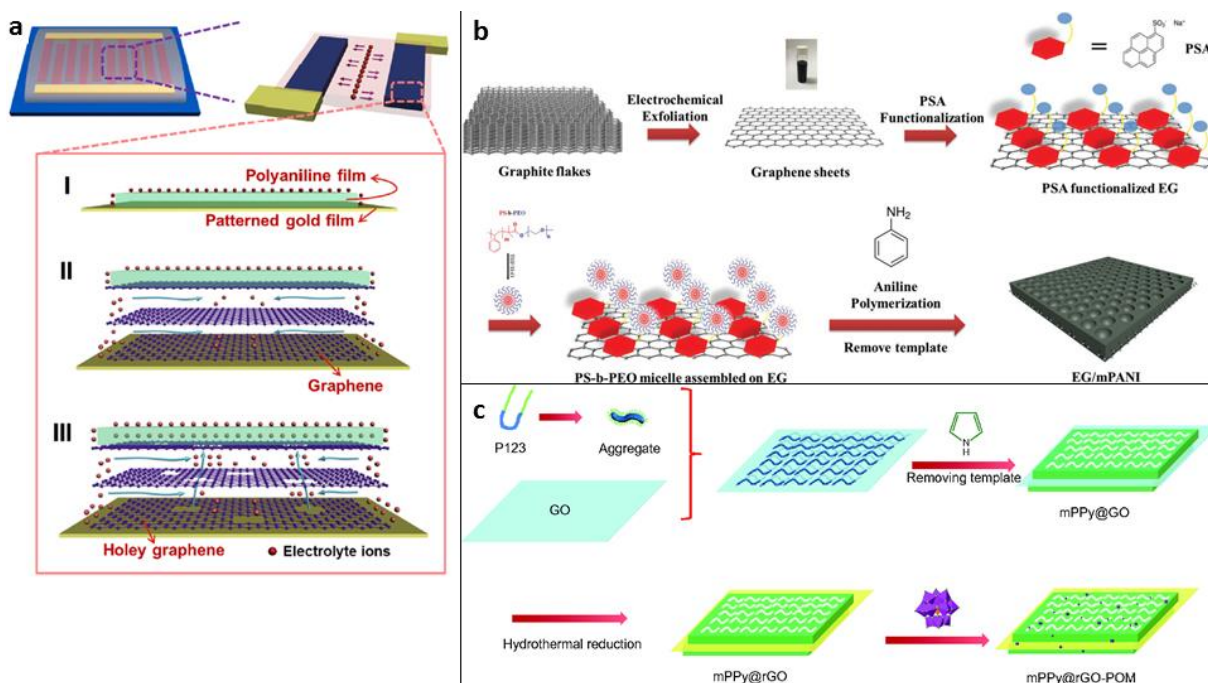
**Figure 14.** (a) Schematic fabrication of RGO-CNT interdigitated MSC (insert: digital photograph of a single MSC). (b) Top-view and (c) cross-sectional SEM images of RGO-CNT-based interdigitated microelectrodes. Reproduced with permission.<sup>[36]</sup> Copyright 2012 Wiley-VCH Verlag GmbH & Co.



**Figure 15.** Schematic illustration of the fabrication process of the RGO/MWCNT nanocomposite electrode. Reproduced with permission.<sup>[138]</sup> Copyright 2017 Elsevier B.V.

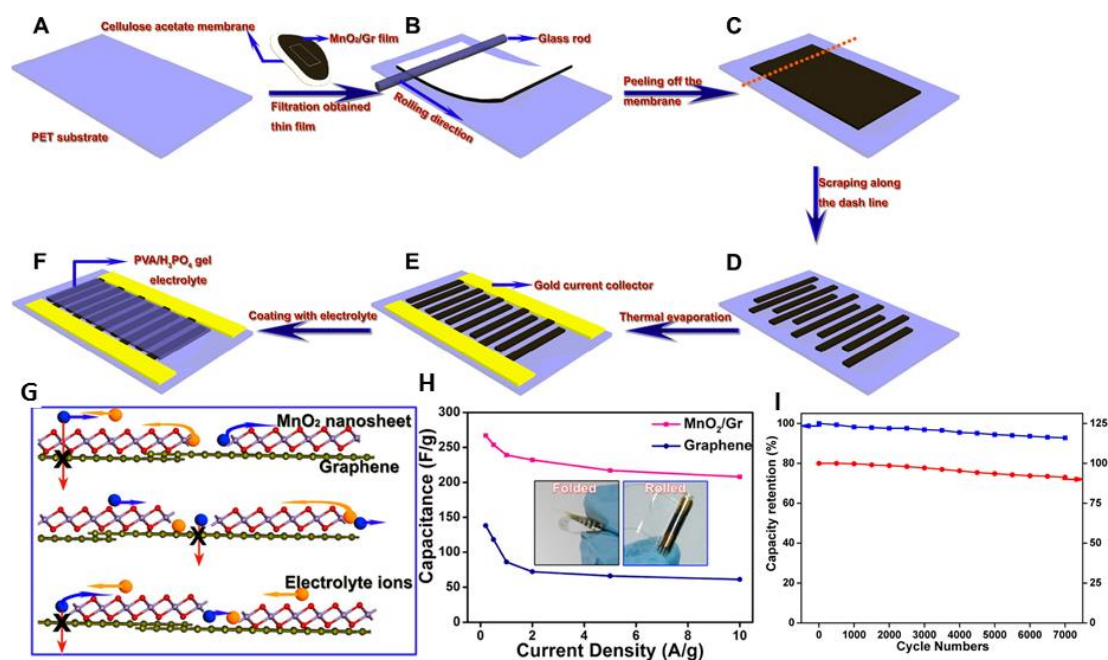


**Figure 16.** Stretchability and cyclability of GCP-MSC. (a–c) Photographs of GCP-MSC tested at different strain rates of (a) 0%, (b) 100%, and (c) 200%. The inserts are the corresponding optical images of microelectrodes. (d) CV curves of GCP-MSCs measured under  $100 \text{ mV s}^{-1}$ , and (e) GCD curves measured at  $0.1 \text{ mA cm}^{-2}$ , with different strain rates. (f) Cycling stability of GCP-MSCs obtained at  $0.5 \text{ mA cm}^{-2}$  for 8000 cycles under different strain states. Reproduced with permission.<sup>[139]</sup> Copyright 2018 Elsevier B.V.

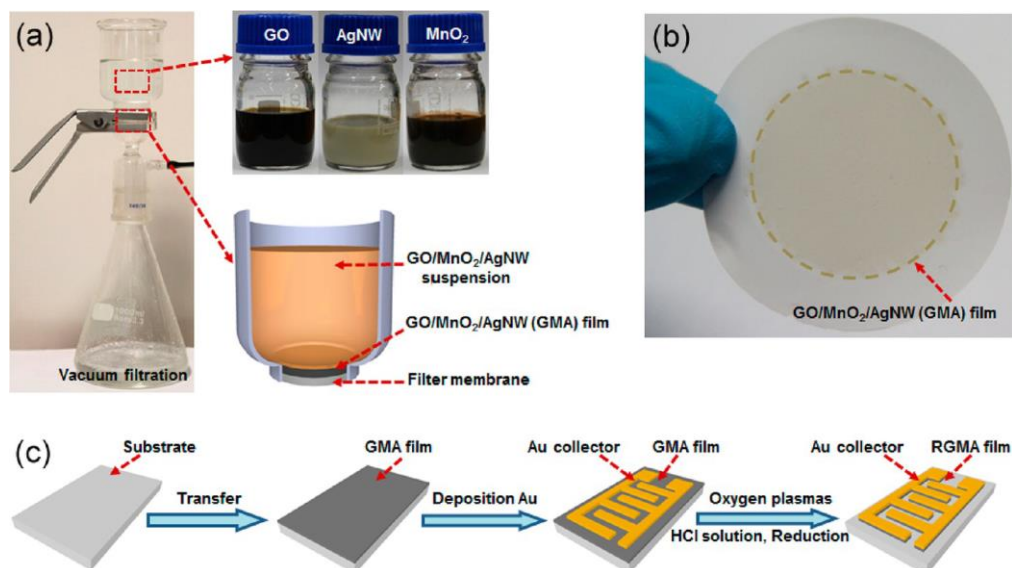


**Figure 17.** a) Different charge storage mechanisms of interdigital electrode-based on-chip MSCs. Reproduced with permission.<sup>[141]</sup> Copyright 2016 Tsinghua University Press and Springer-Verlag. b) Schematic illustration of the synthetic process of EG/mPANI sheets.

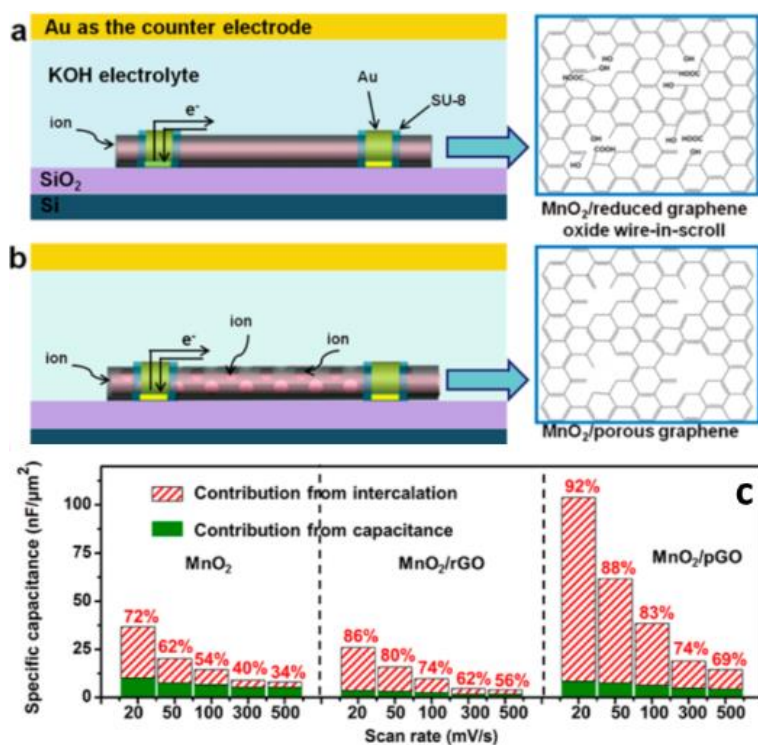
Reproduced with permission.<sup>[142]</sup> Copyright 2017 Wiley-VCH Verlag GmbH & Co. c)  
 Scheme of the fabrication of mPPy@RGO-POM Nano sheets. Reproduced with  
 permission.<sup>[143]</sup> Copyright 2017 Science China Press and Springer-Verlag.



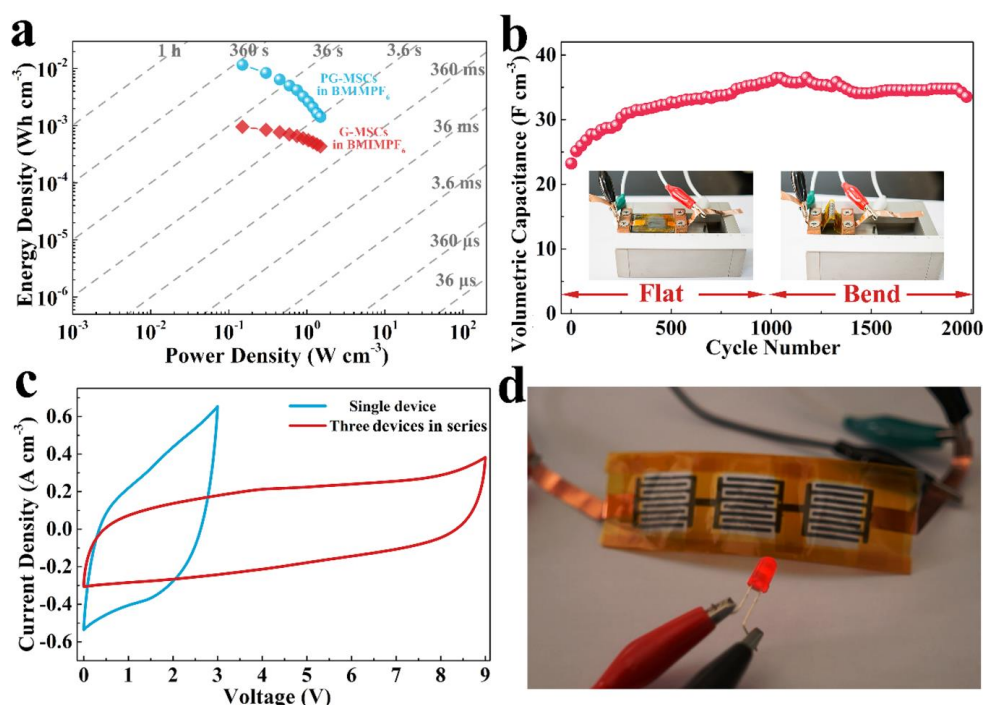
**Figure 18.** (a)-(f) Fabrication step of the MnO<sub>2</sub>/graphene-based MSC. (g) Description of the 2-D planar ion transport mechanism. (h) Specific capacitance values for the MSCs. (i) Capacitance retention (blue curve) and Coulombic efficiency (red curve) of the planar MSC. Reproduced with permission.<sup>[144]</sup> Copyright 2013 American Chemical Society.



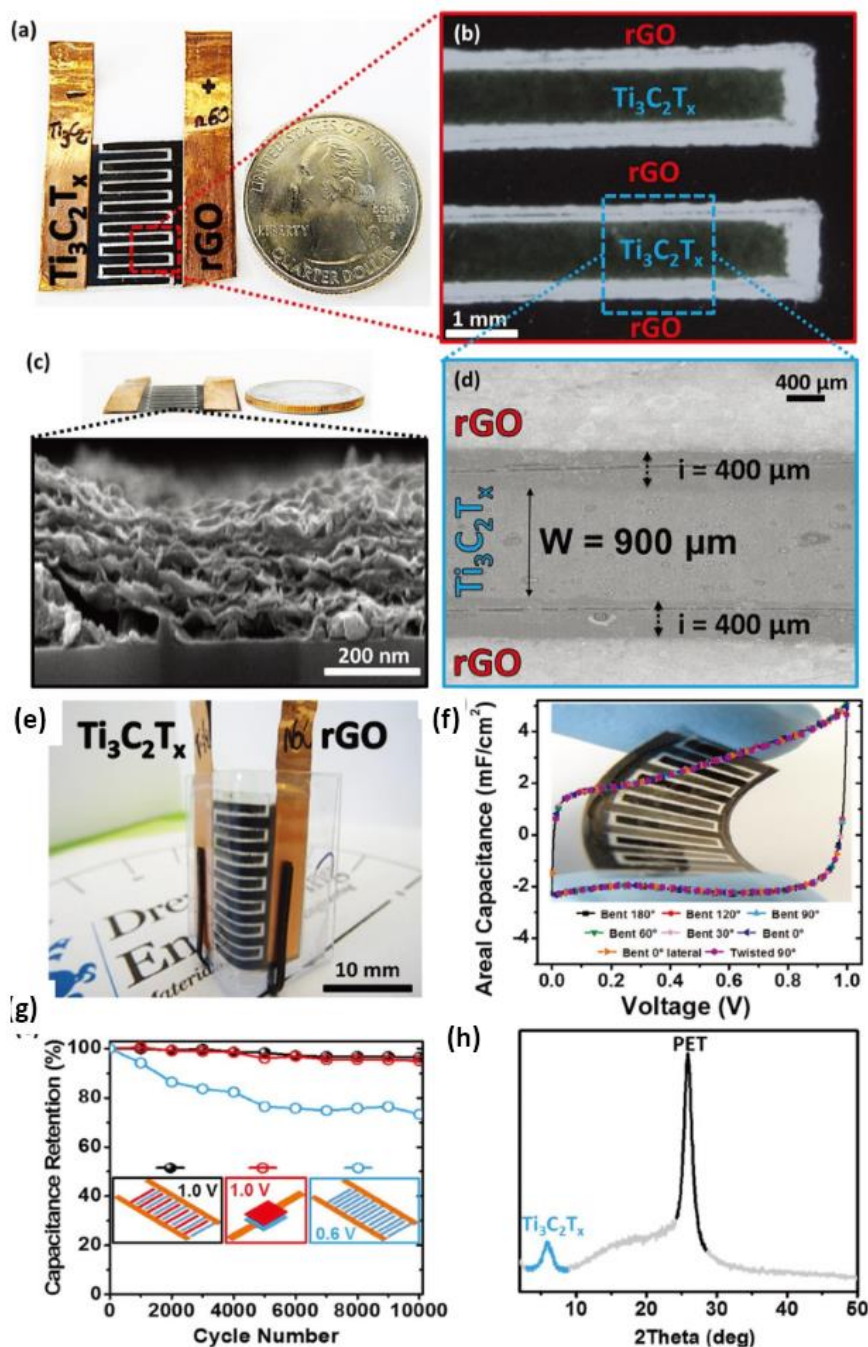
**Figure 19.** (a) Fabrication of the GMA ternary hybrid film via vacuum filtration of the mixture of GO, MnO<sub>2</sub>, and Ag-nanowire suspension. (b) Digital image of the as-obtained GMA film supported on the cellulose acetate membrane after the vacuum filtration. (c) Schematic illustration of the fabrication procedures for RGMA-MSC on an Al substrate. Reproduced with permission.<sup>[135]</sup> Copyright 2015 American Chemical Society.



**Figure 20.** (a) Schematic illustration of a  $\text{MnO}_2/\text{RGO}$  nanowire. Ions transport only through the gap between the graphene and the  $\text{MnO}_2$  nanowire. (b) Schematic illustration of a  $\text{MnO}_2/\text{pGO}$  nanowire. Ions transport through not only the gap between the graphene and the  $\text{MnO}_2$  nanowire but also the pores in the graphene. (c) Bar chart of total capacitance in  $\text{nF}/\mu\text{m}^2$  together with the percentage contribution from capacitance and intercalation as a function of different materials with scan rates of 20, 50, 100, 300, and 500  $\text{mV/s}$ . Reproduced with permission.<sup>[40]</sup> Copyright 2016 American Chemical Society.

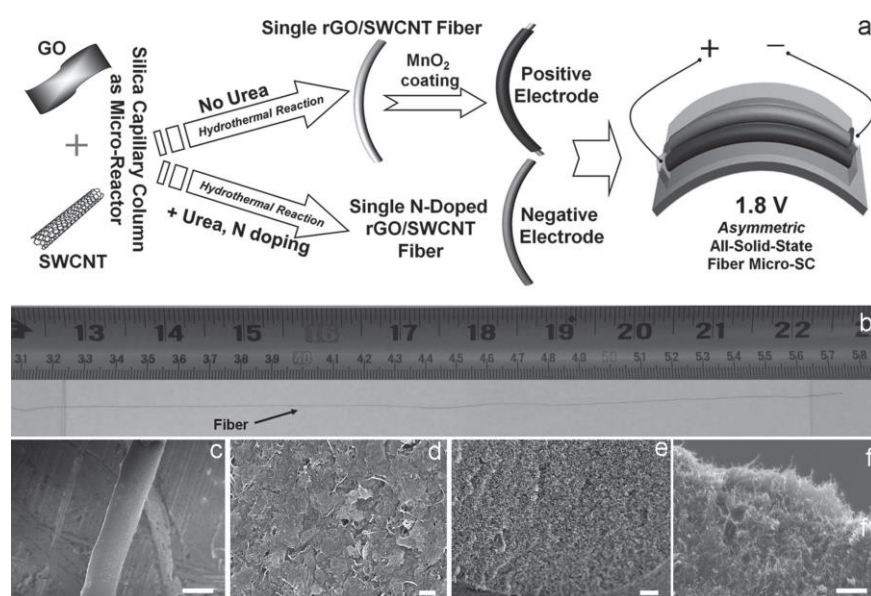


**Figure 21.** Electrochemical performance of PG-MSC. (a) Ragone plot of PG-MSC and G-MSC. (b) Cycling stability of PG-MSC at  $0.44 \text{ A cm}^{-3}$  for 2000 cycles under flat and bending state. The inserts are optical images of PG-MSC in flat and bend states. (c) CV curves at  $100 \text{ mV s}^{-1}$  of single and three serial PG-MSC. (d) Photograph of three serial PG-MSC used to power a light-emitting diode (LED). Reproduced with permission.<sup>[139]</sup> Copyright 2017 American Chemical Society.

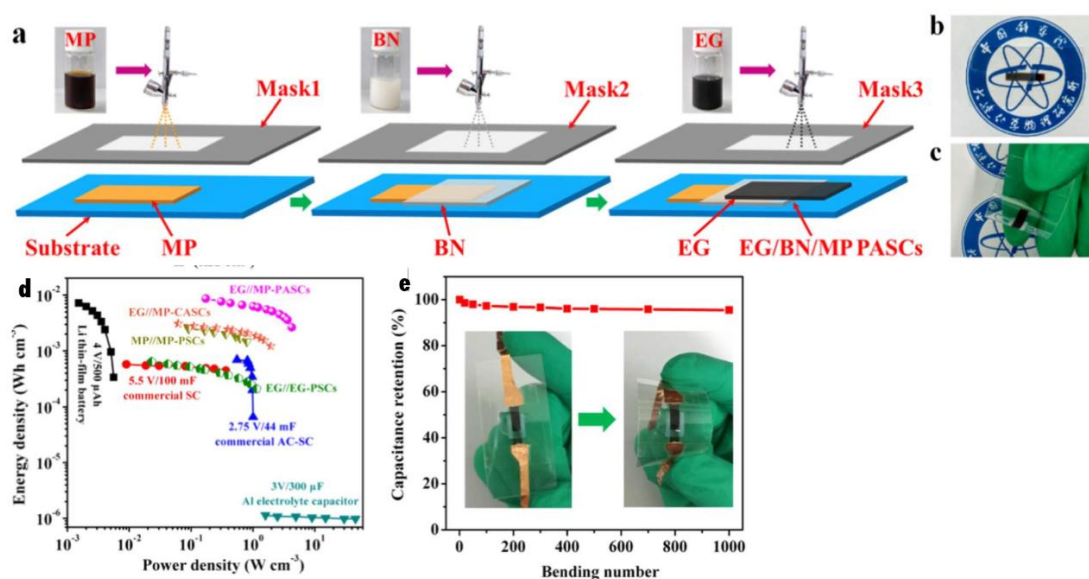


**Figure 22.** a) Digital image showing a top-view of the asymmetric MSC device along with a quarter U.S. dollar coin for size comparison, b) zoom-in image of  $\text{Ti}_3\text{C}_2\text{T}_x$  and RGO interdigitated electrode configurations and the interspace. c) Side view of the device with a U.S. quarter dollar coin and SEM cross-sectional image of the  $\text{Ti}_3\text{C}_2\text{T}_x$  electrode. d) Top-view SEM image of the interdigitated fingers, showing one  $\text{Ti}_3\text{C}_2\text{T}_x$  electrode between two RGO electrodes. e) MSC with two microscope slides to hold it at  $90^\circ$  angle. f) CV recorded at 2 mV

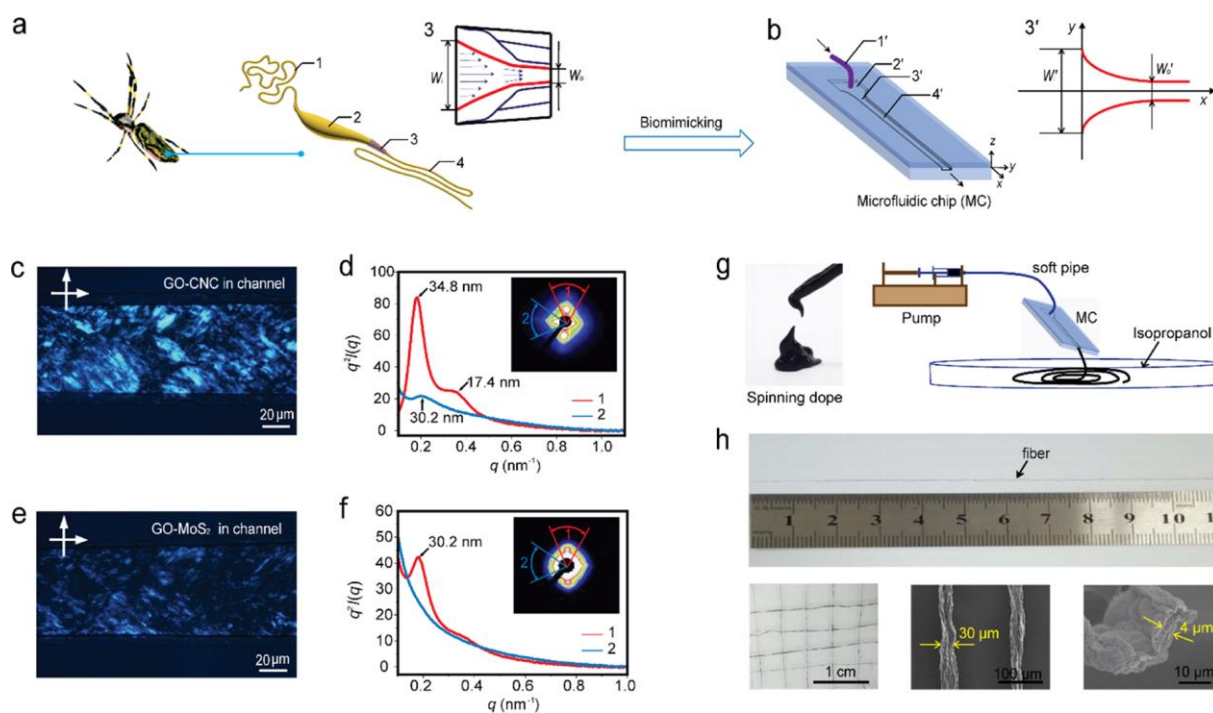
s<sup>-1</sup> while the device is bent and twisted at different angles, with a flexible MSC without a current collector in the background. g) Capacitance retention of the three different MSCs at 0.2 mA cm<sup>-2</sup> while held at an angle of 30°. From the left to the right interdigitated asymmetric MSC (black), sandwich asymmetric MSC (red), and interdigitated symmetric MSC (blue). h) XRD of the asymmetric interdigitated MSC after 10000 cycles. Reproduced with permission.<sup>[149]</sup> Copyright 2017 WILEY-VCH Verlag GmbH & Co.



**Figure 23.** (a) Schematic illustration of the design and fabrication of the asymmetric fibre-based MSC; (b) The optical image of a 26 cm-long RGO/SWCNT (GCF) all-carbon fibre; (c–f) SEM images of the GCF fibre: (c) overview, (d) surface, (e) cross-section, and (f) fractured end. Scale bars: 50  $\mu$  m for (c), 100 nm for (d), and 1  $\mu$  m for (e) and (f). Reproduced with permission.<sup>[153]</sup> Copyright 2014 WILEY-VCH Verlag GmbH & Co.

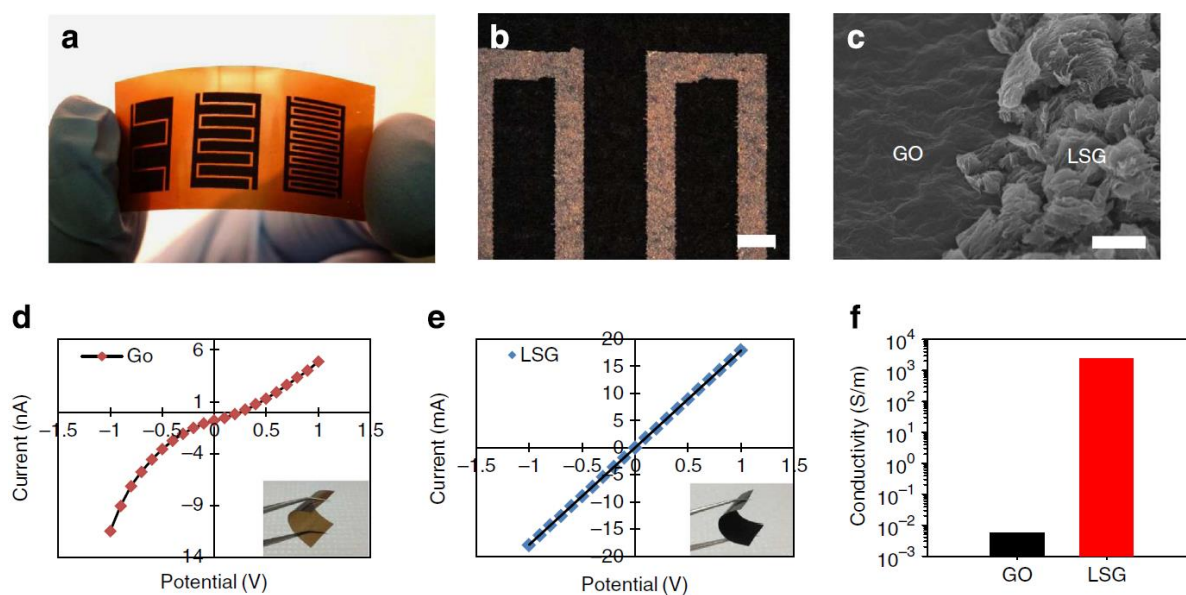


**Figure 24.** Fabrication and characterization of EG//MP-MSC based on EG/BN/MP monolithic film. (a) Schematic of the stepwise fabrication of EG//MP-MSC. (b, c) Digital image of EG//MP-PASC with flat (b) and bending (c) states on PET substrate. (d) Ragone plot of EG//MP-MSCs and other commercially available energy storage devices. (e) Cycling stability of EG//MP-MSC tested under repeated bending state. Insert is the photographs of EG//MP-MSC under flat and bending states. Reproduced with permission.<sup>[154]</sup> Copyright 2017 Elsevier B.V.

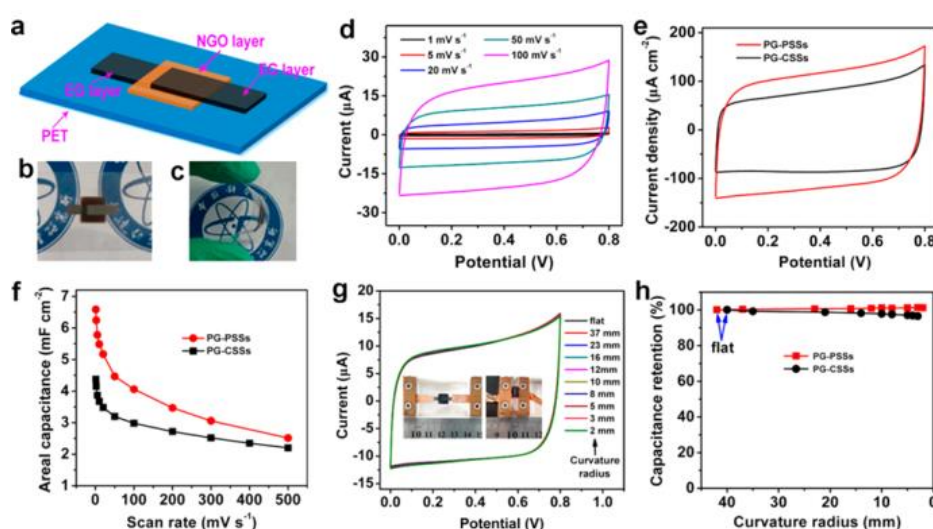


**Figure 25.** (a) Major ampullate gland of a *Nephila clavipes* with its winding tail (segment 1), central ampulla (segment 2), conical funnel (segment 3), and S-shaped duct (segment 4). (b) Biomimetic MC. (c–f) Liquid crystals formed in the MC channel under shearing: (c, d) POM and (e, f) SAXS patterns. (g) Schematic spinning process via a MC starting from the high-viscosity spinning dopes. (h) Ribbon-like microfibers. Reproduced with permission.<sup>[155]</sup>

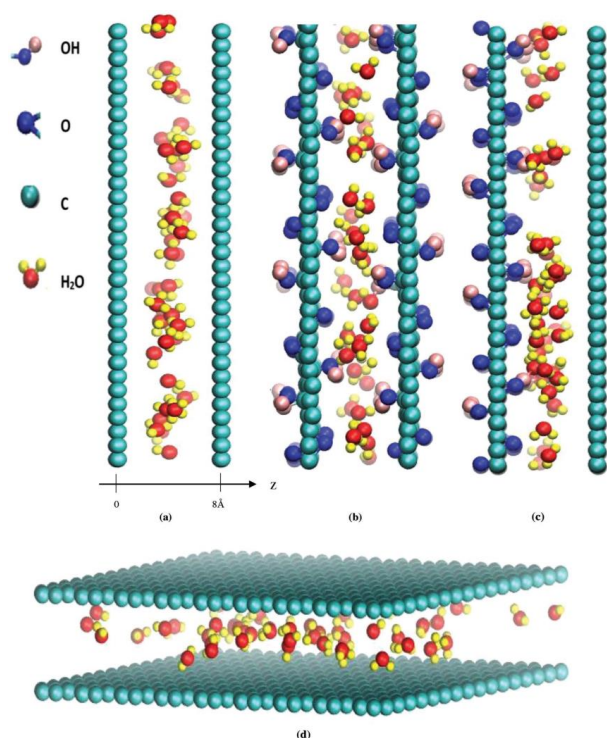
Copyright 2018 American Chemical Society.



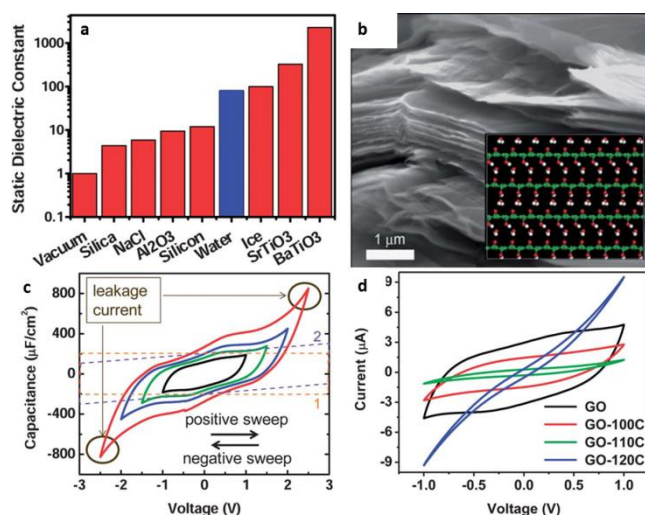
**Figure 26.** Characterization of LSG micro-devices (a) A digital photograph of the laser-scribed micro-devices. (b) An optical microscope image shows interdigitated fingers with 150-μm spacing. The dark area corresponds to LSG and the light area is GO. Scale bar, 200 μm. (c) A tilted-view SEM image shows the direct reduction and expansion of the GO film after exposure to the laser beam. Scale bar, 10 μm. (d) and (e) show the I–V curves of GO and LSG, respectively. (f) A comparison of electrical conductivity values for GO and LSG. Reproduced with permission.<sup>[157]</sup> Copyright 2013 Macmillan Publishers Limited.



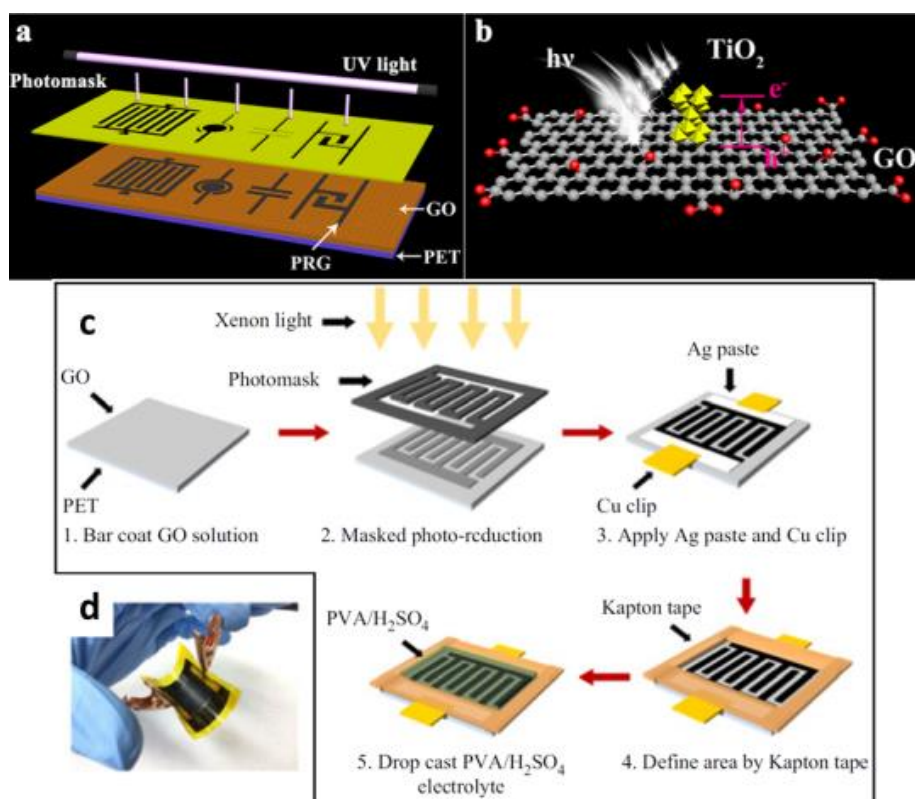
**Figure 27.** (a) Schematic of a rectangle-shaped PG-PSS made up of an EG/NGO/EG layer-structured film on a single PET substrate. (b,c) Optical images of rectangle-shaped PG-PSSs under (b) flat and (c) bending states. (d) The CV of the rectangle-shaped PG-PSSs with  $\text{H}_2\text{SO}_4/\text{PVA}$  gel electrolyte, and scan rates from 1 to  $100 \text{ mV s}^{-1}$ . (e) The CV of the rectangle-shaped PG-PSSs and PG-CSSs with a scan rate of  $50 \text{ mV s}^{-1}$ . (f) Performance comparison of areal capacitance of PG-PSSs with PG-CSSs. (g) The CV curve of the rectangle-shaped PG-PSSs bent at different states from  $42^\circ$  (almost flat, insert) to  $2 \text{ mm}$  ( $\geq 180^\circ$ , insert). (h) Capacitance retention as a function of curvature radius. Reproduced with permission.<sup>[162]</sup> Copyright 2017 American Chemical Society.



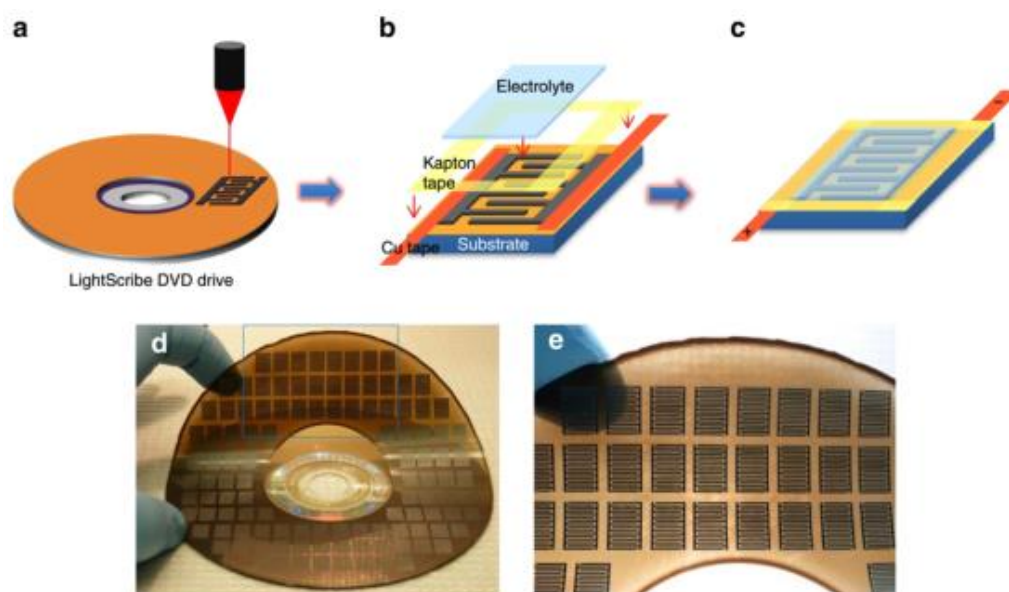
**Figure 28.** (a) Two RGO sheets with the distance of  $8 \text{ Å}$ , (b) two GO sheets with the distance of  $8 \text{ Å}$ , and (c) one GO and one RGO sheets with the distance of  $8 \text{ Å}$ , respectively; (d) is a 3D schematic of this model in (a). Reproduced with permission.<sup>[55]</sup> Copyright 2018 WILEY-VCH Verlag GmbH & Co.



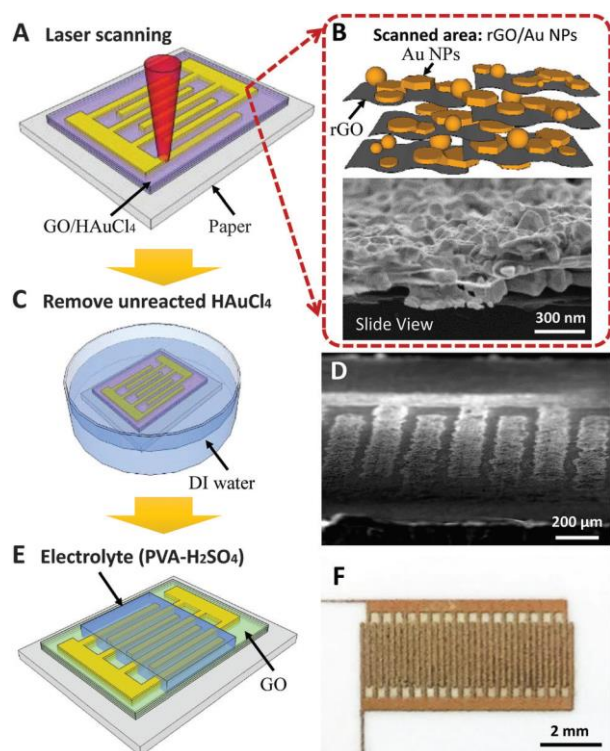
**Figure 29.** a) Dielectric constants of various inorganic materials. b) Cross sectional SEM image of a hydrated graphene oxide film. The insert shows the hydrogen bonding between water molecules and graphene oxide sheets. c) Relationship between dielectric capacitance and voltage of the water-dielectric capacitor in which the hydrated GO film is used as the dielectric spacer. The dashed rectangular curves are CV profiles for 1: ideal dielectric capacitor and 2: dielectric capacitor with resistance. d) CV of the hydrated GO film and films annealed at 100, 110 and 120°C. Reproduced with permission.<sup>[163]</sup> Copyright 2012 The Royal Society of Chemistry.



**Figure 30.** (a) Schematic of one-step fabrication process for photo reduction graphene based MSC (PRGMSC) with different geometries. (b) Photo reduction mechanism of  $\text{TiO}_2$  nanoparticle-assisted reduction of a GO film under ultraviolet irradiation. Reproduced with permission.<sup>[192]</sup> Copyright 2017 American Chemical Society. (c) Schematic illustration of the fabrication process of flash printed (FP)-MSC and (d) optical image of a flexible FPMSC. Reproduced with permission.<sup>[41]</sup> Copyright 2018 ETIR.



**Figure 31.** (a–c) Schematic fabrication process of planar MSCs using a using a LightScribe DVD burner. (d,e) Over 100 micro-supercapacitors are written on a single disc. Reproduced with permission.<sup>[28]</sup> Copyright 2013 Macmillan Publishers Limited.



**Figure 32.** Schematic illustration and photos of fabrication of RGO/Au-MSCs (micro-supercapacitors) onto a paper substrate. The fabrication process includes: (A) direct FS laser writing of RGO/Au microelectrodes, (B) the SEM image of RGO/Au microelectrodes, (C) removal of unreacted HAuCl<sub>4</sub> by rinsing in DI water, (D) SEM image of the interdigitated RGO/Au microelectrodes, (E) spreading the PVA/H<sub>2</sub>SO<sub>4</sub> electrolyte onto the microelectrodes, and (F) the optical image of the final RGO/Au FS-MSC. Reproduced with permission.<sup>[198]</sup> Copyright 2016 The Royal Society of Chemistry.

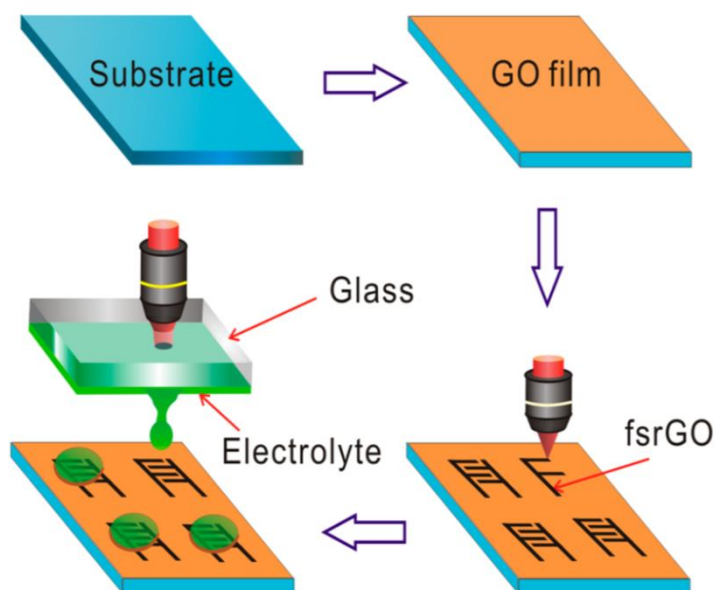
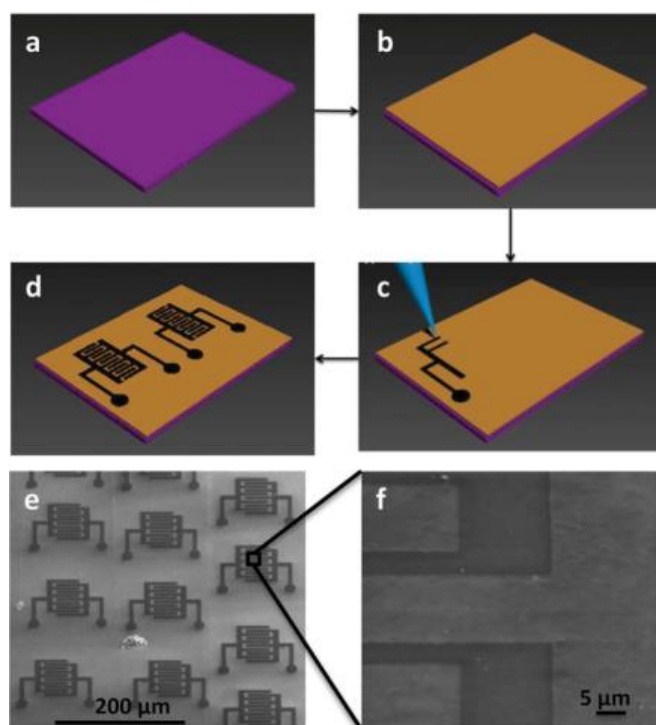
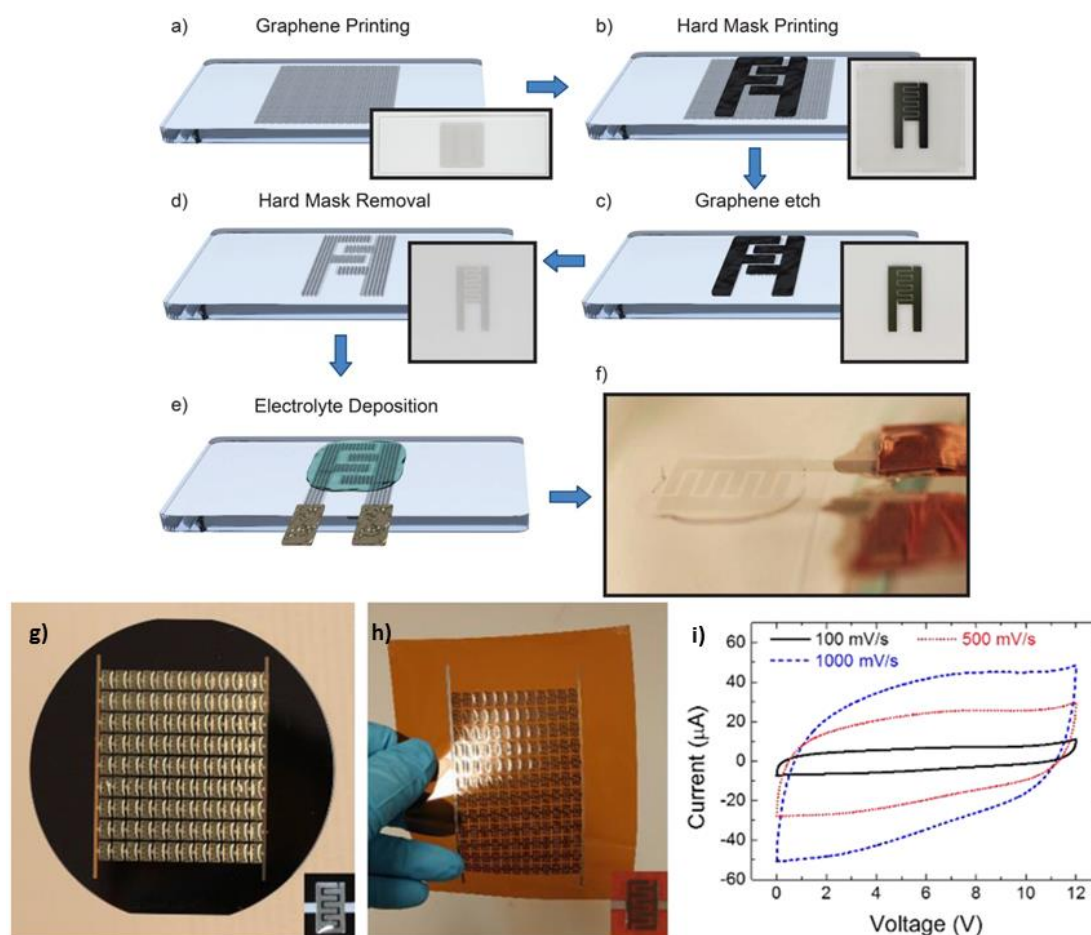


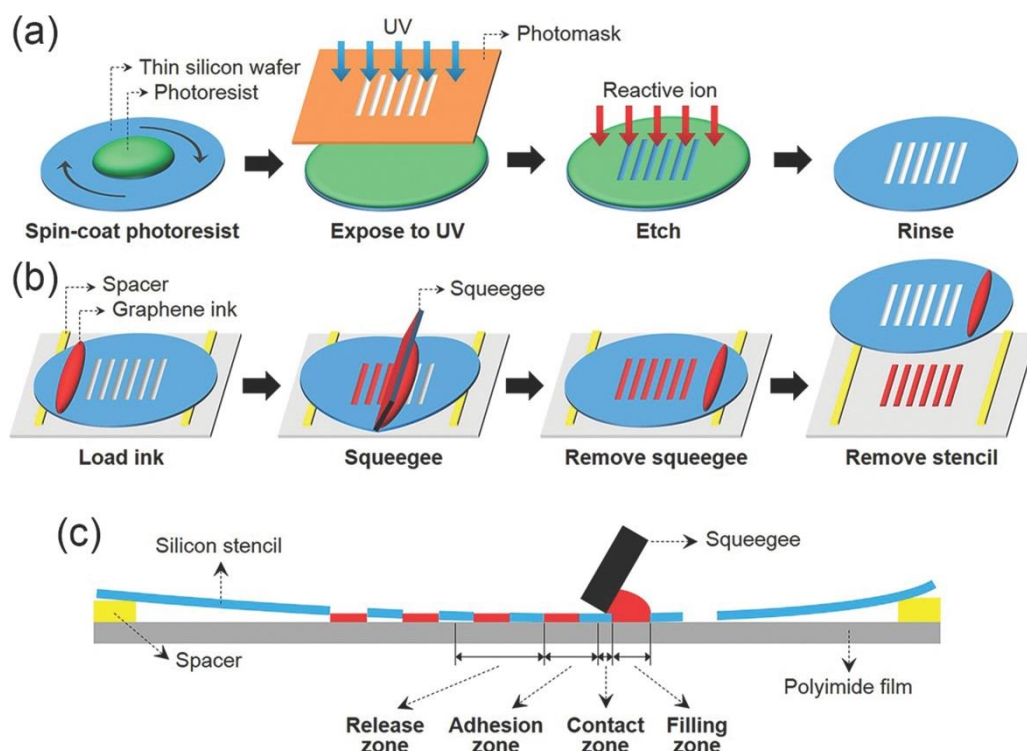
Figure 33. Fabrication of integrated MSC on a GO film using fs laser processing. The micro electrolyte droplet is transferred on top of the interlaced microelectrodes using the fsLIFT technique. Reproduced with permission.<sup>[199]</sup> Copyright 2018 American Chemical Society.



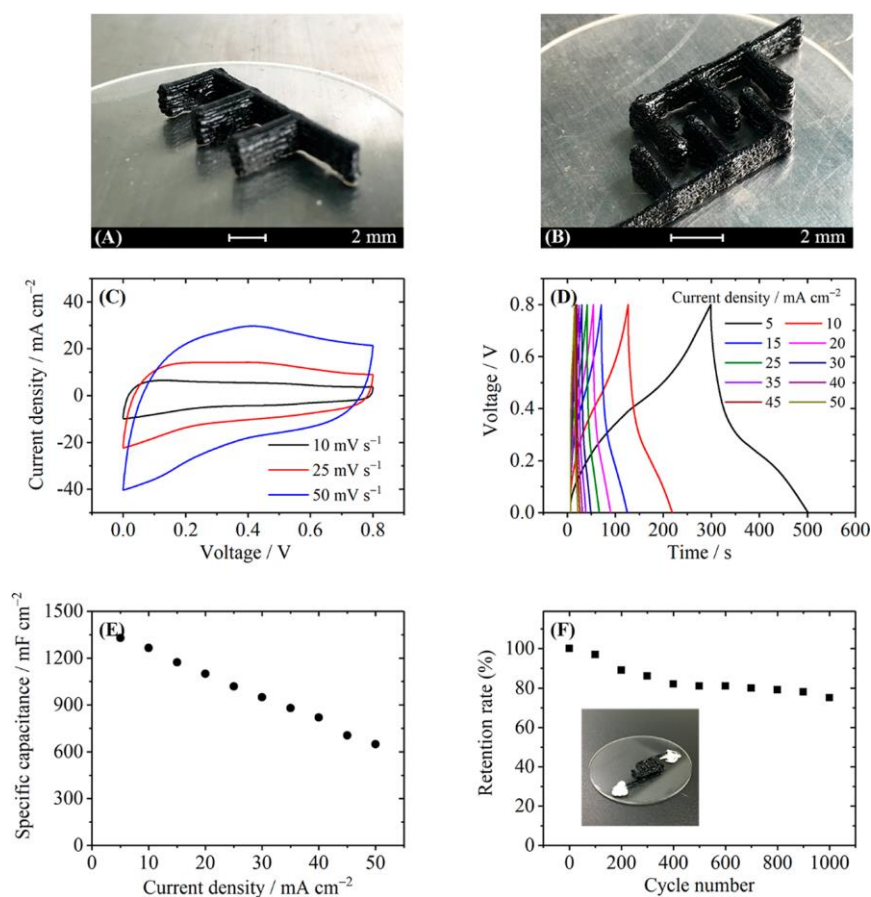
**Figure 34.** Fabrication of MSC with FIB-RGO (a)  $\text{SiO}_2$  layer on a silicon substrate (b) GO is spin-coated (c) RGO structures written by FIB to produce (d) interdigitated devices (e) Individual MSC (f) featuring a  $1\ \mu\text{m}$  inter electrode spacing. Reproduced with permission.<sup>[200]</sup> Copyright 2015 WILEY-VCH Verlag GmbH & Co.



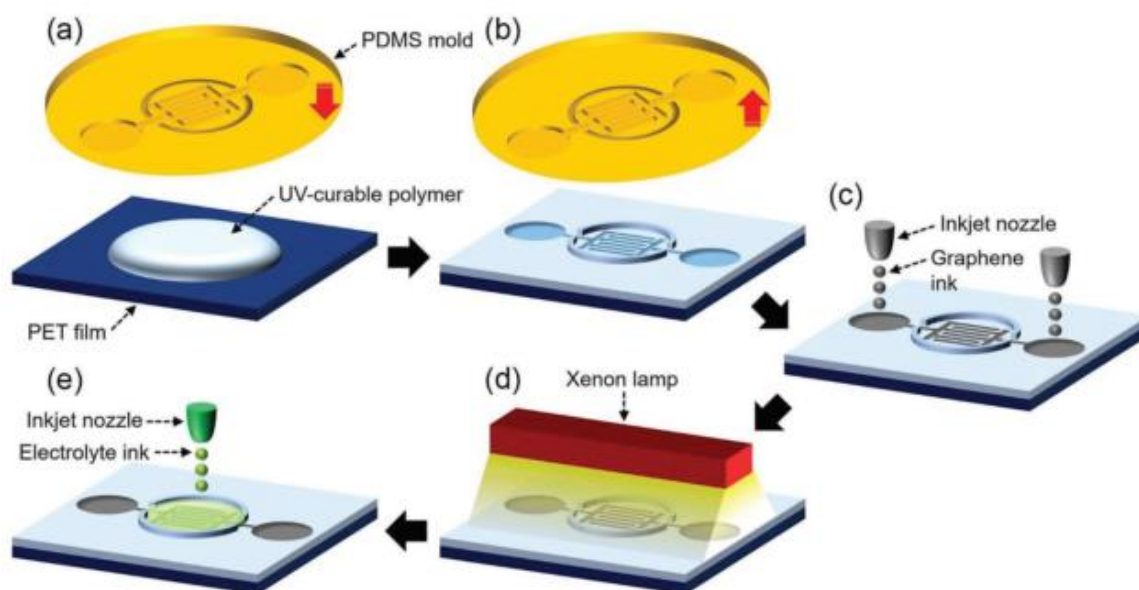
**Figure 35.** Schematic of the fabrication process of the transparent MSC. (a) Graphene flakes were printed on the glass substrate. (b) A hard mask was printed with silver ink. (c) Exposed graphene flakes were etched with  $O_2$  plasma. (d) The hard mask was removed with nitric acid solution. (e) Gel electrolyte was deposited by drop casting. (f) digital photograph of a device during characterization, with fingers of  $600\ \mu\text{m}$  wide,  $2.5\ \text{mm}$  long and the gaps between fingers are  $200\ \mu\text{m}$ . Reproduced with permission.<sup>[202]</sup> Copyright 2017 The Royal Society of Chemistry. (g, h) Images of MSC array on Kapton. (i) CV of MSC array at different scan rates with a voltage window of  $12\ \text{V}$ . Reproduced with permission.<sup>[203]</sup> Copyright 2017 American Chemical Society.



**Figure 36.** a) Fabrication of a thin silicon stencil through conventional lithography techniques. b) Schematic of screen printing using the silicon stencil and a pristine graphene ink. c) Cross-sectional illustration of the screen printing method with the flexible silicon stencil during printing. Reproduced with permission.<sup>[205]</sup> Copyright 2014 WILEY-VCH Verlag GmbH & Co.

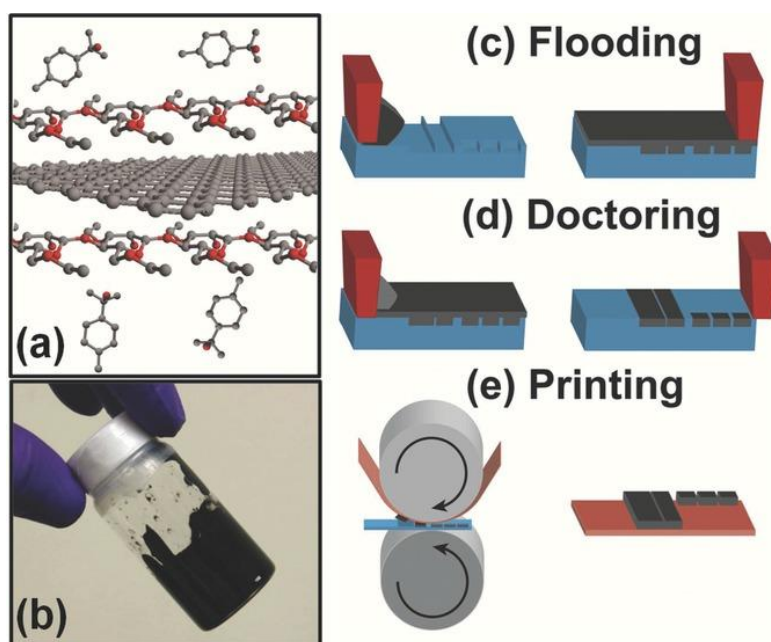


**Figure 37.** 3D printed planar MSC and its capacitive performance. (A, B) Optical images of the printed interdigital electrodes. (C) CV of the planar MSC at different scanning rates. (D) The GCD curves at different current densities. (E) The specific capacitances at different current densities. (F) Capacitance retention rate for 1000 cycles at 50  $\text{mA cm}^{-2}$ . Reproduced with permission.<sup>[206]</sup> Copyright 2018 American Chemical Society.



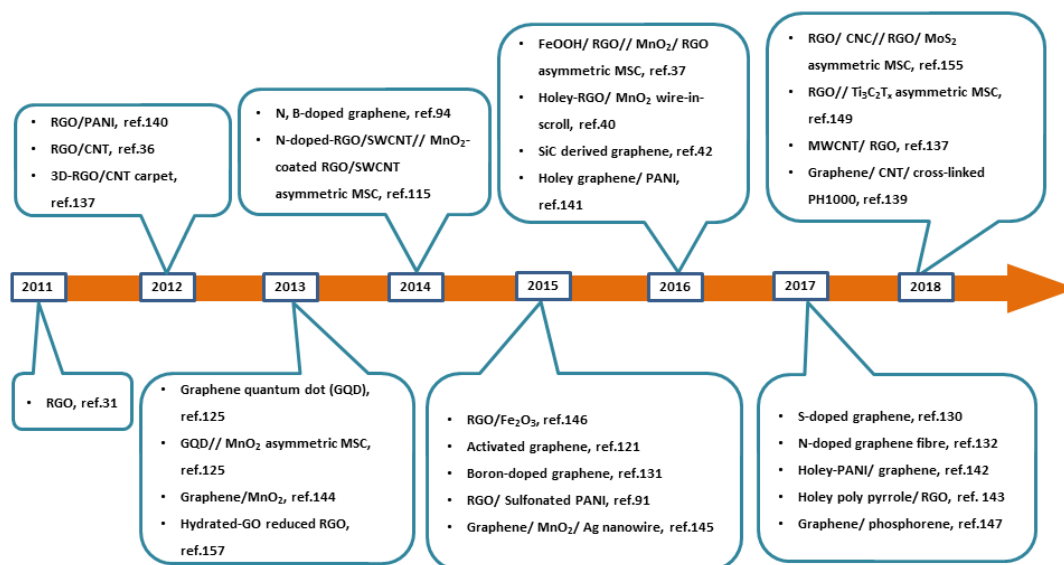
**Figure 38.** Fabrication of MSC via the SCALE process. a) UV-curable polymer was coated on a PET film and pressed by a PDMS stamp. b) The stamp was delaminated from the polymer coating after UV curing of the photopolymer. c) Graphene ink was inkjet-printed onto the ink receivers for electrodes. d) The printed graphene was photonicallly. e) Electrolyte ink was inkjet-printed onto the electrolyte receivers. Reproduced with permission.<sup>[207]</sup>

Copyright 2017 WILEY-VCH Verlag GmbH & Co.

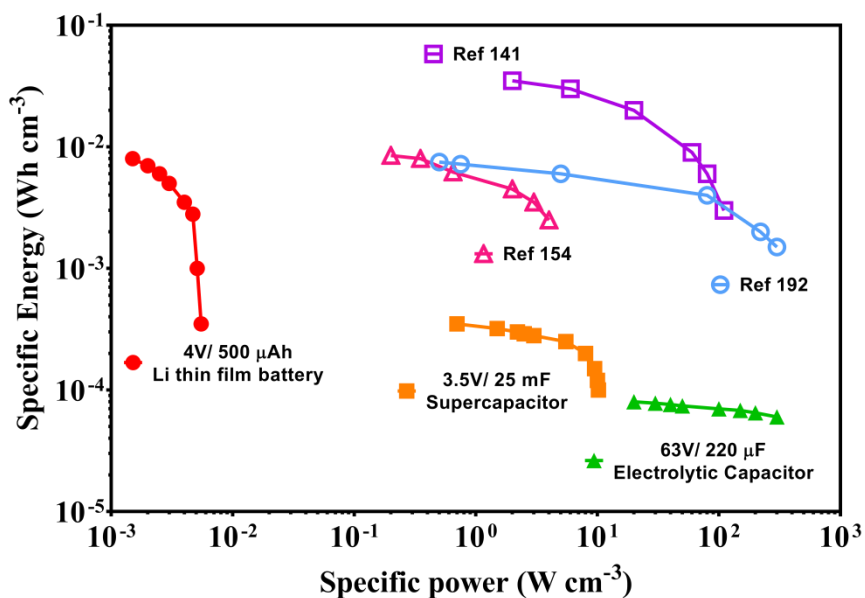


**Figure 39.** Development of the graphene ink for gravure printing. (a) Schematic of the ink. (b) Optical image of the formulated ink. (c-e) Illustration of the gravure printing method decomposed into three steps: (c) flooding of the gravure cells; (d) doctoring; (e) printing.

Reproduced with permission.<sup>[208]</sup> Copyright 2014 WILEY-VCH Verlag GmbH & Co.



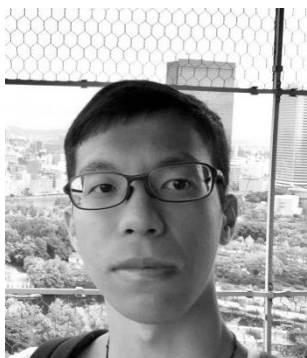
**Figure 40.** Time line of development of graphene-based MSCs. (Asymmetric designs are specifically identified by “//”)



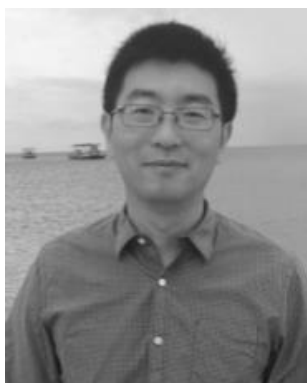
**Figure 41.** Ragone plot comparison of lithium thin-film battery, conventional supercapacitor, electrolytic capacitor and some advanced Graphene-based planar MSCs (ref 141, 154, 192).<sup>[141, 154, 192, 208]</sup>

**Table 1.** Summary of recent advances in graphene-based micro-supercapacitors

Electrode materials	Substrate	Electrolyte	Specific capacitance	Cycle stability	Energy density	Power density	Fabrication Technique	Ref.
Porous RGO film	PET	PVA/ H <sub>2</sub> SO <sub>4</sub>	37.95 mF cm <sup>-2</sup>	95% retained after 10000 cycles	1.45 mWh cm <sup>-3</sup>	-	Ice-drying, laser carve	(57)
RGO	PET	EMImNTF <sub>2</sub>	233 F cm <sup>-3</sup> (Vol.)	100 % retained after 10000 cycles	7.7 mW h cm <sup>-3</sup>	312 W cm <sup>-3</sup>	Photolithography	(192)
Electrochemically exfoliated graphene	Paper	PVA/H <sub>2</sub> SO <sub>4</sub>	5.4 mF cm <sup>-2</sup>	90 % retained after 5000 cycles	-	-	Direct ink printing	(201)
RGO	Si/SiO <sub>2</sub>	1 M Na <sub>2</sub> SO <sub>4</sub>	102 mF cm <sup>-2</sup>	95 % retained after 1000 cycles	-	-	Focused ion beam	(200)
Graphene	Glass & PET	PVA/ H <sub>2</sub> SO <sub>4</sub>	41.8 F cm <sup>-3</sup> (Vol.)	95 % retained after 1000 cycles	-	-	Direct ink printing	(224)
RGO/MWCNTs	PET	PVA/H <sub>3</sub> PO <sub>4</sub>	46.6 F cm <sup>-3</sup> (Vol.)	88.6 % retained after 10,000 cycles	6.47 mW h cm <sup>-3</sup>	10 mW cm <sup>-3</sup>	Direct Laser writing	(138)
Sulfur-doped graphene	Si/SiO <sub>2</sub>	PVA/ H <sub>2</sub> SO <sub>4</sub>	553 mF cm <sup>-2</sup>	95. % retained after 10000 cycles	3.1 mW h cm <sup>-3</sup>	1191 W cm <sup>-3</sup>	Photolithography	(130)
Activated graphene/ Exfoliated graphene	Si	PVA/ H <sub>2</sub> SO <sub>4</sub>	89.5mF/cm <sup>-2</sup>	99.6% retained after 10,000cycles	4.0 mW h cm <sup>-3</sup>	18.9 W cm <sup>-3</sup>	Oxygen plasma etching	(121)
Graphene quantum dot	Au	EMIMBF <sub>4</sub> /A N electrolyte	468.1 μF cm <sup>-2</sup>	97.8% retained after 5000 cycles	0.474 μWh cm <sup>-2</sup>	56.7 μW cm <sup>-2</sup>	Electrophoretic deposition	(125)
Boron-doped graphene	Polyimide	PVA/ H <sub>2</sub> SO <sub>4</sub>	16.5 mF cm <sup>-2</sup>	90% retained after 12,000 cycles	-	-	Laser induction	(131)
Nitrogen-doped RGO	Free-standing fibre	H <sub>3</sub> PO <sub>4</sub> /PVA * EMIBF <sub>4</sub> /PVD F-HFP #	1132 mF cm <sup>-2</sup> * 306.3 mF cm <sup>-2</sup> #	97.1% retained after 10,000 cycles* -#	-* 95.7 μWh cm <sup>-2</sup> #	-* 15 W cm <sup>-2</sup> #	Thermal reduction	(132)
Graphene/carbon nanotube/cross-linked PI1000 film	Rubber substrate	H <sub>3</sub> PO <sub>4</sub> /PVA	107.5 mF cm <sup>-2</sup>	93.2% retained after 8000 cycles	0.54 μWh cm <sup>-2</sup>	1.22 mW cm <sup>-2</sup>	Mask-assisted filtration	(139)
Hydro-RGO/ PANI	SiO <sub>2</sub>	PVA/ H <sub>2</sub> SO <sub>4</sub>	271.1 F·cm <sup>-3</sup> (Vol.)	99.5% retained after 5000 cycles	24.1 cm <sup>-3</sup> mWh	1,000 W cm <sup>-3</sup>	Hydrazine hydrate treatment	(141)
Hydro-PANI/ exfoliated graphene	Si/SiO <sub>2</sub>	1M H <sub>2</sub> SO <sub>4</sub>	3 mF cm <sup>-2</sup>	94% retained after 1000 cycles	6.67 mWh cm <sup>-3</sup>	480 W cm <sup>-3</sup>	Filtration and oxygen plasma etching	(142)
Hydro-poly pyrrole/ RGO- poly oxometalate	Exfoliated graphene-Nylon	PVA/ H <sub>2</sub> SO <sub>4</sub>	115 mF cm <sup>-2</sup>	80% retained after 2000 cycles	4.8 mWh cm <sup>-3</sup>	645.1 mW cm <sup>-3</sup>	Hydrothermal reduction	(143)
RGO/ MnO <sub>2</sub> / Ag wire film	Alumina/ PET	0.5 M Na <sub>2</sub> SO <sub>4</sub> * Ionic liquid gel #	4.42 F cm <sup>-3</sup> * 2.72 F cm <sup>-3</sup> #	- * 90.3% retained after 6000 cycles #	0.45 mWh cm <sup>-3</sup> * 2.3 mWh cm <sup>-3</sup> #	89.1 mW cm <sup>-3</sup> * 162.0 mW cm <sup>-3</sup> #	Oxygen etching	(77)
Hydro-RGO/ MnO <sub>2</sub> nanowire in scroll	Si/SiO <sub>2</sub>	6M KOH	104 nF/μm <sup>2</sup>	-	-	-	Hydrazine hydrate treatment	(40)
RGO/ Fe <sub>2</sub> O <sub>3</sub>	PET	PVA/ KOH	347μF cm <sup>-2</sup>	92.08% retained after 32,000 cycles	1.61 mWh cm <sup>-3</sup>	9.82 W cm <sup>-3</sup>	Photolithography	(146)
Graphene/ Phosphorene	PET	BMIMPF <sub>6</sub> ionic liquid	37 F cm <sup>-3</sup> (Vol.)	84.5% retained after 10,000 cycles	11.6 cm <sup>-3</sup> mWh	1.5 W cm <sup>-3</sup>	Mask-assisted filtration	(147)
RGO/ Mxene	PET	PVA/ H <sub>2</sub> SO <sub>4</sub>	2.4 mF cm <sup>-2</sup>	97% retained after 10,000 cycles	8.6 mW h cm <sup>-3</sup>	-	Mask-assisted printing	(149)
RGO/FeOOH// MnO <sub>2</sub>	Polyimide	PVA/ LiCl	21.9 mF cm <sup>-2</sup>	84% retained after 2000 cycles	2.4 cm <sup>-3</sup> mWh	2.891 W cm <sup>-3</sup>	Laser induction	(37)
Exfoliated graphene// MnO <sub>2</sub> / poly (3,4-ethylene diglythiophene)-poly (styrene sulfonate)	PET	PVA/ LiCl	9.6 mF cm <sup>-2</sup>	92% retained after 5000 cycles	8.6 cm <sup>-3</sup> mWh	4.2 W cm <sup>-3</sup>	Mask-assisted printing	(154)
RGO/ cellulose nanocrystals// MnO <sub>2</sub>	Kapton	PVA/H <sub>3</sub> PO <sub>4</sub>	121 F cm <sup>-3</sup> (Vol.)	97% retained after 10,000 cycles	100 μWh cm <sup>-2</sup>	~10 <sup>2</sup> mW cm <sup>-2</sup>	Spinning	(155)
RGO	PET	PVA/ H <sub>2</sub> SO <sub>4</sub>	233.0 F cm <sup>-3</sup> (Vol.)	~100% retained after 10,000 cycles	7.7 cm <sup>-3</sup> mWh	312 W cm <sup>-3</sup>	TiO <sub>2</sub> -assisted UV reduction	(192)
RGO/ PANI	Polystyrene	PVA/ H <sub>2</sub> SO <sub>4</sub>	1329 mF cm <sup>-2</sup>	75% retained after 1000 cycles	-	-	3D printing	(206)
Graphene	PET	PVA/ H <sub>2</sub> SO <sub>4</sub>	5.0 μF cm <sup>-2</sup>	-	-	-	Roll-to-roll stamping	(209)



Jiaxing Liang is a Master of Philosophy candidate in the faculty of Chemical Engineering at the University of New South Wales under the supervision of Dr Da-wei Wang. He received his bachelor degree in New Energy Materials and Devices from South China Normal University in 2017. His major research interest is electrochemical energy storage, including lithium-ion batteries, supercapacitors and lithium-ion capacitors.



Da-Wei Wang is currently a Senior Lecturer and a Scientia Fellow in School of Chemical Engineering, UNSW. His research interest spreads from the synthesis and surface/interface processes of two-dimensional energy materials, to the design of advanced electrochemical energy devices, including supercapacitors, metal/sulfur batteries, metal-ion batteries and electrolyzers. Da-Wei has contributed 2 book chapters, >100 journal publications, 8 patents and over 20 keynote/invited presentations, which received >13,000 citations with an H-index of 40 (Google Scholar).



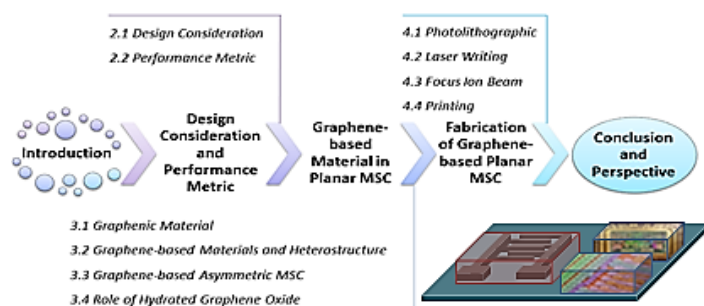
Prof. Francesca Iacopi has 20 years' industrial and academic expertise in Materials and Devices for Semiconductor Technologies, with over 120 peer-reviewed publications and 9 granted patents. Her research emphasis is on the translation of basic scientific advances in nanomaterials and novel device concepts into industrial processes. She was recipient of an MRS Gold Graduate Student Award (2003), an ARC Future Fellowship (2012), and a Global Innovation Award in Washington DC (2014). She is currently Head of Discipline, Communications and Electronics, in the Faculty of Engineering and IT of the University of Technology Sydney.

**This review provides an analysis of the extensive recent advances in graphene -based micro -supercapacitors.** There is an increasing interest in miniaturized power sources that can integrated with electronics microsystems, rigid or flexible. Graphenic carbon, in all of its different forms, has proven a versatile, robust and high -performance material for electrodes in micro -supercapacitors. Substantial further advances are expected from the control of the pore structure of the material, the tailoring of porosity to the electrolyte and the use of hybrid material combinations.

**Keywords** micro- supercapacitors, graphene, thin -films, electrochemical performance, fabrication

L. Jiaying, A.K. Mondal, D. Wang\*, F. Iacopi\*

**Title** Graphene-based planar micro-supercapacitors: Recent advances and future challenges



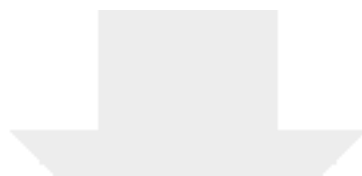


[Click here to access/download](#)

**Production Data**

[RightsLink Printable License-figure1.pdf](#)

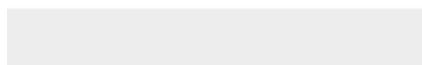
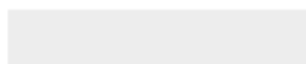


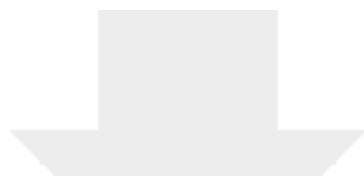


[Click here to access/download](#)

**Production Data**

[RightsLink Printable License-figure10.pdf](#)

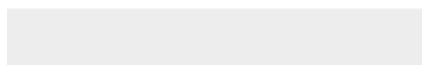
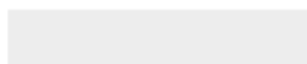


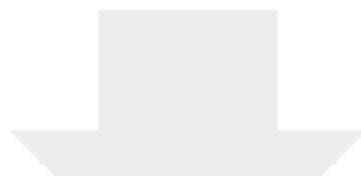


[Click here to access/download](#)

**Production Data**

[RightsLink Printable License-figure13.pdf](#)

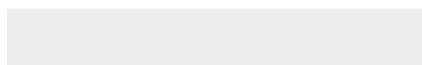
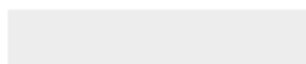


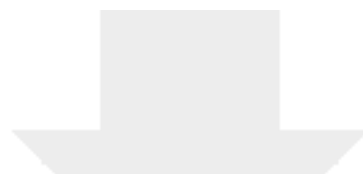


[Click here to access/download](#)

**Production Data**

[RightsLink Printable License-figure14.pdf](#)

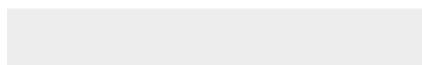
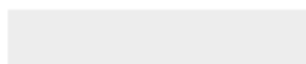


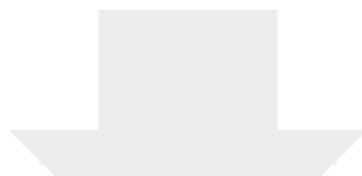


[Click here to access/download](#)

**Production Data**

[RightsLink Printable License-figure15.pdf](#)

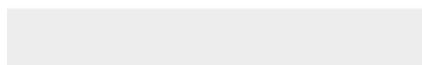
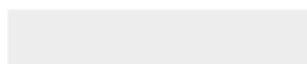




[Click here to access/download](#)

**Production Data**

[RightsLink Printable License-figure16.pdf](#)





[Click here to access/download](#)

**Production Data**

[RightsLink Printable License-figure17a.pdf](#)





[Click here to access/download](#)

**Production Data**

[RightsLink Printable License-figure17b.pdf](#)



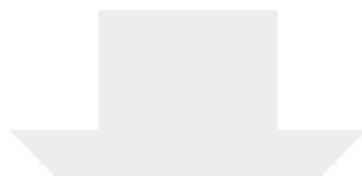


[Click here to access/download](#)

**Production Data**

[RightsLink Printable License-figure17c.pdf](#)

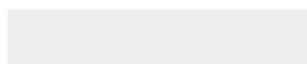


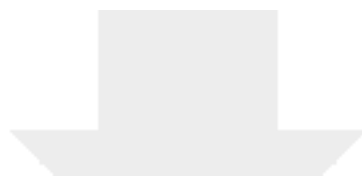


[Click here to access/download](#)

**Production Data**

[RightsLink Printable License-figure22.pdf](#)

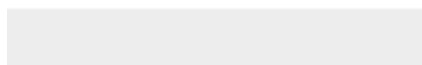
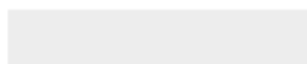


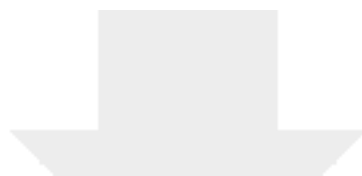


[Click here to access/download](#)

**Production Data**

[RightsLink Printable License-figure23.pdf](#)

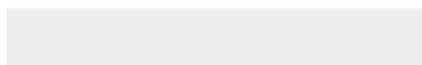




[Click here to access/download](#)

**Production Data**

[RightsLink Printable License-figure24.pdf](#)





[Click here to access/download](#)

**Production Data**

[RightsLink Printable License-figure26 and 31.pdf](#)

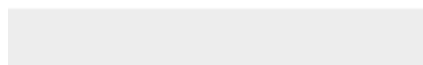
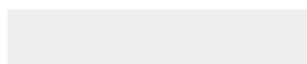


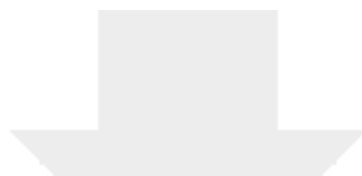


[Click here to access/download](#)

**Production Data**

[RightsLink Printable License-figure30 cd.pdf](#)

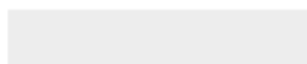


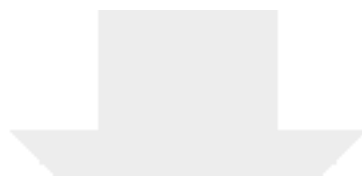


[Click here to access/download](#)

**Production Data**

[RightsLink Printable License-figure34.pdf](#)

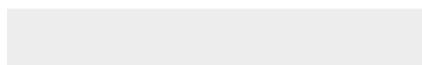
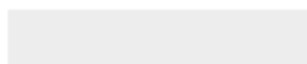


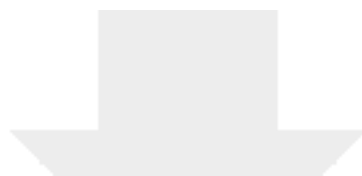


[Click here to access/download](#)

**Production Data**

[RightsLink Printable License-figure36.pdf](#)

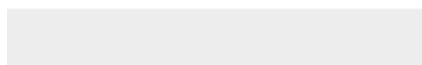
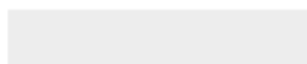


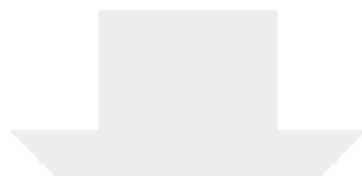


[Click here to access/download](#)

**Production Data**

[RightsLink Printable License-figure38.pdf](#)

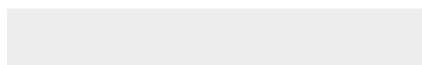
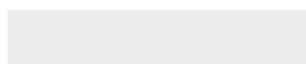




[Click here to access/download](#)

**Production Data**

[RightsLink Printable License-figure39.pdf](#)





[Click here to access/download](#)

**Production Data**

[RightsLink Printable License-figure3a,b.pdf](#)



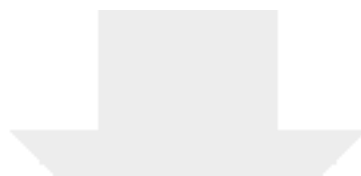


[Click here to access/download](#)

**Production Data**

[RightsLink Printable License-figure3c and 28.pdf](#)

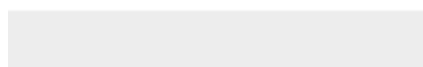
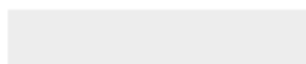




[Click here to access/download](#)

**Production Data**

[RightsLink Printable License-figure3d.pdf](#)



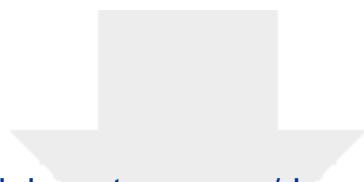


[Click here to access/download](#)

**Production Data**

[RightsLink Printable License-figure4.pdf](#)

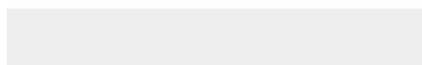
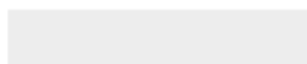




[Click here to access/download](#)

**Production Data**

[RightsLink Printable License-figure5 and 6.pdf](#)






[Click here to access/download](#)

**Production Data**

[RightsLink Printable License-figure7.pdf](#)





[Click here to access/download](#)

**Production Data**

[RightsLink Printable License-figure8.pdf](#)





[Click here to access/download](#)

**Production Data**

[RightsLink Printable License-figure9.pdf](#)





Click here to access/download  
**Production Data**  
Rightslink-figure11.pdf





Click here to access/download  
**Production Data**  
Rightslink-figure12.pdf





Click here to access/download  
**Production Data**  
Rightslink-figure18.pdf





Click here to access/download  
**Production Data**  
Rightslink-figure19.pdf





Click here to access/download  
**Production Data**  
Rightslink-figure20.pdf





Click here to access/download  
**Production Data**  
Rightslink-figure21.pdf







Click here to access/download  
**Production Data**  
Rightslink-figure27.pdf





Click here to access/download  
**Production Data**  
Rightslink-figure29.pdf







Click here to access/download  
**Production Data**  
Rightslink-figure32.pdf





Click here to access/download  
**Production Data**  
Rightslink-figure33.pdf





Click here to access/download  
**Production Data**  
Rightslink-figure35 a-f.pdf








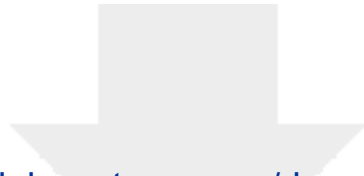
Click here to access/download  
**Production Data**  
Rightslink-figure37.pdf





Click here to access/download  
**Production Data**  
figure1.tif





[Click here to access/download](#)

**Production Data**

figure3 a (left) and b (right) .tif

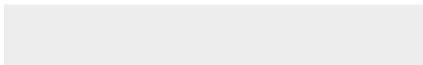
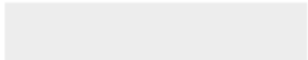






[Click here to access/download](#)

**Production Data**  
figure3d.tif





Click here to access/download  
**Production Data**  
figure4.tif



[Click here to access/download](#)

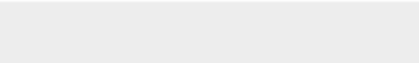
**Production Data**  
figure5a.tif





[Click here to access/download](#)

**Production Data**  
figure5b.tif





[Click here to access/download](#)

**Production Data**  
figure5c.tif





Click here to access/download  
**Production Data**  
figure6.tif



[Click here to access/download](#)

**Production Data**  
figure7ab.tif





[Click here to access/download](#)

**Production Data**  
figure7c.tif





[Click here to access/download](#)

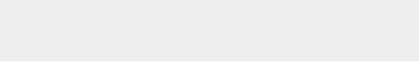
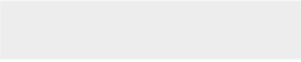
**Production Data**  
figure7d.tif





[Click here to access/download](#)

**Production Data**  
figure7e.tif

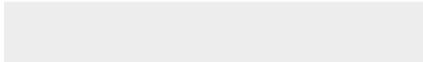







[Click here to access/download](#)

**Production Data**  
figure8a-f.tif





[Click here to access/download](#)

**Production Data**  
figure8g.tif







[Click here to access/download](#)

**Production Data**  
figure8i.tif





Click here to access/download  
**Production Data**  
figure9.tif



[Click here to access/download](#)

**Production Data**  
figure10.tif





[Click here to access/download](#)

**Production Data**  
figure11a-g.tif





[Click here to access/download](#)

**Production Data**  
figure11h,i.tif





[Click here to access/download](#)

**Production Data**  
**figure11j.tif**





[Click here to access/download](#)

**Production Data**  
figure12.tif








[Click here to access/download](#)

**Production Data**  
figure14.tif








[Click here to access/download](#)

**Production Data**  
figure16.tif





[Click here to access/download](#)

**Production Data**  
figure17a.tif






[Click here to access/download](#)

**Production Data**  
figure17b.tif





Click here to access/download  
**Production Data**  
figure17c.tif



[Click here to access/download](#)

**Production Data**  
figure18a-f.tif






[Click here to access/download](#)

**Production Data**  
figure18gh.tif





Click here to access/download  
**Production Data**  
figure18i.tif



[Click here to access/download](#)

**Production Data**  
figure19.tif





[Click here to access/download](#)

**Production Data**  
figure20ab.tif





Click here to access/download  
**Production Data**  
figure20c.tif







[Click here to access/download](#)

**Production Data**  
**figure22a-d.tif**





[Click here to access/download](#)

**Production Data**  
figure22e-h.tif

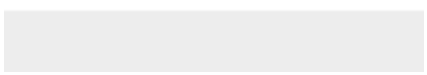
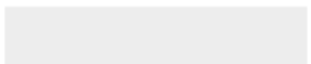






[Click here to access/download](#)


**Production Data**  
**figure24a-c.tif**





[Click here to access/download](#)

**Production Data**  
figure24d.tif



Click here to access/download  
**Production Data**  
figure24e.tif





[Click here to access/download](#)

**Production Data**  
figure26.tif





[Click here to access/download](#)

**Production Data**  
figure27.tif

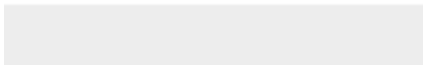






[Click here to access/download](#)

**Production Data**  
figure29.tif





[Click here to access/download](#)

**Production Data**  
figure30ab.tif





[Click here to access/download](#)

**Production Data**  
**figure30cd.tif**












[Click here to access/download](#)

**Production Data**  
figure34.tif



[Click here to access/download](#)

**Production Data**  
figure35a-f.tif





[Click here to access/download](#)

**Production Data**  
figure35g-i.tif



[Click here to access/download](#)


**Production Data**  
figure36.tif





[Click here to access/download](#)


**Production Data**  
figure37.tif





[Click here to access/download](#)

**Production Data**  
figure38.tif





[Click here to access/download](#)

**Production Data**  
figure39.tif





[Click here to access/download](#)

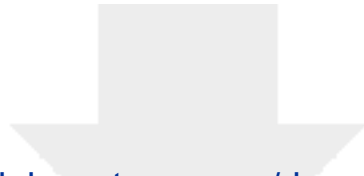
**Production Data**  
figure40.tif





[Click here to access/download](#)

**Production Data**  
Ragone plot.tif



[Click here to access/download](#)

**Production Data**

TOC-110x20mm.pptx





Click here to access/download  
**Production Data**  
TOC-110x20mm.tif

